Theoretical investigation of the hydrogen electrocatalysis in alkaline media on bimetallic Ni-based electrodes

Debora Heloisa Capella Salmazo

UNIVERSITÉ DE STRASBOURG

ÉCOLE DOCTORALE DES SCIENCES CHIMIQUES

THÈSE présentée par :

Debora Heloisa CAPELLA SALMAZO

soutenue le : 07 december **2018**

pour obtenir le grade de : **Docteur de l'université de Strasbourg**

Discipline/ Spécialité : Chimie

Etude théorique de l'électrocatalyse des réactions de l'hydrogène en milieu alcalin sur des électrodes bimétalliques à base de Ni

THÈSE dirigée par :

[Mme SAVINOVA Elena]	PR PRUPH, ECPM Université de Strasbourg
[M SCHMICKLER Wolfgang]	Professour, Universität Ulm

RAPPORTEURS :

[M FILHOL Jean-Sébastien]	PR PRUPH, Institut Charles Gerhard Monpelier
[M TIELENS Frederik]	PR PRUPH, Vrije Universiteit Brussel

AUTRES MEMBRES DU JURY :

[M MARQUARDT Roberto]	PR PRUPH, Institut de Chimie de Strasbourg
[M BONNEFONT Antoine]	MCF - MCUPH, Institut de Chimie de Strasbourg
[Mme JUAREZ Fernanda]	Autre, Universität Ulm

Debora Heloisa CAPELLA SALMAZO

Etude théorique de l'électrocatalyse des réactions de l'hydrogène enmilieu alcalin sur des électrodes bimétalliques à base de Ni

Résumé

Le mécanisme de la réaction d'oxydation de l'hydrogène (HOR) dans Ni (111) est bien connu et se fait par étapes de Volmer-Heyrovsky, en milieu alcalin. . Il a été proposé que la formation d'eau puisse jouer un rôle important. Dans cette thèse, j'ai étudié les surfaces de nickel et de nickel bimétallique en utilisant la théorie de la densité fonctionnelle (DFT). J'ai calculé des magnitudes thermodynamiques (comme les énergies libres d'adsorption de Gibbs) et des propriétés cinétiques (comme des barrières d'activation pour la formation d'eau). Plusieurs surfaces Ni / Cu ont été analysées. Celle qui contient 25% de Cu (sur la couche supérieure) a les meilleures performances: 1) l'énergie d'activation est de 0,2 eV, et 2) OH et H ne doivent pas être fortement adsorbés dans la plage de potentiel HOR.

Mots-clés: nickel, bimétallique, hydrogène, OH, DFT

Résumé en anglais

The mechanism of hydrogen oxidation reaction (HOR) in Ni(111) is well-known and it happens through Volmer-Heyrovsky steps, in alkaline media. However it was proposed that water formation could play an important role. In this thesis, I have studied nickel and bimetallic nickel surfaces using density functional theory (DFT). I calculated thermodynamical magnitudes (like Gibbs energies of adsorption) and kinetic properties (like activation barriers for water formation). Several Ni/Cu surfaces were analyzed. The one with 25% of Cu (on top layer) has the best performance because: 1) the activation energy is 0.2 eV, and 2) OH and H are not to strongly adsorbed on the HOR potential range.

Keywords: nickel, bimetallic, hydrogen, OH, DFT

Acknowledgements

The last four years of my life have been full of experiences. Moving to Europe, and living in France and Germany have changed me in certain ways that I never thought would be possible. In this page, I am going to thanks all people who help me in this journey.

I wish to express my gratitude to Prof. Dr. Elena Savinova who accepted to guide me during my Ph.D. She gave me the opportunity to work in the fascinating Fuel Cell world and supported me in many ways. Our project included also Prof. Dr. Wolfgang Schmickler who encouraged me in the new way of working with computers.

I would like to say thanks for all the coworks and staff from The Institute of Chemistry and Processes for Energy, Environment and Health and The Institute of Theoretical Chemistry who without their knowledge many thinks could have passed unnoticed.

In these years, I have met people from different cultures and parts of the world. They have been making me more understanding person and my network grows exponentially. Thank all of you.

To my family, this period has been a hard time. I am living more than twelve-hour flight distance, and they are always there supporting me and, eventually, coming to visit me. My special thanks to my mom who always believes on me even when I could not.

My last thanks is for my scholarship, CNPQ, that select me among so many students and truly believe in this project since the beginning and approved all changes we had performed in order to conclude in a good way. Without it, I could not have done this work.

List of Abbreviations

AFC Alkaline Fuel Cells

AMFC Alkaline Membrane Fuel Cell

DFT Density Functional Theory

FC Fuel Cell

GGA Generalized Gradient Approximation

HER Hydrogen Evolution Reaction

HOR Hydrogen Oxidation Reaction

KS Kohn-Sham

LDA Local Density Approximation

MCFC Molten Carbonate Fuel Cell

NEB Nudged Elastic Band Method

PAFC Phosphoric Acid Fuel Cell

PAW Projector Argument Wave

PBE Perdew Burke and Erzenhof

PES Potential Energy Surface

PEMFC Proton Exchange Membrane Fuel Cell

PP Pseudopotential

SAE Solid Alkali Electrolyzers

SAFC Solid Alkaline Fuel Cell

SOFC Solid Oxide Fuel Cell

Contents

Chapter 1

Introduction

Since the industrial revolution, the demand for energy has been increasing exponentially, and the main energy sources are non-renewable such as petroleum, coal, natural gas these correspond to about 80% of the amount of energy produced and used nowadays. These are finite resources and they will not last indefinitely, the most optimist data available suggest about 150 years. Therefore, renewable energy sources are necessary to keep the lifestyle of our society.

There are few types of infinite (or semi-infinite) sources, *e. g.* nuclear fission, geothermal, wind, solar, hydroelectric, and biomass. The first one is quite controversial because the process includes radioactive components, their transportation, manipulation, storage requiring special procedures and equipment. The others have fluctuations in time because they depend on natural processes. Therefore, devices that convert electrical energy from renewable sources into chemical energy, which can be stored and used whenever required, and those, which convert the chemical energy of a fuel directly into electricity could be the key to energy demand problems.

One of the most promising fuels is hydrogen, and it could be obtained from water in different ways: Electrolysis, Radiolysis, Thermolysis, Ferrosilicon method, Photobiological water splitting, Photocatalytic water splitting among others, and they are beyond the topic

of this thesis.

Conversion of the energy stored in the form of hydrogen fuel can be conveniently performed in a fuel cell. Recently, Solid Alkaline Fuel Cell (SAFC) based on anion-exchange membranes has been proposed as a new type of polymer electrolyte membrane fuel cells. They are more resistant to carbon dioxide than the liquid electrolyte-based Alkaline Fuel Cells (AFC) and, in contrast to the proton-exchange membrane fuel cells, do not require the usage of the noble metals. Besides, the oxygen reduction reaction may be catalyzed by a non-precious material such as silver or transition metal oxides and is more efficient in the alkaline compared to the acidic environment.

The hydrogen oxidation is, however, slower under alkaline conditions, due to losses occurred through significant overpotential on the anode in the SAFC. Thus, the prospects for SAFC depend primarily on the researcher's ability to develop active and stable catalysts for the hydrogen oxidation reaction (HOR). In the meantime, the back reaction - the hydrogen evolution reaction (HER) in alkaline media - is of importance for the development of Solid Alkali Electrolyzers (SAE). This justifies a strong practical interest in the study of the hydrogen reactions (HOR and HER) in alkaline electrolytes.

Alkali electrolyzers are usually made using Ni as the cathode material. However, above the equilibrium potential of the hydrogen electrode, Ni undergoes oxidation, while below the equilibrium potential Ni hydrides are formed. While metallic Ni has some activity in the HOR and HER, although about 100 times lower than that of Pt in hydrogen reactions, surface passivation with oxides reduces the activity and makes it of little interest as an anode of a SAFC.

Combining Ni with a second metal allows some adjustments:

- to change the electronic properties of Ni, by affecting hydrogen adsorption energy and decreasing their propensity to oxidation (electronic effect).

- to create active centers for water activation (bi-functional effect).

The literature describes some indications of the positive influence of some metals on the Ni activity. However, the information available is quite controversial due to uncertainties in an active surface area, and the composition of the bimetallic surface. It is often not clear whether the increased activity is due to a synergism between two metals or an increase of surface area.

In the last decade, significant progress in the theory of electrocatalysis has been made due to its importance for energy conversion. Nowadays, thanks to the application of Density Functional Theory (DFT), which will be described below, it has become possible to perform reliable quantum mechanical calculations for systems with hundreds of atoms.

While these can give valuable results for the thermodynamics of electrochemical reactions, they cannot adequately represent an electrochemical interface, because the required ensemble would be too large and because charged particles are difficult to represent. This precludes the investigation of the kinetics of electrochemical charge-transfer reactions solely by DFT. Therefore, much of the present work is focused on semi-empirical correlations between thermodynamic quantities, such as adsorption energies, on the one hand, and kinetic properties, on the other hand, which are ultimately based on Sabatier's principle. Nonetheless, activation barriers were calculated in some selected cases. In this thesis, bi-metallic Ni surfaces are studied using DFT for hydrogen reactions. The theoretical approach is used in order to obtain insights on different surface combinations and different materials at the atomic level.

In what follows, the literature review is presented with the focus in Fuel Cell (FC), their types, uses and challenges followed by the hydrogen reactions and finished with properties of Ni electrodes.

Chapter 2

Literature Review

The most relevant topics for understanding this thesis are discussed in the next pages. In this work, I use theory as a guide in the search for novel bi-metallic Ni-based catalysts for the Hydrogen Evolution Reaction (HER) and Hydrogen Oxidation Reaction (HOR). At the beginning of the literature review, a short introduction about FCs is made, followed by HER and HOR reactions and the parameters that determine their kinetics. In the end, but not less important, the properties of Ni electrodes in these reactions are discussed.

2.1 Fuel Cells

2.1.1 Design

FCs are devices which convert chemical energy into electric one directly and spontaneously. More precisely, this device uses electrochemical reactions. The fuel is oxidized at the anode, and oxygen is reduced at the cathode [1]. In Fig 2.1, a FC scheme is shown.

FCs are usually divided into few types [2–4], and the electrolyte substance is used for the categorization. They are also sub-divided in two main groups according to their operation temperature: Molten Carbonate Fuel Cell (MCFC) and Solid Oxide Fuel Cell (SOFC), which operate at temperatures higher than 473K and because of that they belong to the group

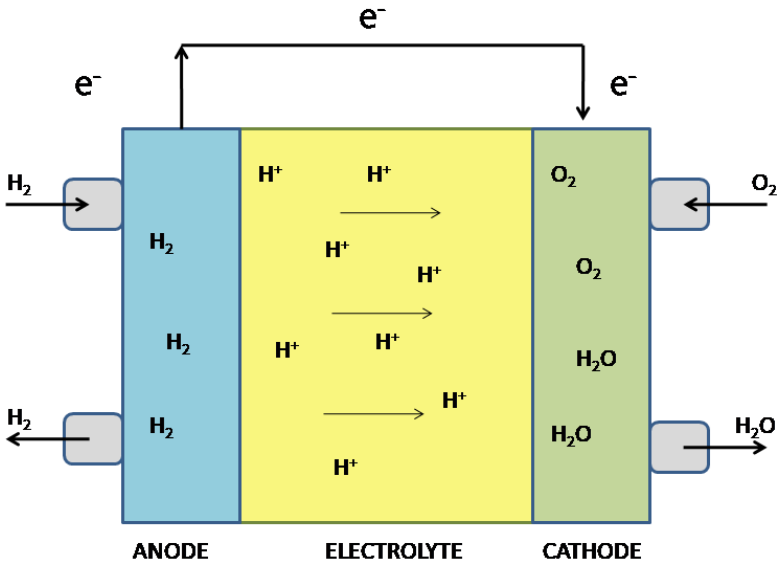

Figure 2.1: Schematic representation of a Proton Exchange Membrane Fuel Cell (PEMFC).

of high-temperature fuel cells; Phosphoric Acid Fuel Cell (PAFC), PEMFC, and AFC are known as low-temperature FCs.

As mentioned before, the reactions occur in separate segments of a fuel cell connected by an external circuit where the electrons produced at the anode can pass. There is a region filled with electrolyte, (which can be liquid, solid or polymer), where current is carried by ions.

A few issues are related to each side of the FC. This document is focused on studying reactions at the anode, and how its composition affects electrocatalysis.

2.1.2 Types

There are a few types of FCs, each one has different applications, their own temperature of operation, advantages, and disadvantages. The most relevant pieces of information are described in the Table 2.1.

Table 2.1: Fuel cell types. Adapted from [4]

Type	Electrolyte	Range of operation (°C)	Advantages	Disadvantages	Applications
AFC	KOH (OH^-)	60 - 90	- High efficiency	-CO_2 sensitivity - No fuel reforming	-Aerospace -Military
PEMFC	Nafion® (H_3O^+)	80 - 90	- Flexible operation	- CO poisoning - Cost and efficiency	-Portable vehicle propulsion - Aerospace
PAFC	H_3PO_3 (H_3O^+)	160 - 200	-Electricity and heat -CO tolerance	- Corrosion	- Stationary applications -Co-generation of heat and electricity
MCFC	Molten Salt (CO_3^{2-})	650 - 700	- Tolerant to CO/CO_2 -Ni based electrode	- Recycling of CO - Three phase interface	- Stationary applications - Co - generation of heat and electricity
SOFC	ZrO_2 (O^{2-})	800 - 900	- Fuel reforming inside the cell	- Thermal expansion	- Stationary applications -Co-generation of heat and electricity

The PAFCs were the first type of FC commercialized by the United Technology Corporation. Nowadays, there are about 100 in operation in the world with an initial efficiency of 42%. Their advantages are high CO tolerance and the possibility of co-generation of heat and electricity. The PAFCs require utilization of noble metals at the anode and the cathode, the electrode kinetics being strongly affected by the electrode flooding and adsorption of phosphate anions.

For the high-temperature fuel cells, non-noble materials can be used as catalysts. Their operation temperature increases the reaction kinetics and permits fuel reforming inside of it. [4]

The AFCs were used in the 1950s on the NASA Apollo program, and they are still used in many aerospace programs. Recently, interest in AFC has increased due to advantages over other FCs such as low operating temperature (23 -70 °C) and faster reaction kinetics at the cathode than in acidic conditions resulting in higher cell voltages.

One of the disadvantages is related to KOH electrolyte. [5] It is sensitive to CO_2 that requires clean gases at the anode and the cathode to feed the system. If air is used, CO_2 might react with KOH generating K_2CO_3 which reduces performance because of changes in the electrolyte conductivity and formation of solid deposits. The volume of electrolyte must be correct, otherwise, there is electrode flooding or drying. Many solutions have been proposed for reducing the problem of carbonate formation, for example, by circulating the electrolyte, however, with limited success.

Most of the AFCs use a noble metal catalyst that makes them expensive and inappropriate for large scale commercialization.[6] Nickel is one of the most promising catalysts to replace platinum. However, the performance of pure metallic Ni electrode toward HER in alkaline media is still much lower than that of palladium or platinum because of strong adsorption of the hydrogen intermediate on the catalyst surface. More details about nickel catalysts are given in section 2.3.

2.2 Hydrogen Reactions

2.2.1 Hydrogen reactions in Acidic Media

The HER/HOR overall reaction can be written as [7]:

$$2H^+ + 2e^- \rightleftharpoons H_2 \tag{2.1}$$

Reactions of the hydrogen electrode were the first electrochemical reactions ever studied. The HER model proposed by many is considered as follows:

$$H^+ + e^- \rightleftharpoons H_{ads} \tag{2.2}$$

$$2H_{ads} \rightleftharpoons H_2 \tag{2.3}$$

$$H_{ads} + H^+ + e^- \rightleftharpoons H_2 \tag{2.4}$$

The mechanism can occur in two ways Tafel(eq. 2.3)- Volmer (eq. 2.2) or Heyrovsky (eq. 2.4) Volmer (eq. 2.2). In the first case, the H_2 is dissociated in a chemical step followed by charge transfer, and then, proton hydration. In the other case, there is charge transfer in both reactions. The mechanism strongly depends on the nature of the electrode, on the electrolyte composition, and on the electrode potential. Depending on the conditions the Tafel-Volmer mechanism can switch into Heyrovsky-Volmer or a combination of the two.

A high-performance catalyst must fulfill criteria for good catalytic activity, chemical and mechanical stability, and low cost. References [8] and [9] provide a resume of the properties of a good catalyst: low hydrogen over-voltage at industrial applications, no potential drift, good chemical and electrochemical stability, long lifetime and no release of process-deleterious products, high adhesion to the support, low sensitivity to poisoning by impurities, low sen-

sitivity to current shut down, no safety or environmental problems in the manufacturing process, and being easy to prepare.

In the next pages, the factors which interfere in the rate of these reactions are discussed in detail with emphasis to the electrode material, the heat of adsorption, and pH.

2.2.2 Electrode Material

The exchange current density in the HER can vary by up to 10 orders of magnitude depending on the electrode material. Many authors have tried to establish correlations between the rate of HER and physical and chemical properties of the electrode materials [10]. Hence, a relation between the exchange current density versus the adsorption energy of H atom on the electrode was studied. The trend is known as the Volcano plot because of its shape and is related to Sabatier´s principle which says that the interaction between the catalyst and an adsorbate intermediate should be neither too strong nor too weak. In Fig 2.2, a version compiled by Trasatti is shown.

In 1972 when Trasatti compiled this plot, the hydride formation energy of E_{M-H} was used instead of the hydrogen adsorption energy because at that time no reliable data about adsorption energies were available. For lower values of E_{M-H}, the Volmer reaction (eq. 2.2) is energetically uphill and, consequently, unfavorable. When the E_{M-H} increases, less energy is necessary for adsorption and the reaction becomes faster. In terms of Gibbs energy of hydrogen adsorption, its value is close to zero is considered as an optimum. If the value of E_{M-H} becomes higher and higher, the kinetics of the Volmer reaction increases but in the second step, the initial state energy becomes lower and lower. This way, a strong adsorption bond has to be broken in Heyrovsky or Tafel step making these steps rate determining.

There is a descending branch, but those metals are covered by an oxide film whose presence impedes the reaction. This surface oxidation was disregarded when the plot was proposed, and if this is taken into account, there is no clear evidence for the volcano plot and just the ascending branch is evident.

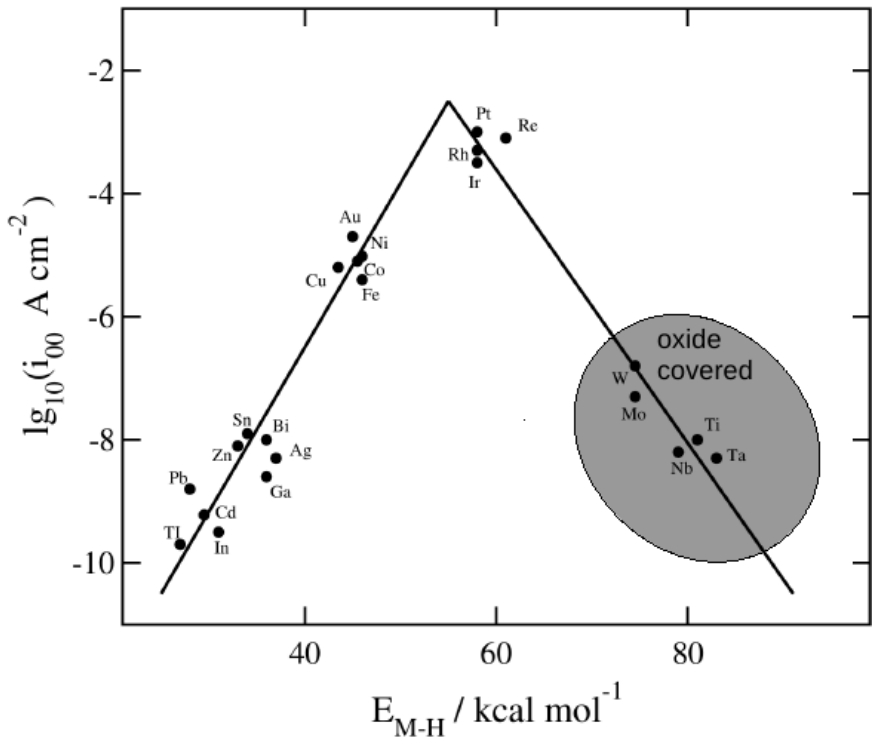

Figure 2.2: Trasatti´s version of the volcano plot for HER. i_{00} is the standard exchange current density of the reaction and E_{M-H} is the binding energy between metal and hydrogen atoms. Data taken from [11]

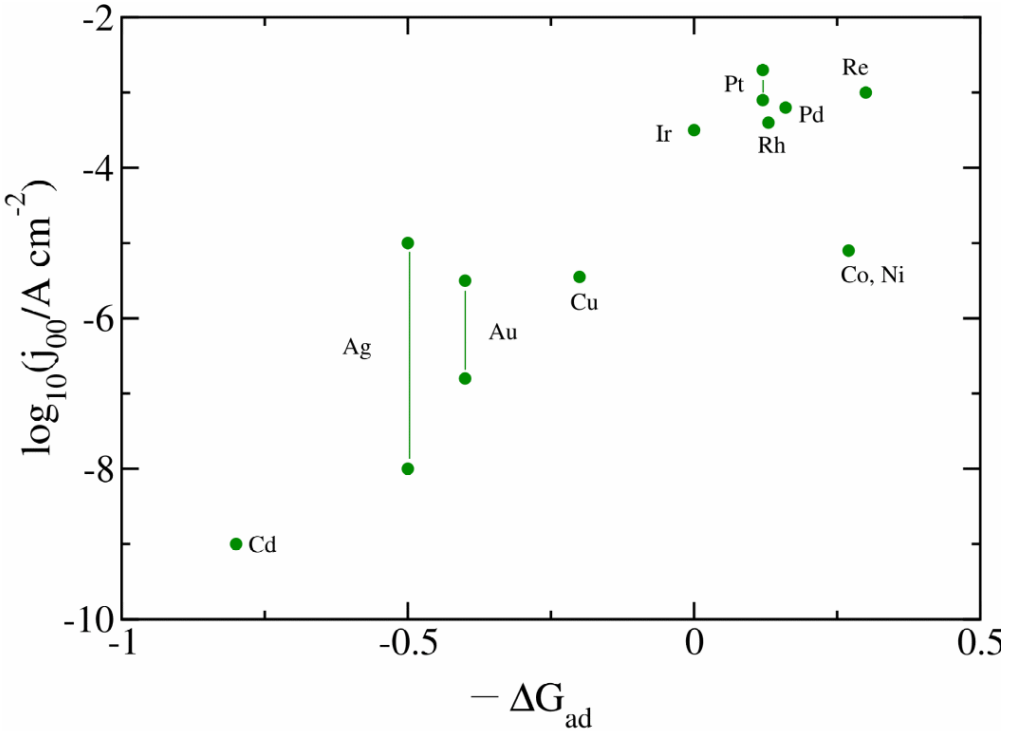

Figure 2.3: Modern version of volcano plot for HER. Adapted from (12)

Values of ΔG_{ad} of hydrogen atom adsorption with an accuracy of 0.1 eV were obtained by DFT calculations, and a new volcano plot was compiled. In the case of Ag and Au there is a spread of experimental data, and in these cases, the extreme values are indicated in Fig. 2.3. The higher ones are more trustworthy because they have been obtained by flame-annealed single crystals [12]. The *sp* metals are bad catalysts for the HOR/HER, so just the adsorption energy of Cd is shown. There is a tendency for the rate to increase with decreasing ΔG_{ad} as in Trasatti's plot. However, there is still little evidence for the descending branch. As it is observed in Fig. 2.3, just Co, and Ni have a low, negative Gibbs adsorption energy, and small reaction rates. Re has lower adsorption energy than Co and Ni. Ni, Co, Re are the metals with the most exergonic adsorption. In experimental conditions, the other metals which adsorb hydrogen strongly are covered by oxides or hydroxides.

On several d-metals two types of adsorbed hydrogen exist: a strongly adsorbed species, which does not participate in the HOR/HER, and a weakly adsorbed species with $\Delta G_{ad} \approx$

= 0 which acts as the intermediate of reaction in hydrogen electrode reactions. In particular, this is the case on Pt and Re. Hence, the ΔG_{ad} values plotted on the x axis are relevant for only part of the metals.

2.2.3 Theoretical dependence between the reaction rate and adsorption energy

Sabatier´s principle and the volcano relationship suggest that the optimal value for the Gibbs energy of adsorption of hydrogen is $\Delta G_{\mathrm{ad}} \approx 0$. Here I illustrate this relation using a simple quantitative model by simplifying the overall reaction mechanism and considering the HER as an ideal case of an electrochemical reaction with a single intermediate following ref. [13]. This can be rationalized using the reduction of H^+ to H_{ads} as shown in Eq. 2.5. For convenience, the other steps of the mechanism are summarized by the letter P as long as the following discussion is based on the intermediate state H_{ads}.

$$H^+ + e^- \rightleftharpoons H_{ads} \rightarrow P \tag{2.5}$$

The volcano relationship results from the balance of the rates of the individual steps. When $\Delta G_{\mathrm{ad}} \ll 0$ the first step is highly exergonic and therefore expected to be fast. However, the second step will be endergonic and hence slow. Vice versa, if $\Delta G_{\mathrm{ad}} \gg 0$ the first step will be endergonic and slow and the second step fast. For a stationary reaction the overall rate is fastest when both steps have about the same rate, i.e. when $\Delta G_{\mathrm{ad}} \approx 0$; this is the essence of Sabatier´s principle. Obviously, this simple reasoning holds only if there are no other factors, such as activation energies, which may strongly affect the rate.

Considering the rates of formation and removal of H_{ads} (eq. 2.5) and the Heyrovsky step (eq. 2.4), which seems to be the dominant mechanism on nickel electrodes [14] the following kinetic equations are given by:

$$\begin{aligned} \upsilon_{ads} &= C_{\mathrm{H^+}}\kappa_1(1-\theta) \\ \upsilon_{des} &= \kappa_{-1}\theta \\ \upsilon_{reac} &= C_{\mathrm{H^+}}\kappa_2\theta \end{aligned} \tag{2.6}$$

where θ is the fraction of surface sites which are covered by H_{ads} and $\mathrm{C}_{\mathrm{H^+}}$ is the concentration of protons; κ_1, κ_{-1}, and κ_2 are kinetic constants for adsorption, desorption, and Heyrovsky reaction, respectively.

As long as $C_{\mathrm{H^+}}\kappa_1 \ll \kappa_{-1} + C_{\mathrm{H^+}}\kappa_2$, the H_{ads} coverage is negligible. On the other hand, if $C_{\mathrm{H^+}}\kappa_1 \gg \kappa_{-1} + C_{\mathrm{H^+}}\kappa_2$, the surface is almost completely covered by H_{ads}. As the adsorption strength rises, κ_1 increases and both κ_{-1} and κ_2 decrease. Hence, θ increases monotonically with raising adsorption strength.

The adsorption of hydrogen on the electrode surface changes the Gibbs energy of activation. According to the Brønsted-Evans-Polanyi rule [15], the relationship between the activation energy and the change in the Gibbs energy for an elementary reaction is linear, i.e.

$$\Delta G^{\#}_{1,ads} = \Delta G^{\#}_{1} + \alpha\Delta G_{ads} \tag{2.7}$$

where $\Delta G^{\#}_{1}$ is the change in the Gibbs energy when there is no interaction with the surface, and α correspond to the Brønsted coefficient, which is equivalent to the transfer coefficient in electrochemistry. In the same way, the activation energies for desorption reaction could be written as:

$$\Delta G^{\#}_{-1,ads} = \Delta G^{\#}_{1} - (1-\alpha)\Delta G_{ads} \tag{2.8}$$

and

$$\Delta G^{\#}_{2,ads} = \Delta G^{\#}_{2} - (1-\beta)\Delta G_{ads} \tag{2.9}$$

where β is called Brønsted coefficient for the second reaction. Using equations 2.8 and 2.9 the rate constants for the corresponding steps can be expressed as follows:

$$\kappa_1 = A_1 e^{-\Delta G^{\#}_{ads}/RT} = A_1 e^{-\Delta G^{\#}_{1}/RT} e^{-\alpha \Delta G_{ads}/RT} = \kappa_1^{'} e^{-\alpha \Delta G_{ads}/RT} \tag{2.10}$$

$$\kappa_{-1} = \kappa_{-1}^{'} e^{(1-\alpha)\Delta G_{ads}/RT} \tag{2.11}$$

$$\kappa_2 = \kappa_2^{'} e^{(1-\beta)\Delta G_{ads}/RT}$$

It is important to point out that $\Delta G_{ads} < 0$ and thus κ_1 rises, while κ_{-1} and κ_2 decrease with increasing adsorption energy, as expected. To a first approximation $\alpha = \beta = 0.5$ and the steady-state coverage of the reaction intermediate θ_{ss} can be expressed as follows:

$$\theta_{ss} = \frac{1}{1 + (\frac{\kappa'_{-1}}{C^{+}_{\mathrm{H}}\kappa'_1} + \frac{\kappa'_2}{\kappa'_1}) e^{\frac{\Delta G_{ad}}{RT}}} \tag{2.12}$$

From these the stationary current can be expresses as 2.13:

$$i = \mathrm{i}_{ox} - i_{red} = F\kappa'_1 e^{\frac{\alpha \Delta G_{ads}}{RT}} [1 - \theta_{ss}(\Delta G_{ads})] - \left(\kappa'_{-1} - \kappa'_2\right) e^{\frac{-\alpha \Delta G_{ads}}{RT}} \theta_{ss}(\Delta G_{ads})\} \tag{2.13}$$

where i_{ox} and i_{red} are the currents of oxidation and reduction reactions, F is Faraday constant, R is universal gas constant, and T is temperature. Plots of $\ln i$ and of θ_{ss} vs ΔG_{ads} as calculated from eq. 2.12 and eq. 2.13 are shown in Fig 2.4.

The coverage increases with ΔG_{ads} showing a sigmoidal shape, while the current (and

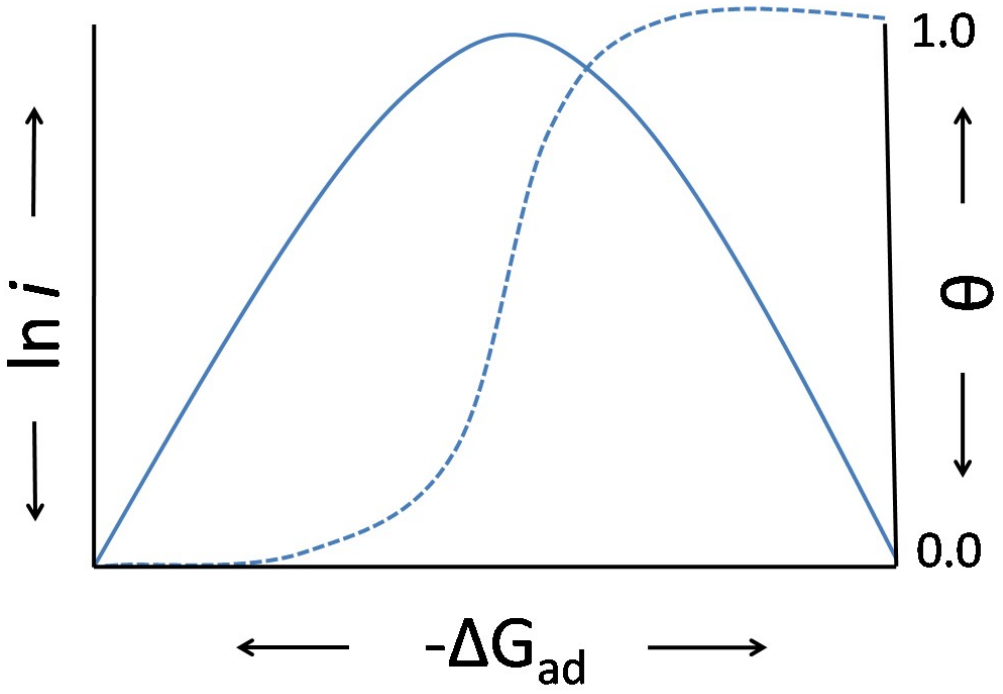

Figure 2.4: Catalytic activity (solid line) and coverage of intermediate H (dashed line) as function of the standard Gibbs energy of adsorption of H for the reaction scheme. Data adapted from [13]

thus the catalyst activity) shows a maximum versus the adsorption strength.

According to eq. 2.12 and eq. 2.13 if θ is low, the rate determining step is the adsorption.

Therefore the best catalyst is the one for which $C_{\mathrm{H^+}}\kappa_1 = \kappa_{-1} + C_{\mathrm{H^+}}\kappa_2$. This means, the standard Gibbs energies of formation of H_{ads} from $\mathrm{H_2}$ is similar to formation of P from H_{ads}.

As mentioned in the previous section, many metals are covered by a thin layer of oxides such as Ni, Ti, Mo, and W [16], [17], [18]. Considering that oxygen adsorbs stronger than hydrogen, there is a reduction in the overall rate of reaction. Impurities present in the electrolyte may also affect the reaction rate in case they are adsorbed on the surface.

So far, the influence of the electrode potential in the reaction rate was neglected but it has a strong effect on the catalytic activation. It does not only affects the activation energies but also the surface charge densities. This means that the surface charge at the metal/electrolyte interface is controlled by the electrode potential under the operating conditions and influenced

by adsorbed ions/molecules, and also changes the Gibbs adsorption energy.

2.2.4 pH dependence

Many factors affect the HER and the most important ones are the adsorption interaction between reactants/reaction products and the electrode (catalyst) [19], [20], [21]. Increasing pH from 0 to 14 in aqueous electrolyte solutions changes *e.g.* the surface state and may also influence adsorption of reactants/intermediates. The acid anion adsorption is replaced by adsorption of OH ions. This can happen even in the vicinity of the reversible hydrogen electrode potential.

There are differences between the HER in acidic and alkaline media. In the Volmer step eq. 2.15, this is not a proton but a water molecule which reacts on the electrode surface to produce an adsorbed hydrogen atom and negatively charged OH^-. Then, this hydrogen atom can combine with another adsorbed hydrogen to generate a hydrogen molecule that leaves the surface (Tafel step eq. 2.14) or interacts with another water molecule to produce a hydrogen molecule and a hydroxide ion (Heyrovsky step eq. 2.16).[7]

$$2H_{ads} \rightleftharpoons H_2 \tag{2.14}$$

$$H_2O + e^- \rightleftharpoons H_{ads} + OH^- \tag{2.15}$$

$$H_{ads} + H_2O + e^- \rightleftharpoons H_2 + OH^- \tag{2.16}$$

Metal affinity to H^+ and OH^- species cause differences in the behavior in acidic and alkaline media. At platinum in alkaline solutions, the coverage with oxygen-containing species increases when the pH is higher. When the OH species adsorb on the surface, the water content in the inner part of the double layer is reduced, and this makes the reaction 2.17 possible.[22]

$$H_{ads} + OH_{ads} \rightleftharpoons H_2O \tag{2.17}$$

On metals with higher affinity to OH, such as Ni, efficient oxidation of hydrogen is possible only at high coverage of OH. [23] The kinetics of H_{ads} on metal surfaces has been studied in detail [24, 25], but the OH^- produced from the H_2O step and their adsorption on the surfaces for HOR/HER is unexplored. Markovic [26] has demonstrated an enhancement of the HER rate upon deposition of Ni oxide/hydroxide on the electrode surface and suggested that an effcient HER in an alkaline electrolyte requires optimization of both the hydrogen atom and the water molecule adsorption. Hence, he suggested that the HER can be optimized by the density and nature of the sites required for H_2O dissociation, OH^- and metal H_{ad} energetics. Therefore, a balance between the transition state energies for H_2O dissociation and final state energies of OH_{ads} must be found. Considering the Brønsted-Evans-Polanyi rule [15], this results in a lower activation barrier for H_2O, also resulting in the poisoning of the sites, which are required for re-adsorption of H_2O.

2.3 Nickel

2.3.1 History and uses of Nickel

The use of Nickel started more than 2000 years ago and it began in China where it was used in alloys. Just in 1751 A. F. Cronstedt isolated the metal in Sweden and gave the name of Nickel.[27]

The amount of nickel relative to the total amount of substance on Earth is 1.8% being the seventh most abundant element. However its mass-abundance in Earth's crust is only 9 ppm. The main producers are Russia, Canada, and New Caledonia. Its use is wide from daily routine to highly advanced aerospace components. The annual amount produced is about 1400 tons. Most of it is used in alloys (84%) followed by plating processes (9%) and

the rest are small applications such as coins, electronics or batteries. Nickel-based catalysts are the most efficient catalysts for methane reforming to produce hydrogen. [28], [29] The catalytic activity can be attributed to the adsorption of hydrogen and hydrocarbons. Besides, Ni plays an important role in AFC and Alkaline Membrane Fuel Cell (AMFC) as cathode material. [30], [31] However, nickel is more associated with the NiCd and NiMH batteries and the research on these topics have been ample in the last decades. Recently, the NiMH applications have been replaced by lithium-ion batteries, and the focus has changed to FCs.

2.3.2 Electrochemical properties of Nickel and Nickel oxidized surfaces

The Pourbaix diagram is a thermodynamical multidimensional map where all possible stable (equilibrium) phases of an aqueous electrochemical system, *e.g*, passivation, corrosion and metallic phase can be seen. In Fig. 2.5, the Ni Pourbaix is shown [32].

At negative potentials Ni is in metallic form, but when the potential increases to values higher than -0.5 V vs. standard hydrogen electrode, the Ni^{2+} ions are predominant in an acidic electrolyte. In acid media, until ca. pH 3, corrosion is the only process while between pH 3 and 9 the formation of $Ni(OH)_3$ can also occur at high potentials. Above pH 12 and intermediate potential values, the NiO oxide transforms into a soluble form, $HNiO_2^-$, and at potentials above 1 V, the Ni^{3+} oxide form is prevalent.

Ni has the electronic configuration $3d^8\ 4s^2$, thus the oxidation states are 0 to IV. In general, the chemistry of Ni is based on the Ni(II) form and its species. The Ni(III) complexes have low stability in aqueous solutions being stable in acidic media.

According to Bode et al. [33] there are two forms of $Ni(OH)_2$ and NiOOH. Their electrochemical reactions are shown in Fig. 2.6. The α-$Ni(OH)_2$ are described having a tilted turbostratic structure with large volume [33], [34]. The structures of α and γ phases are strongly dependent on OH^- concentration and the cations in the solution because of their presence between the layers. [35] Consecutively potential sweeps in alkaline solution trans-

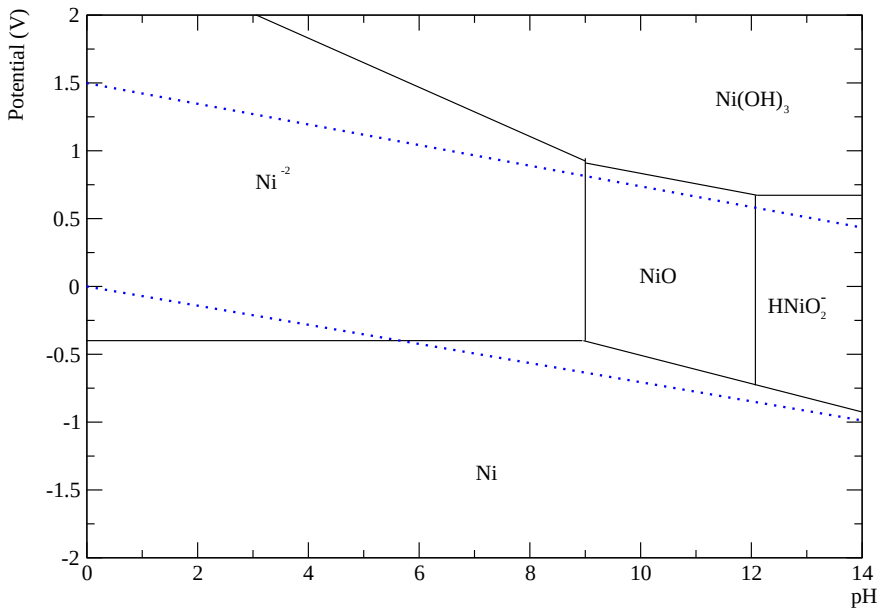

Figure 2.5: Pourbaix diagram for Ni at 25°C. Adapted from [32]

form the α-Ni(OH)$_2$ to β-Ni(OH)$_2$ reducing the volume in 59% due to the radical decrease in the layer spacing. When α-Ni(OH)$_2$ is thermodynamically unstable, the phase is positively charged and it will be transformed to γ - NiOOH. At the time of reverse charging the γ -phase may be reversed back to α-Ni(OH)$_2$ or directly to β-Ni(OH)$_2$. [36] After a few potential cycles in an alkaline solution the β -phase stabilizes on the electrode surface and the γ -NiOOH phase can only be regained by overcharging of the system.

2.3.3 Cyclic Voltammetry of Ni Electrodes

From cyclic voltammetry (CV) information about the formation of oxides and hydroxides on nickel electrodes in alkaline solution can be obtained and this will be discussed in relation to Fig. 2.7 and the literature available. [17], [37], [38]

Recent studies showed that air-oxidized nickel has a bi-layer composition α-Ni(OH)$_2$ at the oxide/solution interface and non-stoichiometric NiO$_x$ at oxide/metal interface. [17], [38]

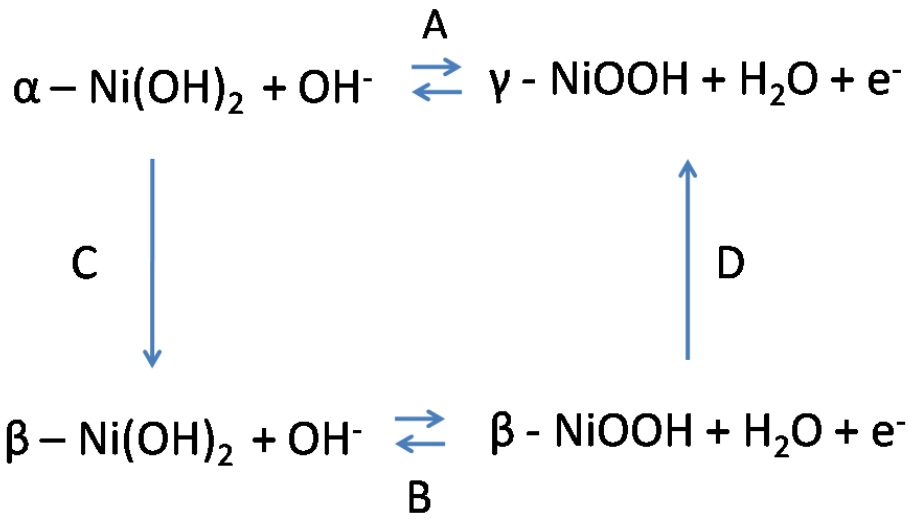

Figure 2.6: Bode diagram for Ni. A and B are electrochemical reactions and C and D are chemical. Adapted from [33]

When a freshly polished electrode is immersed in 0.1 M KOH electrolyte and a potential sweep is made from the open circuit potential in the negative direction, the small peak will appear before hydrogen evolution (a'). Many authors believe this peak a' is the reduction of α- $Ni(OH)_2$ or NiO_x. [39], [40] Nonetheless, the β- $Ni(OH)_2$ is not reduced under peak a' and will be rearranged in more stable β - phase. [17] This way, a' is only seen if the electrode potential is not extended into the NiOOH formation. However, the reduction of α- $Ni(OH)_2$ is not complete and leaves some oxidized species at the metal surface.

At potentials below -1.0 eV vs. Hg/HgO electrode, the water reduction takes place with hydrogen gas (H_2) formation and hydrogen absorption, and formation of Ni hydrides. [17], [38], [40] When the direction of the potential sweep has reversed the peak a appears. The latter peak and the plateau that immediately follows correspond to the oxidation of Ni to α- $Ni(OH)_2$ or NiO_x, and at the end of this plateau the formation of β- $Ni(OH)_2$ begins. If the potential is higher, the peak c is formed and can be attributed to α/β- $Ni(OH)_2$ to

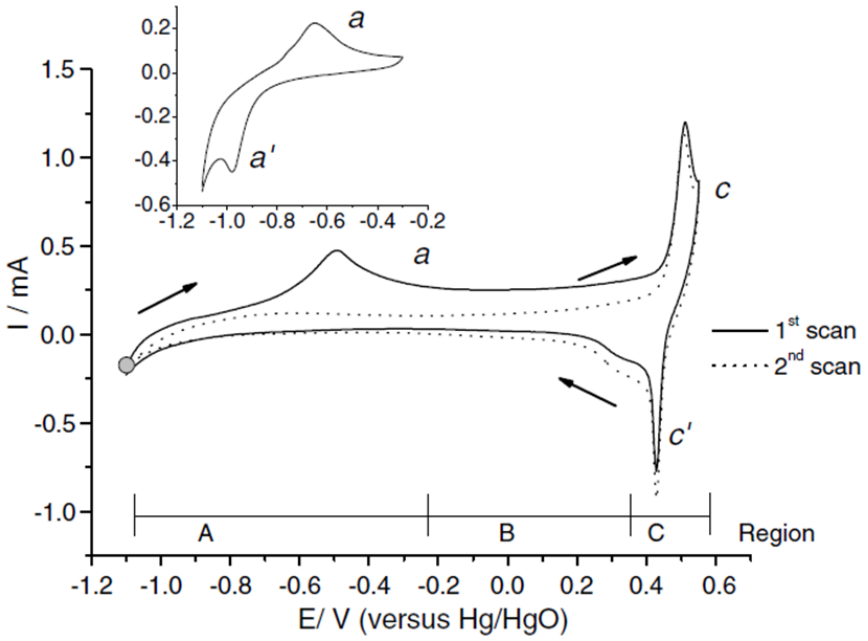

Figure 2.7: Cyclic voltammograms of Ni(111) in 1M KOH. Data take from [16]

γ/β-NiOOH, and shortly after this, the oxidation of water. If during the O_2 evolution, the sweep in Fig. 2.7 is reversed, the O_2 evolution will stop and the reduction of γ/β-NiOOH to α/β- $Ni(OH)_2$ starts creating the peak c'.

The α and γ phases have a strong dependence on the OH^- concentration and the type of cations in the solution since they intercalate in the structure [41–43]. After few potential scans in alkaline media, the α- $Ni(OH)_2$ converts to β - $Ni(OH)_2$ with volume reduction because water and ions are removed from the space between the layers. The difference visualized in the first and the second scan is due to this phenomenon. However, the α - $Ni(OH)_2$ is converted to γ - NiOOH when the first is thermodynamically unstable. In the reverse scan, the γ species change to α - $Ni(OH)_2$ or β - $Ni(OH)_2$ as can be seen in Fig. 2.7.

Since the mid of last century, the HER on metallic Ni has received special attention. The reactions follow the typical general Volmer-Tafel or Volmer-Heyrovsky pathways.[44], [45].

Using the double-charging method to calculating the degree of coverage on Ni, Denavathan

et al. [45] investigated HER. At current densities up to 0.5 mA.cm^{-2}, the results suggested that the rate determining step was Volmer. They calculated the gradient of log i_c vs log θ (where i_c was the cathodic current density and θ was the coverage value) obtaining 2. Therefore, a fast Tafel recombination process was suggested as the desorption step.

Ahn *et al.* [46] synthesized Ni - based dendrites, particles and films applying controlled electro-deposition procedure using nickel chloride. The activities in HER were shown to increase in the order of dendrite > particle > film > foil because of highly (111)-populated Ni dendrite structures when compared to polycrystalline Ni particles and films. However, this conclusion is in contradiction with Floner *et. al* [23] who demonstrated that HOR is structure-sensitive, decreasing in the order 110, 100, and 111, Ni(110) being 6 times more active than polycrystalline Ni.

LeRoy *et al* [47] observed an increase in overpotential over time because of hydride formation. Other authors confirmed hydride formation by X-ray diffraction and scanning electron microscopy [48]. The presence of hydrides changes the pathway into a desorption-limited reaction, which helps to increase the voltage on the Tafel slop. The HER intermediates and a reaction between metallic nickel and dissolved hydrogen are the origins of hydrides. [49]

Weininger *et al.* [50] observed the Ni oxidation or electrochemical adsorption of the hydroxide anion in the low potential region. There is also a possibility to the hydrogen intermediate on the surface to be replaced by hydroxide anions to form water and nickel, which reduces the catalytic activity.

At ambient conditions, Ni has the tendency to be oxidized, resulting in the formation of a thick oxide layer consisting of a mixture of NiO and $Ni(OH)_2$. [16], [17], [18] Some increase of activity has been reported for surfaces where pure nickel and oxidized Ni as NiO co-exist [51] or β - $Ni(OH)_2$. [52], [53], [54] The changes in the activity were attributed to the synergy effect and the enhancement of the rate of the water dissociation step. [54], [52].

Especially on non-precious metals, the number of oxide-hydroxide interfaces must be maximized. Gong *et al.* [52] developed a nanoscale nickel oxide-nickel (NiO/Ni) interfaces

using low-pressure decomposition. Comparing NiO/CNT(Carbon NanoTubes) and Ni/CNT activities through HER, there is a significant improvement in the HER.

Oshchepkov *et al.* [55] concluded that the electrochemical and electrocatalytic properties of nickel in the hydrogen oxidation and hydrogen evolution reactions had high dependence of the electrode pretreatment. If the contact with air was minimized, their electrocatalytic activity in the hydrogen electrode reactions is low for either Ni-nanoparticles deposited on carbon supports or polished Ni. The ambient exposed electrode or controlled chemical conditions had an opposite behavior, increasing the catalytic activity for HER due to the presence of NiO confirmed by ex situ angle-resolved XPS measurements. Similar behavior was observed for Ni electrodes subjected to controlled electrochemical oxidation. While fully oxide-passivated Ni surface is inactive in the HOR/HER, a partially oxidized Ni surface, where both metallic Ni and NiO (or Ni hydroxide) sites co-exist, shows high HOR/HER activity. Combining experimental data with microkinetic modeling, it was concluded that NiO reduces the adsorption energy of hydrogen intermediate and consequently, increases the rate of the Volmer step.

Hetero-structure interfaces are another option of interface creating more opportunities of adjustment for adsorption/desorption energies and consequently, more active catalysts. Subbaraman *et al.* [56] constructed a nano-sized $Ni(OH)_2$ clusters on platinum electrode to improve the catalytic activity. The presence of $Ni(OH)_2$ clusters on Pt(111) reduced the surface area by 35% but the activity for HER $Ni(OH)_2$/Pt increased about seven times. They affirmed that oxygen atoms interacted with $Ni(OH)_2$ domain and hydrogen with the surface next to the boundary. Deposition of $Ni(OH)_2$ improved the activity of several metal electrodes. [57] In the specific case of $Ni(OH)_2$/Ni the activity boosted about four times compared with other surfaces without nickel structures. The presence of $Ni(OH)_2$ clusters was suggested to facilitate water dissociation on the surface and stabilize the cations nearby with the formation of a compact double layer attracting more molecules for dissociation.

Krstajic *et. al* [44] combining steady-state voltammetry and impedance spectroscopy concluded that Volmer-Tafel mechanism occurs in a certain potential interval and then, changes

to the Volmer-Heyrovsky mechanism. Kreysa *et. al* [58] claimed the step of Tafel recombination as the rate determining because of slow H_{ads} surface diffusion.

In general, Ni structures with a high surface area is expected to provide a good catalyst to HER. However, there are still limitations regarding the intrinsic activity of metallic Ni. Another relevant remark is that the H, OH^-, and H_2O adsorption energies are extremely important for the catalytic activity of any surface and can be calculated easily with DFT and other theoretical approaches. Therefore, the comparison of experimental data with models can lead to new insights into the HOR/HER mechanism.

The reaction activation energy depends on many factors such as the energy of adsorption, breaking and/or formation of bonds, the medium reorganization energy, which is determined by the solvent composition and type [59]. Changing the pH, the reactants and products of the reaction can be modified.

One of the reasons for lower activity for HER/HOR is related to a lower state density of d-band electrons requiring a higher potential to maintain the same current density. Hydrogen adsorption is determined by the catalyst properties and electrolyte ionic composition. The hydrogen adsorption is a relevant step on HER and understanding how it behaves is essential. Ni adsorbs hydrogen strongly blocking available reaction sites.[25], [46]. Consequently, new catalysts have to be designed in order to change the electronic structure of Ni and weaken hydrogen adsorption.

Fajin *et al.* [60] studied water splitting using DFT method. They estimated the activation energy in 0.71 eV on Ni (111). With the same method, Sebastiani *et al.* [61] created surfaces with and without steps to study water splitting. They conclude that the binding is stronger on the step and the water is bonding to a surface through oxygen. Pozzo *et al.* [62] claimed the most favorable site is a top site.

Recently, modeling of experimental HOR/HER current potential curves became a useful tool. Using them, many important parameters like Gibbs adsorption energy of an intermediate (H_{ads}) and rate of Volmer, Heyrovsky and Tafel steps for various electrode materials in acidic

or alkaline media can be extracted. On nickel electrodes at pH higher than eight, just the HER part was studied and the processes on HOR part ignored. [58], [44], [63], [64] The difference between a freshly polished nickel electrode surface and a partially oxidized one was mentioned above. However, the mechanism was just analyzed on metallic Ni.

Therefore, the theoretical approach is one of the most powerful tools available for developing new catalysts. Comparing with the experimental approach, a larger number of different catalysts can be studied in a shorter period of time. Calculating the adsorption energy of hydrogen at different coverages, determining the activation and total energies of a given reaction save a lot of time for experimentalists since they provide guidlines which catalysts might be promising.

2.3.4 HER on NiM surfaces

Bimetallic Ni electrodes have been widely studied for the HER. In concentrated alkaline solutions, Ni has an excellent resistance to corrosion, which justifies the interest in its use as a cathode for the HER. There are a few issues related to using Ni alone as a cathode such as low activity, and low resistance to intermittent electrolysis. Therefore, Ni is often combined with other metals in order to increase its catalytic activity. Ni has been alloyed with different metals such as Fe, Cu, Ti, Ru, Mo, Pd, Ir, Ru, and many others.

Abouatallah [65] demonstrated that the addition of V_2O_5 in KOH electrolyte during the HER increased the catalytic activity of Ni cathode with the formation of V deposited. In another publication [66], the same author affirmed electrocatalytic activity of the deposit is not due to increased surface roughness, but changes on its surface state during the reaction.

According to Aaboubi [67], the enhanced performace of NiMn is related to two main factors: increase of the real area of Ni (porosity and roughness) and suitability of the active sites by introducing Mn in the Ni alloy. Dannee [68], using graphite as support for NiMn increased the electrochemical activity for HER in 0.1 M NaOH reducing the Tafel slop and increasing the current density.

NiFe intermetallic systems are considered low cost electrocatalysts for HER [69]. Flis-Kabulska [70] claims that the reasons for this are the high intrinsic activity of NiFe materials and a reduction of the extent of their oxidation. NiFe coatings are corrosion resisistant and are good catalysts for HER.

Jukic [71] studied different compositions of ZrNi amorphous alloys. The catalytic activity increased with the amount of Ni, which was attributed to changing the density of states of the 3d Ni band close to the Fermi level.

Nanocrystalline [72] $Zr_{67}Ni_{33}$ is a better catalyst than an amorphous or nano-/amorphous alloy with the same chemical composition. This could be related to a favorable microstructure. It also adsorbs H under experimental conditions, and the amount is highly dependent on the potential.

Molybdenum is one of the most studied combination. Many different top layer compositions were considered interesting for enhancing the performance, a few of them are: 15% [73], 38.3% [74], 41% [75]. Their composition has a huge dependence on how the alloy is prepared. Some authors advocate that the good performance of this catalyst occurs because the binding energy of the H intermediate is reduced compared to metallic Ni.

Ru is often used in electrocaliysis due to its price being lower than that of Ir, Pt or Pd. Schmidt [22] reported Ni activation by Ru electrodeposition during H_2 evolution in 40% KOH. However, using the spontaneous deposition, Franceschini [63] observed that increasing the amount of Ru resulted in a reduction of the activity. Aging treatment also has an influence on enhancing their performance.

Ni combined with Pd is one of the most studied bimetallic systems for the development of HOR electrocatalysts in alkaline medium. Zitoun [76] *et al.* considered 20 different coverages of Pd on Ni making many surface compositions. The amount of 17% Pd coverage was most efficient reaching the diffusion limit for HOR being even better than pure Pd. This way, the optimum surface coverage requires a small load of the noble metal. [77]

Herranz [78] modified macroporous Ni with Ag nanoparticles and determined that the

enhancement in the HER in alkaline solutions occurred mostly because of the increased surface area. Franceschini [79] showed that the HER is almost the same when Ni is modified with Cu and Ag. The presence of Ag in nanowires and nanoparticles demonstrated a decreased overpotential. The activity of AgNi is associated with a strong synergistic effect between Ag and Ni.

Combinations of a Fe group metal (Ni, Co, Fe) and a refractory metal (Re, Mo, W) are the most promising candidates as Pt-free electrodes for HER. The NiRe alloys are resistant to dilute acids and bases. Both Re and Ni present low overpotentials for HER, thus, accelerating the cathodic reduction process [80].

Ni can be used for increasing catalytic activity of other metals such as Ir. Ni is a good candidate for alloying with Ir because of d-band center theory, a descriptor for the relationship between the distribution of d-band electron and adsorption energy [81].

Another metal that can be combined with Ni is Pt, the most studied metal for HER. In the case of nanoparticles, a low amount of Pt increases the catalytic activity in the alkaline medium. [82] Ni foam activated by Pt showed increased catalytic activity for HER in pH higher than 8 [83]. If the spontaneous metal deposition route is used, this modifies electrocatalytic HER properties during the process. In this type of electrodes, Pt has to be homogeneously distributed for better performance.

Ni macroporous electrode was synthesized by galvanic deposition at high current densities and then modified with Au nanoparticles to evaluate their electrocatalytic behavior towards the HER in alkaline media [84]. This procedure affects positively the activity of Ni for HER without changing the structure.

According to Lupi [85], NiAu alloy nanoparticles are more active than pure Au nanoparticles or NiAu/Au for HER in acid solutions. Their activity is close to that of commercial Pt with an increase in durability. Applying first principles calculations, according to the same author, the best catalyst activity is achieved when Au sites have low coordination numbers.

Recently, copper has received special interest to be combined with nickel because it ad-

sorbs hydrogen weaker than Ni. It is expected that alloying Ni with Cu reduces the enthalpy of hydrogen adsorption, consequently increasing the HER/HOR activity. In addition, copper has high corrosion stability in alkaline media and it is inexpensive compared with Pt or other commercial catalysts available.

Santos *et. al* [86] studied HER for NiCu surfaces using the DFT, the Anderson Newns model, and Marcus theory. The presence of nickel provokes a significant lowering in the activation barrier of Volmer step due to stronger coupling between the hydrogen 1s and d-band on Cu/Ni(111) compared with pure Cu(111). Cherstiouk *et al.* [87] observed the electrocatalytic activity of Ni in the hydrogen reactions in alkaline medium increases with the lower concentration of Cu. The best catalyst had only 5% and it was prepared by the incipient wetness impregnation method. Ahn [88] reported that a catalyst with 59% Ni and 41% Cu performs best. Similarly, Negem [89] reported that 50-50 surfaces were good catalysts.

Chapter 3

Aims and Scope

In this thesis, I explore the realm of bimetallics catalysts for the hydrogen evolution reaction in alkaline media by means of theory. Nickel is a decent catalyst, but it adsorbs hydrogen and also OH too strongly – the latter can inhibit the reaction if it is too firmly bound. Therefore I focus on bimetallic of the composition NiM, where M is a metal that binds hydrogen and OH more weakly. In particular, I shall investigate the following topics:

- Copper is an excellent candidate for the second metal. As summarized in the previous chapter, experiments indicate that certain NiCu clusters are good catalysts. In addition, there is already theoretical work on the surface composition of such clusters. Therefore I shall calculate adsorption energies for H and OH on a variety of surface sites on NiCu. In particular, I am looking for sites where the Gibbs energies of adsorption for OH and H are close to zero in the potential range where hydrogen evolution takes place. As explained in the previous chapter, these are promising sites for catalysis.

- Recently, the recombination reaction $H_{ad} + OH_{ad} \rightarrow H_2O$ has been proposed as an intermediate step for the HER in alkaline media. This is an exciting possibility since the two reactants can be adsorbed on neighboring sites of different composition, one site being optimal for H, the other for OH. A central part of my thesis is devoted to the calculation of activation energies for this step on NiCu surfaces.

- Finally, I shall screen a large number of NiM bimetallic as possible candidates for hydrogen catalysis. For these systems, my focus is on H and OH adsorption energies – the calculation of the corresponding activation energies is beyond the scope of this work since it would have taken too long.

Throughout the investigations, I use density functional theory (DFT) as my workhorse. During the last decades, this method has proved to be efficient and reliable for the theoretical investigation of surface properties and reactions. The calculation of activation energies by DFT can be quite tricky if the configuration space is large. The standard method is Nudged Elastic Band Method (NEB), but this turned out to converge too slowly in many cases. Therefore I calculated potential energy surfaces by restricted geometry optimizations and obtained the activation energies from the saddle points. The method is explained below.

There is one fundamental problem with these and similar investigations: The electrochemical reactions take place at the interface between the electrodes and an aqueous electrolyte. However, the inclusion of a realistic model for the solution is still way beyond the capabilities of DFT. Fortunately, the interaction of water with metal surfaces is generally weak, so its omission is not a problem. Further, the adsorption of hydrogen has been shown to be little influenced by the presence of water. For OH adsorption, the effect of water is somewhat larger, but still of the order of a few tenths of an eV, and thus only a little larger than the usual DFT error, and the relative error when comparing different substrates should be even less. Nevertheless, I express a certain caveat in this respect.

Outline

DFT is introduced in Chapter 4. This method is used in all my calculations, therefore I explain the topics required for understanding my thesis. At the end of this chapter, I will introduce my methodology to find transition states by means of potential energy surfaces Potential Energy Surface (PES)).

Pure Ni(111) surface is the topic of Chapter 5. Adsorption energies of H, O, and OH are

analyzed and compared with literature values in order to evaluate if the proposed set of parameters are accurate for the studies of intermetallic NiM systems. I will also use this surface to establish the accuracy of the PES method to obtain activation energies by comparing my values with previous results, usually obtained using the NEB method.

The adsorption energies of H and OH and the activation energy required for their recombination on the NiCu system are presented in Chapter 6. These results are analyzed in order to select the best top layer composition for HER in case of NiCu systems and the best site for OH adsorption.

Results for H and OH adsorption on a large number of NiM surfaces, where M is a transition metal, are discussed in Chapter 7. The transition metals were selected based on the literature available. The noble ones are Ru, Rh, Pd, Ag, Re, Ir, Pt, and Au; the others are Ti, V, Mn, Fe, Co, Cu, Zn, Zr, Nb, and Mo.

Chapter 8 summarizes briefly the results.

Chapter 4

Theoretical concepts and methodology

In Quantum Chemistry, the wave-function contains all the information about a specific system. To obtain this wave-function the Schrödinger equation has to be solved. However, it is not possible to solve this equation exactly for many-electron systems. In solid state chemistry, the number of electrons involved in the reactions is usually large and effective approaches are required. DFT focuses on the electronic density and therefore it is a faster way to solve the multielectronic problem and to obtain the ground-state energy.

In this Chapter, I shall give a short review of this theory. For those readers who want a deeper understanding of DFT concepts should refer to textbooks on quantum mechanics such as [90]. The chapter starts with a brief discussion about the Schrödinger equation and the Born-Oppenheimer approximation. Afterward, Hohenberg and Kohn theorems and Kohn-Sham equations are shortly reviewed, together with: pseudopotentials and basis sets. Finally, I will define the thermodynamical magnitudes that are used in this thesis, and then explain the method to calculate activation barriers.

4.1 Concepts of quantum chemistry

4.1.1 Many-electron Schrödinger equation

In chemistry, we are just interested in the electrostatic interactions. Usually relativistic effects are negligible if only the valence electrons are considered. If the magnetic effect is also ignored, a system of L nuclei and N electrons is described by the non-relativistic Schrödinger equation with a Hamiltonian of a well-defined form:

$$H = T_{nucl} + T_{el} + V_{nucl-nucl} + V_{nucl-el} + V_{el-el} \tag{4.1}$$

where the operators T_{nucl} and T_{el} describe the kinetic energies of the nuclei and the electrons, respectively. The other terms describe the electrostatic interaction between electrons and nuclei. The terms of the equation are expressed as follows:

$$T_{nucl} = \sum_{I=1}^{L} \frac{\boldsymbol{P}_I^2}{2M_I} \tag{4.2}$$

$$T_{el} = \sum_{i=1}^{N} \frac{\boldsymbol{p}_i^2}{2m} \tag{4.3}$$

$$V_{nucl-nucl} = \frac{1}{2} \sum_{I \neq J} \frac{Z_I Z_J e^2}{\mid \boldsymbol{R}_I - \boldsymbol{R}_J \mid} \tag{4.4}$$

$$V_{nucl-el} = -\sum_{i,I} \frac{Z_I e^2}{\mid \boldsymbol{r}_i - \boldsymbol{R}_I \mid} \tag{4.5}$$

$$V_{el-el} = \frac{1}{2} \sum_{i \neq j} \frac{e^2}{\mid \boldsymbol{r}_i - \boldsymbol{r}_j \mid} \tag{4.6}$$

In the equations above the capital and lower letters in the indexes refer to nuclei and electrons, respectively. M and m are the masses, $\boldsymbol{p}$ and $\boldsymbol{P}$ are the momenta, Z is the atomic

number, $\boldsymbol{r}$ and $\boldsymbol{R}$ are the position vectors, and $e = 1$ in atomic units.

4.1.2 Born-Oppenheimer Approximation

The main idea in the Born-Oppenheimer Approximation is the separation in the time scale of the processes involving electrons and atoms due to the large difference of their masses. The velocity of the electrons is 100 or 1000 times faster than that of the nuclei. Therefore the electrons follow the motion of nuclei almost instantaneously. As a consequence, in practical applications, we can suppose that electrons are moving in the field of fixed nuclei. Under this assumption, nuclear kinetic energy is zero and the potential energy due to the nuclear-nuclear repulsion is a constant value. Then, the electronic Hamiltonian can be written as:

$$\mathrm{H_{el}} = \mathrm{T_{el}} + \mathrm{V_{nucl-el}} + \mathrm{V_{el-el}} \tag{4.7}$$

The electronic wave-function is the solution to the above equation for stationary nuclei. The total energy E_{total} of a system at a given nuclear configuration is the sum of the electronic energy E_{elec} and the constant nuclear repulsion term:

$$\mathrm{E}_{total} = \mathrm{E}_{elec} + \mathrm{E}_{nucl-nucl} \tag{4.8}$$

4.1.3 Density Functional Theory

In Density Functional Theory, the explicit wave-function of the many-body equation is not required and just the ground-state density $n_{\boldsymbol{r}}$ is calculated. This section starts with a brief description of the Hohenberg and Kohn [91] theorems followed by the Kohn-Sham (KS) equations.

Hohenberg and Kohn theorems

All the essential information about a system is contained in the electronic density $n(\boldsymbol{r})$. It determines the Hamiltonian H_{el}, the ground-state wave-function Ψ_0, and the ground-state energy E_0. The energy E_0 can be written as a functional of $n(\boldsymbol{r})$:

$$E_0 = \langle\Psi_0|T_{el} + V_{el-el}|\Psi_0|\rangle + \langle\Psi_0|V_{ext}|\Psi_0\rangle = F(n(\boldsymbol{r})) + \int V_{ext}(\boldsymbol{r})n(\boldsymbol{r})d^3\boldsymbol{r} \tag{4.9}$$

where F is the functional that gives the kinetic and interaction energy. The two theorems of Hohenberg and Kohn are based on these properties and they state that:

Theorem 1 The ground-state density $n(\boldsymbol{r})$ of a system of interacting electrons in a external potential is uniquely determined by its potential and vice-versa. [92]

Theorem 2 The ground-state energy can be obtained variationally and the density that minimises the total energy is the exact ground-state density.

Therefore, when Eq. 4.9 is optimized, the ground-state can be found. However, the functional F is not explicitly known. If F is replaced by the functional for a non-interacting system and a homogeneous electron gas, the Thomas-Fermi Theory is obtained [90].

Kohn-Sham equations

In 1965 Kohn and Sham extended the original "orbital-free" DFT approach to derive an effective single-particle Hamiltonian of non-interacting electrons [93]. Using the KS equations, the system is described as non-interacting particles in a fictitious effective potential $\tilde{V}_e$ with Hamiltonian:

$$\tilde{H} = -\frac{\hbar^2}{2m_e}\bigtriangledown^2 + \tilde{V}_e(\boldsymbol{r}) \tag{4.10}$$

which leads to the same ground-state charge density $n(\boldsymbol{r})$ as the interacting system. In this case, the density is derived from a set of occupied single-particle orbitals ($n(\boldsymbol{r}) =$

$\sum_{i=1}^{N} |\phi_i(\boldsymbol{r})|^2$).

In order to obtain the KS equations, the functional $F[n(\boldsymbol{r})]$ from eq. 4.9 has to be written as:

$$F[n(\boldsymbol{r})] = T_s[n(\boldsymbol{r})] + \frac{1}{2}\int V_h(\boldsymbol{r})n(\boldsymbol{r})d^3\boldsymbol{r} + E_{xc}[n(\boldsymbol{r})] \tag{4.11}$$

where T_s is the kinetic energy functional of a non-interacting system with the same ground-state density as the interacting system and the second term is the functional of the classical electrostatic energy, that corresponds to the Hartree energy. $E_{xc}[n(\boldsymbol{r})]$ is called the exchange-correlation functional and it incorporates all quantum mechanical many-body effects.

Equation 4.9 can be solved variationally using a set of orthonormal single-particle orbitals ϕ_i. The result is a set of coupled single-particle equations with the form:

$$(-\frac{\hbar^2}{2m}\bigtriangledown^2 + V_{ext}(\boldsymbol{r}) + V_H(\boldsymbol{r}) + V_{xc}(\boldsymbol{r}))\phi_i(\boldsymbol{r}) = \epsilon_i\phi_i(\boldsymbol{r}) \tag{4.12}$$

The equations above are the canonical KS equations. The effective potential $\tilde{V}_e$ is given by:

$$\tilde{V}_e = V_{ext}(\boldsymbol{r}) + V_H(\boldsymbol{r}) + V_{xc}(\boldsymbol{r}) \tag{4.13}$$

where $V_{xc}(\boldsymbol{r})$ is the exchange-correlation potential and can be written as:

$$V_{xc}(\boldsymbol{r}) = \frac{\delta E_{xc}[n]}{\delta\tilde{n}(\boldsymbol{r})}|_{\tilde{n}(\boldsymbol{r})=n(\boldsymbol{r})} \tag{4.14}$$

Finally, the ground-state energy can be expressed as:

$$E_0 = \sum_{i=1}^{N}\epsilon_i + E_{xc}[n] - \int V_{ex}(\boldsymbol{r})n(\boldsymbol{r})d^3(\boldsymbol{r}) - V_H + V_{nucl-nucl} \tag{4.15}$$

Exchange correlation functional

The exchange-correlation functional makes the KS-DFT approach different from Hartree-Fock equations. The reliability of DFT implementation depends on the accuracy of the expression of this functional. Since V_{xc} is unknown, several approximations have been developed. The most important ones are Local Density Approximation (LDA) and Generalized Gradient Approximation (GGA).

LDA approximation assumes an exchange-correlation energy ϵ_{xc} per particle based on homogeneous electron gas of density $n(\boldsymbol{r})$ which is defined as:

$$E_{xc}^{LDA} = \int \epsilon_{xc}^{LDA}(n(\boldsymbol{r}))n(\boldsymbol{r})d^3(\boldsymbol{r}) \tag{4.16}$$

The Eq 4.16 provides a relation between the effective potential and the electron density at each point in space. Nonetheless, this equation is strictly valid for constant external potential and it works better in systems with slowly variable densities.

Non-local interactions are included in V_{xc}. Improvements can be made including the gradient of the local density $n(\boldsymbol{r})$ in ϵ_{xc}, but with a higher computational cost. The most common semi-local functionals are summarized under the term of GGA. A very popular choice is the parametrization of Perdew, Burke, and Erzenhof (PBE) [94]:

$$\epsilon_{xc}^{GGA}(n(\boldsymbol{r}), \bigtriangledown n(\boldsymbol{r})) = \epsilon_{xc}^{LDA} \times F_{xc}(n, s) \tag{4.17}$$

$$s = \frac{|\bigtriangledown n(\boldsymbol{r})|}{2nkr}; k_f = (3\pi^2 n)^{\frac{1}{3}} \tag{4.18}$$

where $F_{xc}(n, s)$ is the GGA enhancement factor that depends on the dimensionless gradient s. The extension to spin-polarized systems is straightforward. The calculations in this thesis rely on this functional.

4.1.4 Pseudopotentials

Core electrons screen nuclear charge but they do not largely contribute to chemical bonds. Besides, core states in solids are practically identical to core states in an isolated atom. Reducing the number of mathematical operations on DFT by using only valence electrons eliminates many degrees of freedom and accelerates the process of solving the many-body problem. That is the main idea of the pseudopotential approximation, to express the true wave-function as a combination of smooth pseudo-wave functions and a set of localized core orbitals [90] [95]. In this manner the valence states $|\phi_v\rangle$ are described by the pseudo-wave functions $|\tilde{\phi_v}\rangle$ and all-core states $|\phi_c\rangle$:

$$|\phi_v\rangle = |\tilde{\phi_v}\rangle - \sum_c |\phi_c\rangle\langle\phi_c|\tilde{\phi_v}\rangle = [1 - \sum_c |\phi_c\rangle\langle\phi_c|]\,|\tilde{\phi_v}\rangle \tag{4.19}$$

Replacing the pseudo-functions $|\tilde{\phi_v}\rangle$ on eq. 4.12, the single KS equations yield an equivalent set of equations for the pseudo-wave-function. These pseudo-wave functions have the same one-particle energies but they do not have nodes because of the presence of the non-orthogonal core states.

The general construction scheme of eq 4.19 can be extended by choosing wave-functions with desired properties. For example, norm-conservative pseudopotentials are constructed requiring that: (1) the radial pseudo-wave function $\tilde{\phi_v}$ is smoother than the true valence wave-function ϕ_v, inside of a cutoff radius r_c, and (2) both functions $\tilde{\phi_v}$ and ϕ_v have the same the integrated charge and the same logarithmic radial derivative (at r_c).

Beside all these requirements, there are still many degrees of freedom for different choices of pseudo-wave functions and pseudopotentials, e.g. accuracy, softness, smaller cutoff radius, etc.

The Projector Argument Wave (PAW) is beyond the Pseudopotential (PP) approach and it uses a similar scheme of projection to that of Eq. 4.19 in order to define a linear transformation of a smooth pseudo-wave function into real wave-function. Basically, there is

a separation of the true wave-function into a smooth extended part and a localized part [95].

4.1.5 Basis set

Unlike in organic chemistry, the study of reactions occurring on metal surfaces requires the use of periodic boundary conditions (PBC). For many years a lot of effort has been made to develop reliable software that implements periodic DFT and allows to study systems with periodicity in one, two, and three dimensions. Functions adapted to the crystal symmetry and following the Bloch theorem are the base of these computational programs. Because of the extended and delocalized nature of the crystalline orbitals in metal surfaces, better results have been obtained using a different type of functions to construct them. In the following, three different implementations of the one-electron wave-functions are described.

Plane-waves (PW)

The plane-waves form a universal basis set that does not depend on the nature of the atoms. Although the mathematical operations become easy and simple to solve, the number of plane-waves necessary to describe correctly the wave-functions are huge. A few approximations can be done in order to reduce its number. One of the most important ones is to replace the core electrons by pseudopotentials.

One of the disadvantages of the PWs is that they are expanded to the whole unit cell and therefore it is necessary a large vacuum region avoid interactions between slabs. Nevertheless, there are many advantages, e.g. there is no basis set superposition error (BSSE) in this type of calculations.

Atom-centered basis functions

In this case, contracted orbitals centered on nuclei represent the valence electrons. The main advantage of this method is the reduced computational cost in comparison with the traditional PW approach. The disadvantages are the non-orthogonality of the basis set, which

results in BSSE, and the mathematical problems associated with diffuse functions, especially for systems with small unit cells. Siesta software [96] uses this approach.

Real-space uniform grids

In this method, the domain of the system is discretized using a uniform grid. The method also uses a set of discrete numerical approximations. Most of the calculations in this thesis were performed with GPAW [97], [98], a code that uses this type of basis set. The main advantage is that it reduces the computational cost, especially in large systems with a magnetic moment like nickel.

4.2 Methodology of the thesis

Throughout this thesis, I will use certain thermodynamical and kinetic magnitudes in order to study the properties of the systems. In this section, definitions are shown and I will establish how they are connected to the whole mechanism of the hydrogen oxidation reaction.

4.2.1 Adsorption energy

The adsorption energy E_{ads} of an adsorbate (H, O or OH) on a surface can be defined as:

$$E_{ads} = E_{total} - E_{surface} - E_{adsorbate} \tag{4.20}$$

where E_{total} is the energy of adsorbate on the surface, E_{surf} is the energy of the clean surface, and $E_{adsorbate}$ is the energy of the optimized adsorbate in a gas phase (H_2 molecule, O atom, or OH radical, respectively).

Such energy takes into account the thermodynamical stability of the surface modified by the adsorbate and it is straightforward to notice that lower and more negative values indicate a stronger interaction between the surface and the adsorbate. Besides this interpretation, there are other ways in which the adsorption energy has helped to understand and predict

the thermodynamical and kinetic properties of an electrode. As I mentioned in the previous section 2.2.2, Volcano plots have been used effectively to relate adsorption energies (obtained by simulations) to experimental kinetic parameters (exchange current). In most cases, Volcano plots are giving good results because Sabatier's principle can be applied to the reaction mechanism. In practical terms, this means that the optimal speed of a reaction is reached when the concentration of the intermediates is neither too low nor too high. In HOR/HER this can be translated as that H and OH should be adsorbed on the surface but not too strongly.

Another way to use the adsorption energy to predict kinetic properties is through the Brnsted-Evans-Polanyi principle. It establishes a linear relationship between the activation barrier E_{act} and the enthalpy ΔH of reactions of the same family. It can be expressed as:

$$E_{act} = E_0 + \alpha \, \Delta H \tag{4.21}$$

where E_0 is the activation barrier when ΔH is equal to zero. By means of this principle, the adsorption energies can be used qualitatively to predict the kinetic properties of new materials. However, researchers must be careful with its use because it is just an empirical principle without any demonstration.

In this thesis, I will use a different perspective. Adsorption energies will be used within the ab initio thermodynamics approach, that will allow me to compare the stability of the adsorbates on the surface in a potential scale.

The Gibbs energy ΔG of adsorption is related to the adsorption energy E_{ads} by the equation:

$$\Delta G = E_{ads} + \Delta E_{ZPE} - T\Delta S \tag{4.22}$$

where ΔE_{ZPE} and ΔS are the differences in zero-point-energy (ZPE) and entropy between the adsorbed and the gas phase. Because I am studying the HOR, the two species that I will

consider are H and OH. The reactions involved in their adsorption are different and then they can be consider separately.

The adsorption of hydrogen on the metal surfaces in an electrochemical environment is described by the electrochemical reaction:

$$H^+_{aq} + e^- + \text{surface sites} \longrightarrow H_{ads} \qquad \Delta G_1 \tag{4.23}$$

Unfortunately, periodic DFT calculations are very difficult to perform for charged systems, like H^+. Nevertheless, if we consider that the H^+ and H_2 are in equilibrium through the redox reaction:

$$H^+_{aq} + e^- \Longleftrightarrow {}^1/_2\, H_2 \qquad \Delta G_2 \tag{4.24}$$

then its energy ΔG_2 is equal to zero. We can now combine both reactions using a thermodynamical cycle in order to write the adsorption as:

$${}^1/_2\, H_2 + \text{surface sites} \longrightarrow H_{ads} \qquad \Delta G_3 \tag{4.25}$$

And the relationship among the three energies are:

$$\Delta G_3 = \Delta G_1 - \Delta G_2 = \Delta G_1 \tag{4.26}$$

In this manner it is possible to use reaction 4.25 instead of 4.23 and obtain the same energy (under the equilibrium condition previously mentioned). The main advantage of reaction 4.25 is that both products and reactants can be calculated using periodic DFT calculations. Finally, it is important to emphasize that the Gibbs energies are directly related to the potential of the reaction by the Nernst equation.

Let us consider now the vibrational and entropic terms on eq. 4.22. As I did with the adsorption energy (eq. 4.20), the change of the ZPE and entropy can be written as:

$$\Delta E_{ZPE} = E_{ZPE}^{total} - E_{ZPE}^{surface} - E_{ZPE}^{adsorbate} \tag{4.27}$$

and

$$\Delta S = S_{total} - S_{surface} - S_{adsorbate} \tag{4.28}$$

Some assumptions can be done. The first one is that the entropy of the adsorbate state and the surface are small ($S_{total}, S_{surface} \approx 0$). Therefore, the change of entropy of reaction 4.25 is: $\Delta S = \frac{1}{2} S_{\mathrm{H_2}}$, where $S_{\mathrm{H_2}}$ is the entropy of $\mathrm{H_2}$ in gas phase at standard conditions. The ΔE_{ZPE} for a surface of Cu(111) was calculated by Nørskov and it is very small (0.04 eV). It is expected to obtain similar values on the Ni/Cu surfaces and due to the fact that the calculations of vibrational frequencies are very time demanding and consuming, I neglected ΔE_{ZPE} in the calculation of $\Delta G(\mathrm{H})$. Taken into account all these approximations, the Gibbs energy of adsorption of H is:

$$\Delta G(\mathrm{H}) = E_{ads}(\mathrm{H}) + 0.2 \tag{4.29}$$

Calculating the Gibbs energy of adsorption of OH is not as simple as for the case of H. The adsorption reaction in this case is:

$$\mathrm{OH}_{aq}^{-} + \text{surface sites} \longrightarrow \mathrm{OH}_{ads} + e^{-} \qquad\qquad \Delta G(\mathrm{OH}) \tag{4.30}$$

The main difficulty is that after the adsorption, OH is not completely discharged on the surface. Therefore, the solvation sphere is not completely lost, and the changes on the solvation energy are difficult to estimate. Nevertheless, it can be assumed that the loss in solvation energy will be the same for all the fcc metal surfaces with the same orientation.Therefore I take Pt(111) as our reference surface. With this assumption, the Gibbs adsorption energies from the values of the adsorption on the Pt(111) surface, in eV, are:

$$\begin{aligned} \Delta G(\mathrm{OH}) - E_{ads}(\mathrm{OH}) &= \Delta G^{\mathrm{Pt(111)}}(\mathrm{OH}) - E_{ads}^{\mathrm{Pt(111)}}(\mathrm{OH}) \\ \Delta G(\mathrm{OH}) &= \Delta G^{\mathrm{Pt(111)}(OH)} - E_{ads}^{\mathrm{Pt(111)}(OH)} + E_{ads}(\mathrm{OH}) \\ \Delta \mathrm{G(OH)} &= 0.65\, eV - (-2.3\, eV) + E_{ads}(\mathrm{OH}) \end{aligned} \tag{4.31}$$

The Gibbs adsorption energies ΔG for Pt(111) were obtained from the experimental electrochemical potentials (from cyclic voltammetry) by using the Nernst equation, and the adsorption energy from DFT calculations [99].

4.2.2 Activation energy

The calculation of the activation energy of a reaction requires to have the true reaction path in order to find the transition state. However in some cases, when there are many degrees of freedom or the configurational space is large, it is not easy to find unequivocally the true minimal energy path (MEP). In this thesis, I confronted that situation. On one hand the number of possible sites and combinations was challenging and on the other hand, every calculation was time-consuming. In the spirit of finding a solution, I used the following method to obtain the activation barriers. It consists of creating potential energy surfaces (PES) using all possible positions of OH and H on a particular surface. The details will be explained next.

First, calculations of the adsorption energies of co-adsorbed H and OH radicals were made. To reduce the size of the problem, the following considerations were made:

- the oxygen atom of OH radical was kept fixed on x and y axis. The H was free to move;
- a hydrogen atom was placed on different positions: top, bridge, and fcc sites, at different lateral distances to OH radical. At each H position, the perpendicular separation (z axis)

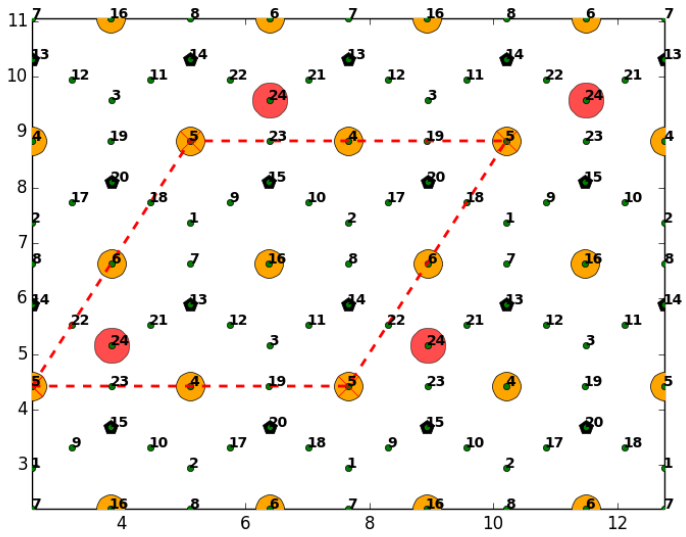

Figure 4.1: Possible adsorption sites for H on Cu(111) with OH adsorbed on fcc site. All the 24 studied sites are labeled. Orange and red circles correspond to Cu atoms and OH radical, respectively. The dashed red lines show the unit cell.

between the H atom and the metal surface was optimized.

Both strings were applied on the same calculation. In this manner for each OH position, different H sites were selected considering symmetry. An example of the procedure is shown in Fig. 4.1 for the case of OH on fcc site of Cu(111) surface. The red circles are OH radicals in fcc position, and the green small circles are H in different positions. The copper atoms of the first layer are the orange circles and the red lines indicate the unit cell. Each system was calculated using the same surface with one OH radical in the same position (red circle) but only one H in one position (indexes labeled from 1 to 24) at a time. The energy for each system was calculated and collected to create a potential energy map by interpolating the values in between (Fig. 4.2).

The energy scale of Fig. 4.2 was created using as zero energy the lowest value of the PES. As it can be observed, the lowest energies (blue regions) correspond to stable minima whereas the regions in red are unstable positions. In this case, a minimum is established near the OH radical and it is because of water formation. The other blue regions are stable positions for

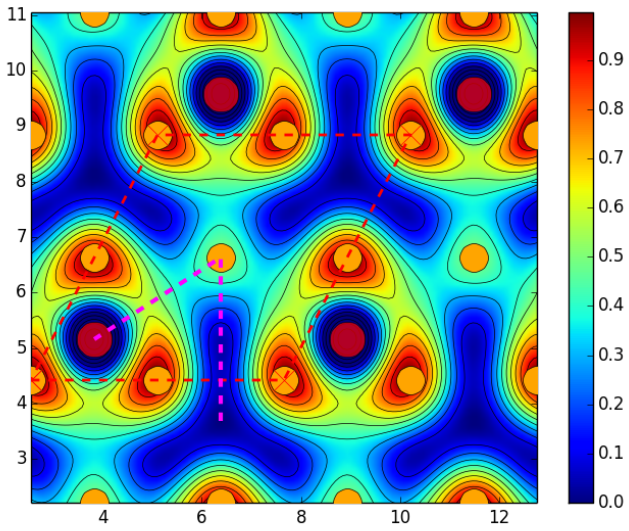

Figure 4.2: PES for Cu(111) with OH on fcc site. The trajectory that corresponds to minimal path is shown with magenta dashed lines. Energy values are in eV. The lowest energy was taken as zero value of the scale.

H adsorption on fcc and hcp sites, far from OH radical.

Knowing the whole PES it is easier and clearer to find out which path is the one with the lowest activation energy. In Fig. 4.2 the MEP has been marked (magenta dashed lines) and it was used to calculate the activation barrier. Extracting the data from this map I obtained the reaction path shown in Fig. 4.3. In this particular example, the reaction starts with OH and H adsorb on fcc positions. Then the H atom diffuses on the surface following the path: hcp–fcc–top–bridge–fcc(OH). The transition state is near to the bridge position and the reaction has an activation barrier of 0.58 eV.

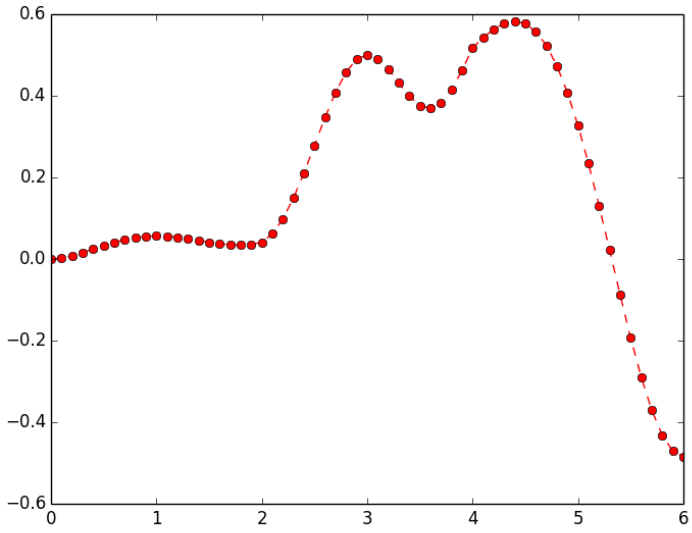

Figure 4.3: Reaction coordinate for OH and H recombination. The initial energy was taken as zero value of the scale. Energy values are in eV.

Chapter 5

Water formation on Cu(111) and Ni(111) surfaces

The first step of HER and many other chemical processes involves the adsorption of species on the surface. In this study, the adsorption energy of H and OH are particularly interesting because they are involved in Volmer reaction and water formation as demonstrated in Chapter 2. The calculations in this chapter were used for checking the model since the E_{ads} for H and OH on pure nickel and copper (111) surfaces are available in the literature, but not for mixed systems NiM (M means any other metal except Ni). Besides these adsorbates, O adsorption was also analyzed. After that, the PES method described in the previous chapter was applied for the pure (111) surfaces with OH in three different positions.

This chapter is organized as follows: in the first section, the adsorption of H, O, and OH are introduced then, the results of PES are shown, a discussion of adsorption, activation, total energies, and PES are presented with a short conclusion in the end.

5.1 Adsorption of H, O, and OH

The adsorption of H, O, and OH radicals was studied in three different positions: fcc, bridge, and on top sites. The details of the computational setup are given in Appendix A. The cor-

Table 5.1: Adsorption energies at nickel and copper (111) surfaces for H, O, and OH radicals. All the energies are in eV.

Metal surfaces	Site	H	O	OH
Ni(111)	bridge	-0.35	-3.42	-2.97
	fcc	-0.49	-5.25	-3.23
	top	-0.39	-3.44	-2.64
Cu(111)	bridge	0.02	-3.92	-2.73
	fcc	-0.19	-4.08	-2.88
	top	-0.08	-0.40	-2.10

responding adsorption energies are shown in Table 5.1. The values were calculated according to Section 4.2.1.

Hydrogen adsorption is stronger on fcc than on bridge sites. However, the energy difference between the three sites is within DFT error (0.1 eV). The reported values on the Ni(111) surfaces are in agreement with previous publications: Mohsenzadeh [100] and Ferrin [101] found that the most stable site is fcc, with energies between -0.4 and -0.6 eV. In the case of Cu(111) surface, the adsorption energies are more positive than on Ni(111). The value reported by Ferrin et al. [101] is -0.18 eV on fcc position, which is comparable to my result. The adsorption energies in fcc sites are not so strong. However when hydrogen is adsorbed on a fcc site, the bridge and top sites are blocked. A different behaviour is observed on Pt(111) [102]. The hydrogen on fcc site is known as upd-hydrogen because its strong adsorption while on bridge and top opd-hydrogen. Observing the table 5.1, opd-hydrogen does not occurs on Cu(111) and Nii(111) due to their compact valence orbital comparing with Pt(111).

The fcc position is also preferable to others in the case of the oxygenated species. In contrast to the H adsorption, there is a clear preference to adsorb on fcc rather than on top sites. The values reported in the literature for O on nickel are between -5.3 and -5.8 eV [103], [100], [104] on fcc sites, and -3.95 eV [104] on top position, which are consistent with my data. In the case of OH adsorption, the energy presented in this chapter is similar to the values reported for Ni -3.41 [100] and -3.50 [104] eV on Ni(111, and -2.41 eV [105] on Cu(111). The most strongly adsorbed species is O due to the tendency of these metals to oxidize.

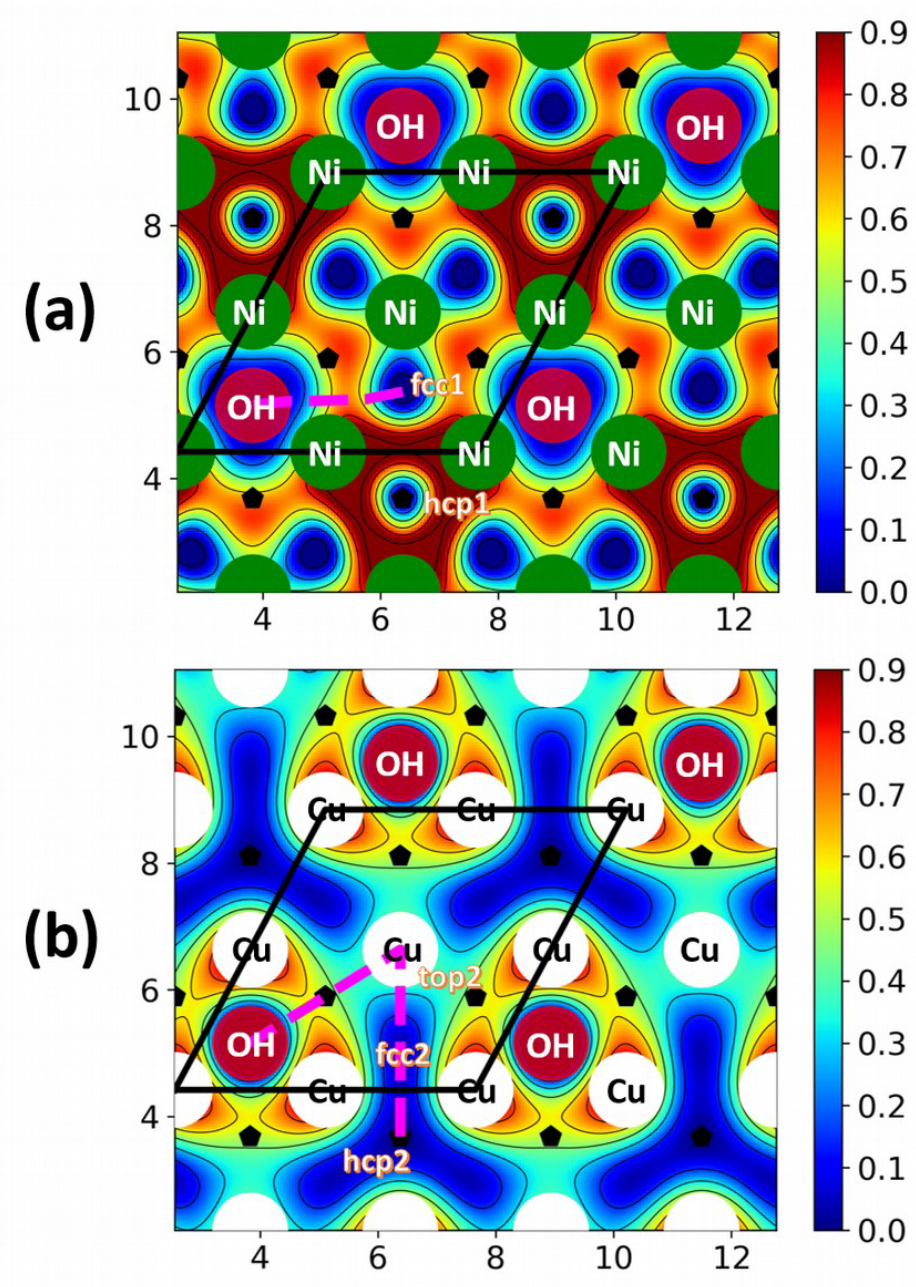

Figure 5.1: PES for co-adsorption of H and OH on: (a) Ni(111), and (b) Cu(111) surfaces. Green, white, and red spheres correspond to nickel, and copper atoms and to OH radical, respectively. The black continuous line shows the unit cell and the magenta dashed line shows the MEP that was used to calculate the activation barrier. Energy scale on the right side is in eV.

5.2 Water formation on Cu(111) and Ni(111) surfaces

In this section, I will present activation energies for water formation on pure nickel and copper surfaces. As mentioned in the previous section, the fcc is the most stable site for the studied adsorbates. Therefore, the PES presented hereafter will only consider OH on fcc positions.

Figure 5.1 shows the PES for the adsorption of H and the formation of water on nickel and copper (111) surfaces. The position of adsorbed OH has been indicated using red spheres, whereas the green and white ones correspond to nickel and copper atoms of the top layer, respectively. Both maps are clearly different and I will start with the description of the one corresponding to Ni(111). Inside of the unit cell local minima, blue regions, are clearly visible. One of them corresponds to the water formation and it is located around OH. The remaining minima correspond to fcc and hcp sites (labeled as fcc1 and hcp1, respectively). It can be noticed that there is a big energy barrier between both sites. The formation of water happens to start from the fcc1 site, with an activation energy of 0.84 eV (see Table 5.2). The reaction is slightly endothermic (ΔE =0.17 eV), being the separated reactants on the fcc positions (H on fcc1 site) more stable than water.

The map for the water formation on Cu(111) has more regions of lower energy (blue areas). As in the case of nickel surface, there are local minima near OH radical (water formation), and on fcc and hcp sites. Nevertheless, the barrier between both of them is negligible. In this case, the reaction path is more complicated and it goes through a top site. The transition state is in a bridge position and the activation barrier is 0.58 eV (see Table 5.2). In contrast to nickel, the reaction is exothermic: ΔE =-0.48 eV. It should be emphasized that even when the final state of this reaction has more negative energy than the reactants, this does not mean that the water is more strongly adsorbed on the Cu surface. The water molecule is physisorbed on the surface and it is more stable than H and OH adsorbed on the surface, due to the weakness of these interactions.

The minimal energy reaction paths have been collected in Figure 5.2. The intermediate and transition states can be easily noticed, and therefore the differences between both sur-

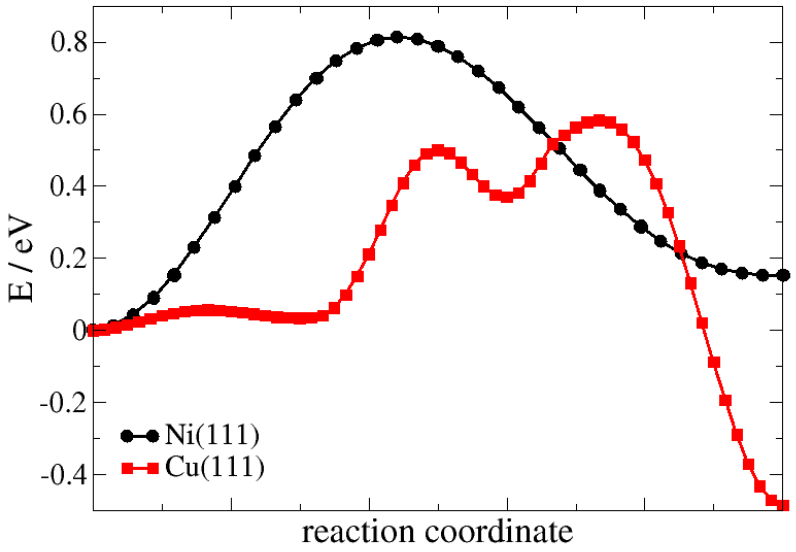

Figure 5.2: MEP for the formation of water on Ni (black curve) and Cu (red curve) (111) surfaces. The path were obtained using the PES shown in Fig. 5.1. All the energies are in eV.

faces. In both cases, the energy of the initial states has been taken as zero. The transition states (TS) are shown in Figure 5.3. On copper, the H atom is on hcp position whereas on nickel the same atom is on bridge site. In the last case, the H atom and OH group are farther than on copper surface. Therefore, the activation barrier is higher on nickel.

The values reported in literature for activation energy are for water dissociation and not for formation. In this scenario, my energy is 1.06 eV for Cu(111), which is comparable with values reported by Fajin et al. 1.16 [106] and 1.19 eV [60]. For Ni, Mohsenzadeh et al. reported 0.69 eV [100] and 0.67 eV [103] those values are comparable with mine, 0.64 eV.

5.3 Conclusions

The adsorption of H, O, and OH, and the formation of water on Cu(111) and Ni(111) has been studied in this chapter. The results are in good agreement with previous theoretical works and they showed that my computational setup is appropriated for this study.I have also confirmed that fcc is the preferable adsorption site for the OH radical; this information is

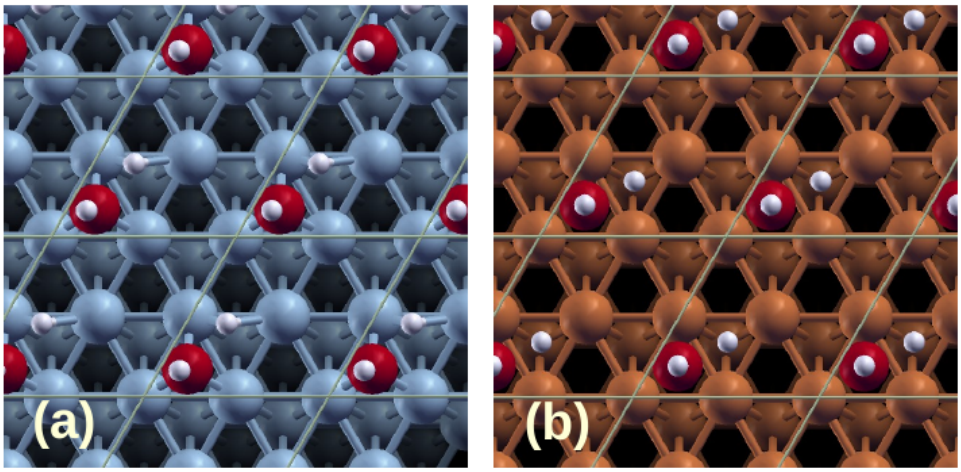

Figure 5.3: Top view of the transition states corresponding to the reaction paths of Fig. 5.2. Dark blue, brown, red, and white spheres represent Ni, Cu, O, and H atoms.

very relevant for preparing the PES and there is no presence of opd-hydrogen on pure nickel and copper (111) surfaces.

So what do these results tell us about water formation on these two surfaces? In order to answer these questions, I have converted the energies of adsorption of H and OH to the RHE scale by recalculating into ΔG (see Table 5.2). On Ni(111) both Gibbs energies of adsorption are negative; therefore, there is a substantial potential range in which both H and OH are simultaneously present on the surface. However, the energy of activation (0.81 eV) is too high for this reaction to take place. Instead, hydrogen evolution takes place via the Heyrovsky pathway [7].

In contrast, on copper the Gibbs energies of adsorption are zero within DFT error. So at 0 V RHE both species can be present, but as soon as an overpotential is applied hydrogen

Table 5.2: Gibbs energy of adsorption ΔG of H and OH, activation barrier E_{act}, and reaction energy ΔE of water formation on nickel and copper (111) surfaces. All the energies are in eV.

Surfaces	$\Delta G(H)$	$\Delta G(OH)$	E_{act}	ΔE
Cu(111)	0.01	0.07	0.58	-0.48
Ni(111)	-0.29	-0.34	0.81	0.17

will leave the surface, while the coverage of OH increases. The energy of activation (0.58 eV) is lower than on nickel. It is difficult to come to a definite conclusion. Perhaps the water formation pathway can contribute in a narrow potential range near 0 V RHE.

So nickel adsorbs both species too strongly, while copper adsorbs too weakly. Therefore, bimetallic surfaces composed of copper and nickel are promising candidates for the water formation pathway.

Chapter 6

Water formation on NiCu surfaces

Many metals could be combined with nickel to improve the hydrogen evolution reaction. Indeed, in Chapter 7. I will examine a manifold of such combinations. In this chapter, I focus on bimetallic surfaces of nickel and copper. We have seen in the last chapter, that the adsorption properties of these two metal complement each other well. In addition, copper is relatively cheap, and in alkaline media, it is more stable against corrosion than the nickel. Also, their lattice constants are quite similar.

Bimetallic NiCu materials have been studied before from a theoretical point of view. Santos et al. observed that a mesomorphic monolayer of Cu on Ni(111) adsorb hydrogen stronger than pure Cu(111), and this is attributed to the chemical effect of the Ni substrate [86]. Gao *et al.* prepared a nanoporous NiCu alloy by potentiostatic electrodeposition, and this surface exhibited high catalytic activity for HER due to the synergetic effect of Ni and Cu [107].

In this chapter, I study bimetallic Ni/Cu layers on top of bulk Ni(111). The adsorption energies of H and OH will be analyzed first, followed by the PES and activation barriers for the water formation. Indeed, I shall demonstrate that several combinations promise to be excellent catalysts for water formation within the hydrogen evolution reaction. So this is the most important chapter of my thesis!

6.1 Representation of NiCu surfaces

As I have already stated, the computational setup of the calculations performed throughout this thesis is described in section A.1. I will not repeat any details here, however, for the sake of clarity, I will explain the structure of the slabs that I used to simulate different contents of copper on Ni(111).

All the surfaces have four metal layers and a (2 x 2) unit cell. Different percentages of Cu content in the top layer were simulated by replacing different numbers of Ni atoms by Cu. In this manner, the 3 bottom layers were formed only by Ni and the topmost layer was prepared as follows:

- 25% Cu on Ni(111): 3 Ni atoms + 1 Cu atom,
- 50% Cu on Ni(111): 2 Ni atoms + 2 Cu atoms,
- 75% Cu on Ni(111): 1 Ni atom + 3 Cu atoms,
- 100% Cu or 1ML of Cu on Ni(111): only Cu atoms

Another system was also considered, a surface with one topmost layer of Ni, the second layer of Cu on top of Ni(111) (see Fig. 6.1 (e)). This system is thermodynamically unstable because the surface energy of nickel is much higher than that of copper [108]. I have studied this system in order to investigate if the underlying copper has a chemical effect on the nickel surface.

6.2 H and OH adsorption energies

In order to gain an overview of the adsorptive properties, I first calculated adsorption energies for H and OH on fcc sites for various surface compositions. The results have been collected in Table 6.1.

Both hydrogen and OH adsorption energies tend to be close either to those on Ni(111) or on Cu(111). If there is more nickel on the surface, the value is closer to Ni(111), and vice

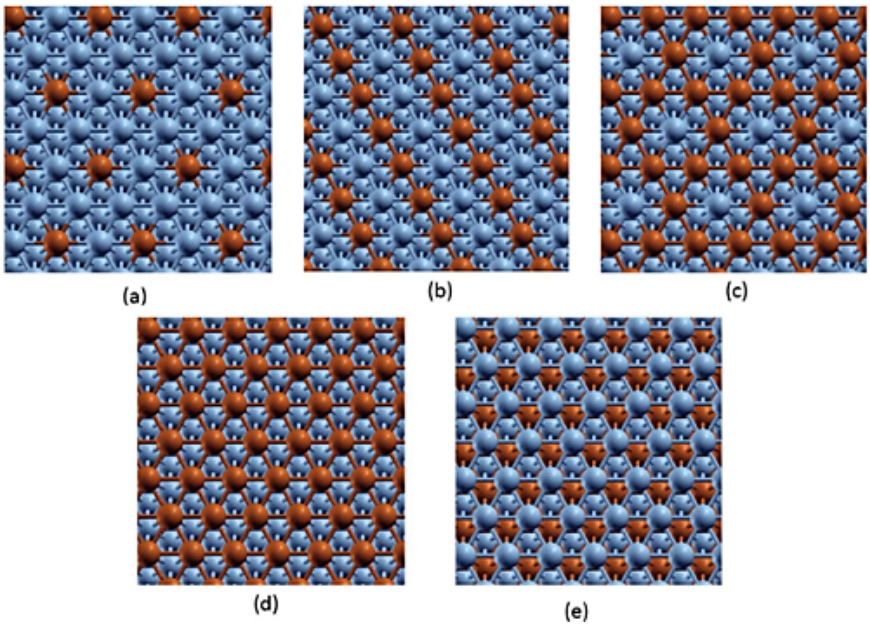

Figure 6.1: Top views of the slabs used to represent mixed CuNi(111) surfaces. Composition of top layer: (a) 25% Cu, (b) 50% Cu, (c) 75% Cu, (d) 100% Cu. System (e) has a a complete topmost layer of Ni and a second layer of Cu on top of Ni(111). Dark blue and brown spheres represent Ni and Cu atoms, respectively.

versa for Cu(111). OH, adsorption is stronger on surfaces with more Ni in the first layer. This seems to indicate that, as far as water formation is concerned, these bimetallic surfaces are not very much better than pure Ni(111) and Cu(111). However, I shall show below, that the energies of activation are substantially reduced.

6.3 Water formation on NiCu surfaces

In this section, I present the potential energy surfaces for water formation, examine likely reaction paths, and corresponding energies of activation. I shall present the results separately for each composition, and at the end arrive at some general conclusions.

6.3.1 25 % Cu on Ni(111)

On this surface OH can adsorb on two different positions: one in between 2 Ni and 1 Cu (Fig. 6.2 (a)), and another surrounded by 3 neighboring Ni atoms (Fig. 6.2 (b)). I will start by

Table 6.1: Adsorption of H or OH on the mixed Cu/Ni(111) systems. All the energies are in eV.

Surface	$E_{ads}(H)$	$E_{ads}(OH)$	$\Delta G(H)$	$\Delta G(OH)$
Ni (111)	-0.49	-3.29	-0.29	-0.34
100% Ni on Cu/Ni(111)	-0.63	-3.39	-0.43	-0.44
25% Cu on Ni (111)	-0.57 (3Ni) -0.24 (1Cu)	-3.31 (3Ni) -3.18 (1Cu)	-0.37 -0.04	-0.36 -0.23
50% Cu on Ni (111)	-0.26 (2Cu)	-2.99 (2Cu)	-0.06	-0.04
75% Cu on Ni (111)	-0.21 (1Ni) -0.09 (3Cu)	-2.82 (1Ni) -2.86 (3Cu)	-0.01 0.11	0.13 0.09
100% Cu on Ni (111)	-0.18	-2.98	0.02	-0.03
Cu (111)	-0.19	-2.88	0.01	0.07

describing the results of the first case.

As can be seen in Fig. 6.2 (a), there are several local minima of different energies. One of the minima with the lowest energy corresponds to water formation (blue region near OH). Fcc sites are also local minima in this potential energy surface. However one of them has higher energy: fcc2. This is not unexpected because in this position the H atom is near to one copper atom. The energy is lower when the H atom is on the fcc1 site, in between 3 Ni atoms. The presence of these two local minima creates two possible pathways for the water formation: P1 from fcc1, and P2 from the fcc2 site. The activation barriers for both of them are rather different: 0.75 eV and 0.26 eV, respectively. The pathway P2 is the more likely reaction path to produce water on this surface because the energy of the initial state is higher, but it is still negative, which makes it a good starting point.

The PES showed in Fig. 6.2 (b) is rather different from the previous case. In this surface, there are local minima on fcc and hcp sites near Ni atoms (fcc3 and hcp3). The energy of H on these sites is very negative and makes the reaction very endothermic ($\Delta E = 0.54$ eV). The high stability of H on these positions also affects the activation barrier: $E_{act} = 0.78$ eV. So there is no favorable reaction path.

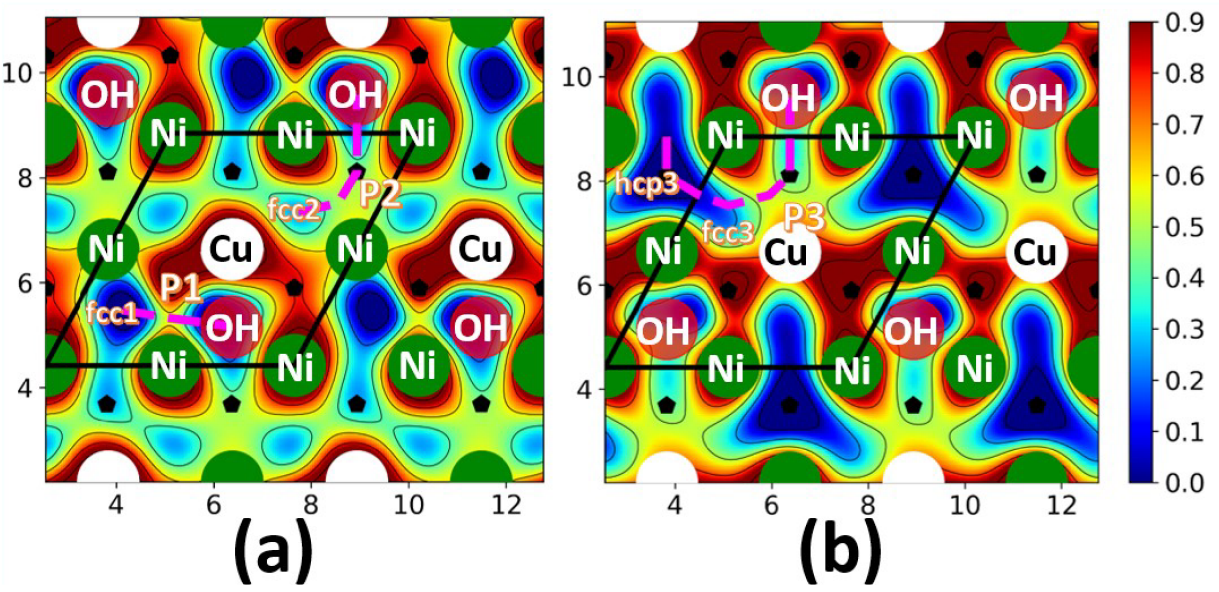

Figure 6.2: PES for 25% Cu on Ni(111) with OH on fcc site. The black and magenta lines correspond to the unit cell and reaction paths. Several paths have been plotted and high symmetry points have been marked. The energy scale on right side in eV.

6.3.2 50 % Cu on Ni(111)

Figure 6.3 shows the PES for the water formation with OH adsorbed among 1 Ni and 2 Cu atoms. In this case, I found 2 possible pathways. Trajectory P1 starts from an fcc site (fcc1), where H is surrounded by 2 Cu and 1 Ni. The energy of the initial state is similar to that of the final state and therefore, the reaction energy is near to zero (within DFT error). Its activation barrier is also low and equal to 0.34 eV.

The second possible pathway P2 has even a lower activation energy (E_{act} = 0.20 eV), and in contrast to pathway P1, the reaction energy is negative (ΔE = -0.23 eV). Both trajectories have the same products and very similar transition states, therefore the initial state is the factor that distinguishes them. Clearly, the lower energy and stability of the fcc2 site favors the formation of water. Both reaction pathways are favorable.

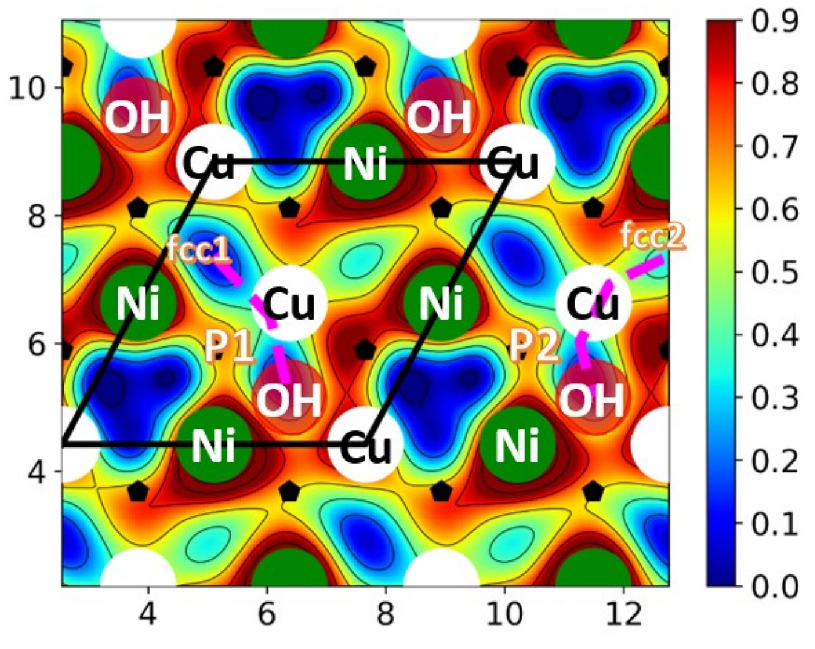

Figure 6.3: PES for 50% Cu on Ni(111) with OH on fcc site. The black and magenta lines correspond to the unit cell and reaction paths. Several paths have been plotted and high symmetry points have been marked. The energy scale on right side in eV.

6.3.3 75 % Cu on Ni(111)

Like in the case of the surface with 25% of Cu, here I placed OH in two different positions: surrounded by 3 Ni atoms (Fig. 6.4 (a)), and among 1 Ni and 2 Cu atoms (Fig. 6.4 (b)). I will start with the first case.

It is rather noticeable in Fig. 6.4 (a) that the energies of most sites have increased. There is still one local minimum with low energy: bridge site (br2). The reaction pathway P2 that starts from this site has a high activation barrier of 0.82 eV and is a rather unlikely trajectory to produce water. A second path P1 begins from an fcc site (fcc1) with higher energy. In consequence, P1 has a low activation barrier of 0.2 eV for water formation. However, it is important to point out that the initial state is very unfavorable, with a Gibbs energy of adsorption of 0.42 eV vs RHE.

When OH is adsorbed near to one nickel atom (Fig. 6.4 (b)) the PES changes. In this scenario, there are local minima on fcc and hcp sites (fcc3 and hcp3) from where the water

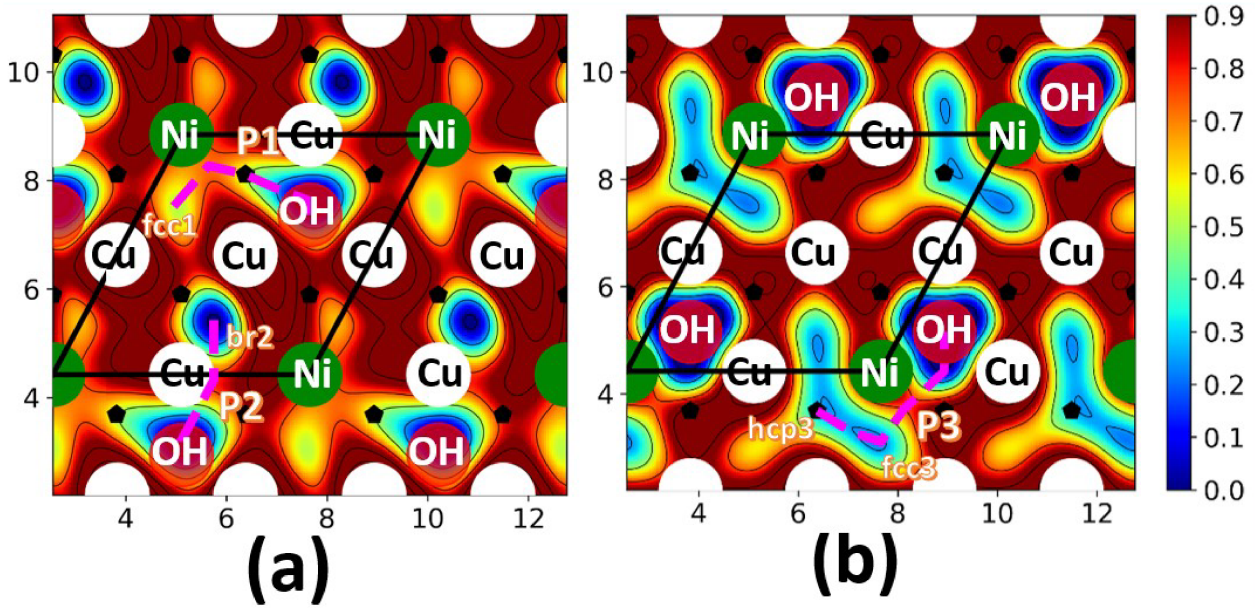

Figure 6.4: PES for 75% Cu on Ni(111) with OH on fcc site. The black and magenta lines correspond to the unit cell and reaction paths. Several paths have been plotted and high symmetry points have been marked. The energy scale on right side in eV.

formation can start. The reaction energy is favourable (ΔE = -0.31 eV) but the activation barrier is relatively high: E_{act} = 0.50 eV. In addition, the energy ΔG_{ini} of the initial state is close to zero, so this is the only favorable reaction path on this surface.

6.3.4 100% Cu on Ni(111)

Figure 6.5 shows the PES for water formation on the surface with 1ML of Cu on top of Ni(111). It can be observed that like on the surface with 75% of Cu, the energies in most of the sites are high. Even the local minimum, the fcc site (fcc1), has high energy. Nevertheless, this does not affect significantly the activation barrier, its value of 0.45 eV is similar to that on the pure Cu(111) surface. Only the reaction energy is more positive in this case than on the pure surface (-0.28 eV vs -0.48 eV). The energy ΔG_{ini} of the initial state (0.34 eV) is positive and close to that on pure copper, making this an unlikely reaction path.

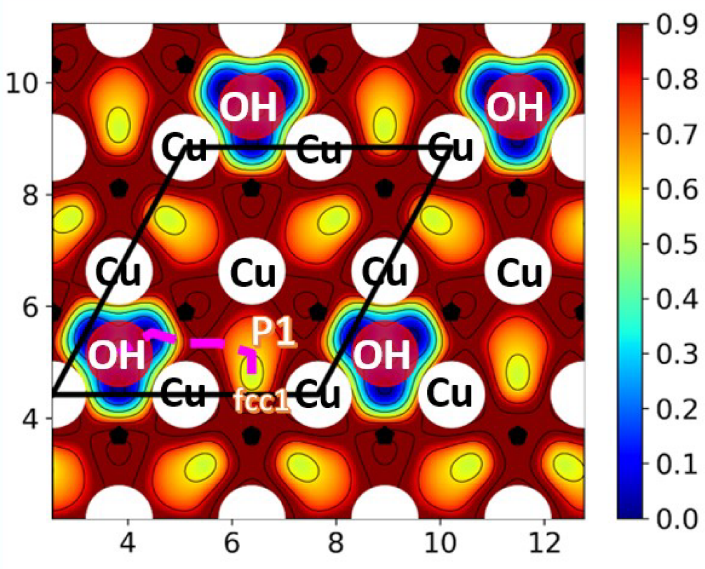

Figure 6.5: PES for 100% Cu on Ni(111) with OH on fcc site. The black and magenta lines correspond to the unit cell and reaction path. High symmetry points have been marked. The energy scale on right side in eV.

6.3.5 1 ML of Ni on top of Cu_{1ML}/Ni(111)

Finally, the PES for the formation of water on the last surface considered is presented in Figure 6.6. In this case, the two local minima, fcc1, and hcp1 sites have similar and very negative energy. The reaction path starting from them has a similar but lower activation barrier than pure Ni(111) (0.71 eV vs 0.80 eV). The reaction energy is more affected by the presence of copper underneath, its value increases from 0.17 eV in pure Ni(111) to 0.51 eV in this system.

6.3.6 Activation barriers

The activation barrier for H_2O formation on the intermetallic Cu/Ni(111) surfaces are presented in Table 6.2; for comparison, I also give the values for pure Cu(111) and Ni(111) already presented in Chapter 5. In addition, I also give the energy ΔG_{ini} of the initial state and the overall reaction energy ΔE.

The Brønsted-Evans-Polanyi suggests, that there should be a linear relationship between

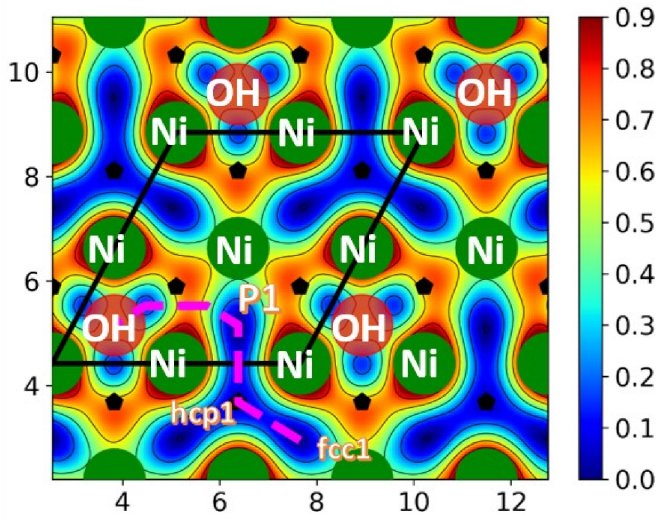

Figure 6.6: PES for 1ML of Ni on Cu_{1ML}/Ni(111) with OH on fcc site. The black and magenta lines correspond to the unit cell and reaction path. High symmetry points have been marked. The energy scale on right side in eV.

the energy of activation and the reaction energy. A brief glance at the table shows, that there is no such correlation.

The energies of activation are given with respect to ΔG_{ini}. Therefore they determine the magnitude of the rate constant. In addition, a negative value of the initial energy assures a high concentration of the reactants. Therefore, the optimum combination is a low value of ΔG_{ini} with a low energy of activation. From the table, we gather that there are four cases for which the activation energies are in the range of 0.2 eV to 0.3 eV: 25% Cu with both H and OH near copper; both listed cases with 50% Cu; 75% Cu with H near 2Cu and OH near 3 Cu. However, for the last case, the initial energy is too high, so this leaves us with three excellent candidates.

6.4 Conclusion

In my investigations of bimetallic NiCu surfaces, I have found several reaction paths which fulfill both criteria for a fast reaction: a negative Gibbs energy ΔG_{ini} for the initial state, and

Surface	initial sites	E_{act}	ΔG_{ini}	ΔE
Ni(111)	fcc	0.81	-0.40	0.17
100% Ni on Cu/Ni(111)	fcc	0.70	-0.30	0.51
25% Cu on Ni(111)	H: 3Ni, OH: 3Ni	0.78	-0.61	0.54
	H: 3Ni, OH: 1Cu	0.75	-0.49	0.16
	H: 1Cu, OH: 1Cu	0.26	-0.07	-0.26
50% Cu on Ni(111)	H: 2Cu, OH: 2Cu	0.34	-0.17	0.05
	H: 1Cu, OH: 2Cu	0.20	0.10	-0.23
75% Cu on Ni(111)	H: 2Cu, OH: 2Cu	0.50	-0.04	-0.31
	H: 2Cu, OH: 3Cu	0.20	0.42	-0.54
	H: 3Cu, OH: 3Cu	0.82	-0.33	0.01
100% Cu on Ni(111)	fcc	0.45	0.34	-0.28
Cu(111)	fcc	0.58	0.37	-0.48

Table 6.2: Activation energy E_{act}, energy ΔG_{ini} of the initial state, and reaction energy ΔE for water formation on a variety of surface sites.

low energy of activation. It is worthwhile to point out that particularly reactive surface sites can dominate the kinetics, even if their surface concentration is low.

Chapter 7

H and OH adsorption on different NiM surfaces

In the previous chapters I have studied the adsorption of H and OH, and their recombination to H_2O, in great detail. In particular, I have calculated potential energy surfaces and energies of activation in order to determine surfaces with good catalytic properties. In this chapter I examine other surfaces with the composition NiM, where M is a transition metal. I limit myself to the calculation of adsorption energies for H and OH – an extensive mapping of potential energy surfaces as I did for NiCu lies outside of the scope of this thesis for reasons of time and space. According to Sabatier's principle, surfaces where the Gibbs energy of adsorption is close to zero for both reactants are excellent candidates for the catalysis of water formation.

Therefore, in this chapter, I combined Ni with different metals such as Fe, Cu, Ti, Ru, Mo, Pd, Ir, Ru and others. In the beginning of the chapter, I study the adsorption of OH and H on three different sites: fcc, top, and bridge. Then, different top layer compositions are analyzed. Finally, I consider the case of a monolayer of Ni on top of a layer of another metal M, and the reverse case, a monolayer of M on top of Ni. All calculation are limited to fcc(111) surfaces. The technical details are described in Appendix A.

7.1 H and OH adsorption energies on different sites

In all cases I have calculated the adsorption energies for three different sites: bridge, fcc, and on top. Fig. 7.1 shows the results for a surface of nickel covered by a complete layer of the transition metal M. For Ni, adsorption is strongest on the fcc site both for H and OH. In the case of the first row transition metals, for hydrogen adsorption (Fig. 7.1 (a) up), most of the metals follow Ni , except for Ti and Mn, where the bridge site is favored. Concerning OH adsorption, fcc is favorable for all metals, but for Zn the bridge site is just as good, and for Fe the top site.

In Fig. 7.1 (b), for the second and third row transition metals the fcc site is usually the most favorable or close to being the most favorable both for H and OH adsorption, with OH on Zr being a notable exception – see Figs. 7.1 (b) and 7.1 (c).

7.2 H and OH adsorption on different top layer compositions

For the investigaton of bimetallic surfaces I have limited myself to adsorption on fcc sites, because this is favored for most of the transition metals investigated.

Adsorption energies of H and OH for NiM metal surfaces of various compositions are shown in Fig 7.2 as a function of the content of the metal M. Thus, 0% of M on the top layer correspond to a pure Ni(111) surface.

The results can serve as a database for good candidates as catalysts for the recombination reaction. The most important range of composition is between 25% and 75%. Thus, from the first row d-metals Zn is a good candidate besides Cu, while Ti is unfavorable. From the 2nd row Ru looks promising, while combinations of Ni with Zr have too high an adsorption energy for OH. Similarly, from the third row Ir seems favorable, and Au not. Naturally, this plot says nothin about the stability of these surfaces, but at can serve to exclude several combinations.

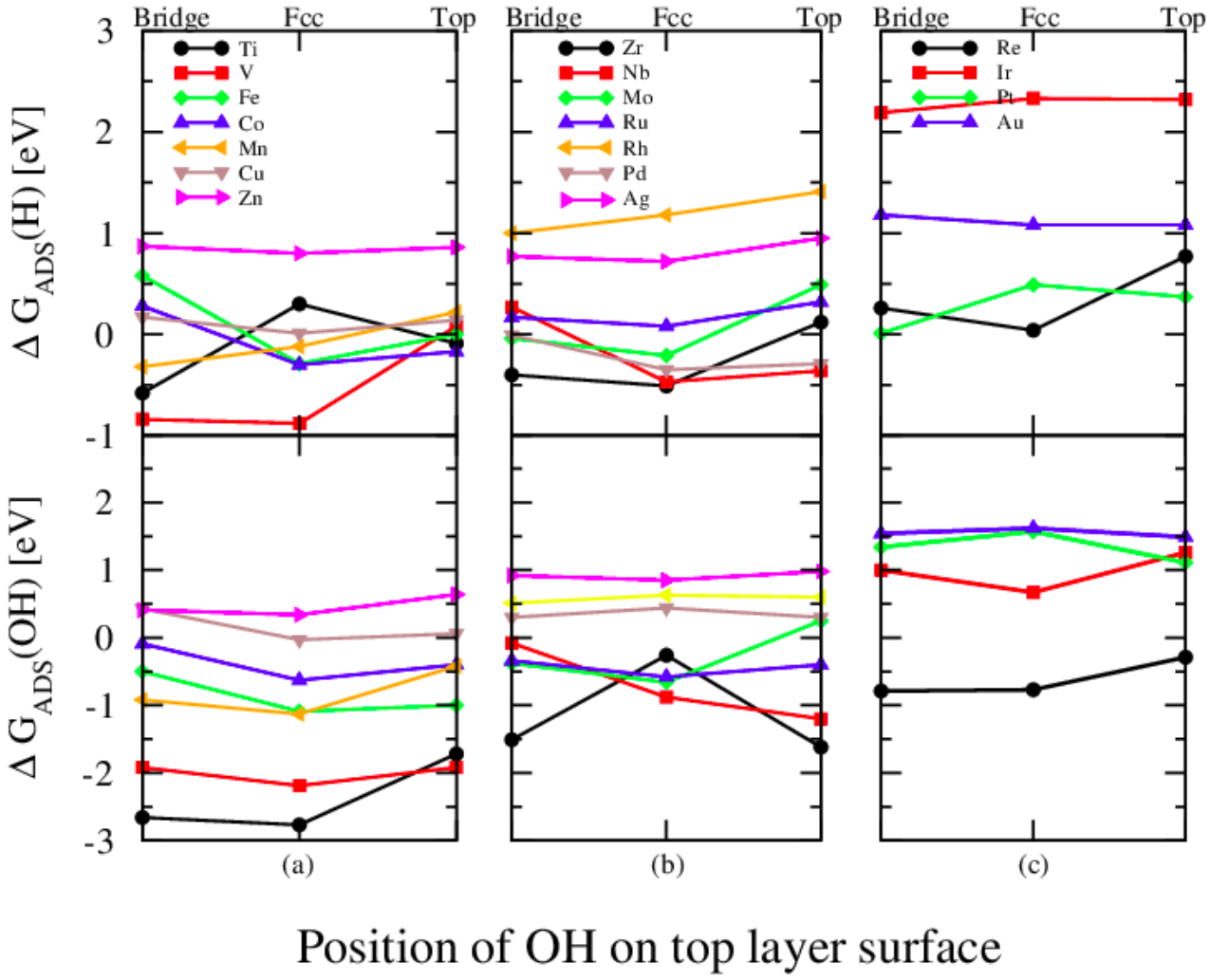

Figure 7.1: H (top) and OH (bottom) adsorption Gibbs energies on the bimetallic NiM surfaces in three different sites. The results are divided according to the position in the periodic table: (a) first row; (b) second row; and (c) third row transition metals.

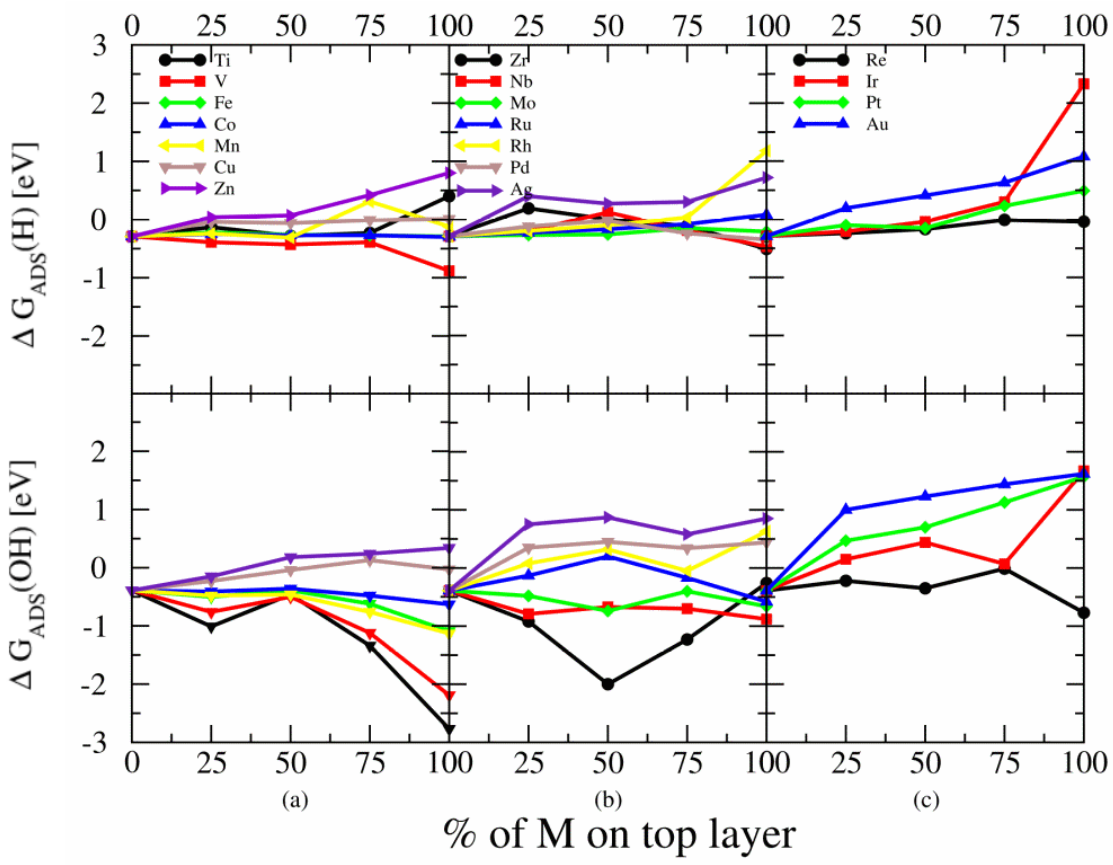

Figure 7.2: H (top) and OH (bottom) adsorption Gibbs energies on the bimetallic NiM surfaces. The results are divided according to the position on the periodic table: (a) first row; (b) second row; and (c) third row d-metals.

7.3 H and OH adsorption on Ni surfaces with M as second layer

In addition I have studied adsorption on a monolayer of Ni on top of a monolayer of M on top of bulk nickel. The results are shown in Table 7.1. For comparison I also give the adsorption energies for a monolayer of M on top of nickel.

The results are not easy to interpret, since there are two different effects: a chemical effect of the underlying layer on the top layer, and a lattice mismatch which induces strain.

Considering the system with Ni on top, there is no clear tendency in the H nor in the OH adsorption energies. But two combinations strike as being promising: Ni on Cu and Ni on

Zr. However, the surface energy of Cu is much lower than that of Ni, so Ni on Cu would not be stable. Unfortunately, the same is true for Zr on Ni. Obviously there is a large difference between M on Ni and Ni on M, but there is no clear correlation.

Table 7.1: Adsorption Gibbs energies on nickel surfaces modified by a monolayer of another metal. Column 1 and 2 give adsorption energies for surfaces with one layer of Ni on top followed by a layer of metal M on top of bulk nickel. Columns 3 and 4 show the data from section for one layer of M above bulk Ni. All energies are in eV.

Metal	$\Delta G(H)$ – (Ni)	$\Delta G(OH)$ – Ni	$\Delta G(H)$ – (M)	$\Delta G(OH)$ – (M)
Ni	-0.29	-0.39	-0.29	-0.39
Ti	-0.15	-0.66	0.4	-2.77
V	-0.23	-0.59	-0.88	-2.19
Fe	-0.35	-0.17	-0.29	-1.09
Co	-0.39	-0.18	-0.30	-0.63
Mn	-0.30	0.12	-0.12	-1.13
Cu	-0.12	0.02	-0.01	-0.03
Zn	0.14	0.52	0.80	-0.34
Zr	0.07	0.1	-0.51	-0.26
Nb	-0.35	-0.09	-0.47	-0.88
Mo	-0.38	-0.29	-0.21	-0.66
Ru	0.42	-1.32	0.08	-0.58
Rh	-0.51	-0.05	1.18	0.63
Pd	-0.57	-0.32	-0.35	0.44
Ag	-0.56	-0.24	0.72	0.85
Re	1.91	0.01	0.04	-0.77
Pt	-0.57	-0.29	0.49	1.57
Au	1.11	-0.62	1.08	1.62

7.4 Discussion

As I pointed out in the previous sections, it is challenging to interpret such a wide range of results in terms of one descriptor. Nevertheless, in this section I will summarize the previous findings and I will show some general trends of these systems.

The systems with lower percentage of the second metal have shown to be the most promising. In the Figure 7.3 the Gibbs energies of adsorption of H and OH on those surfaces have been collected and displayed according to the position of the second metal on the Periodic

Table.

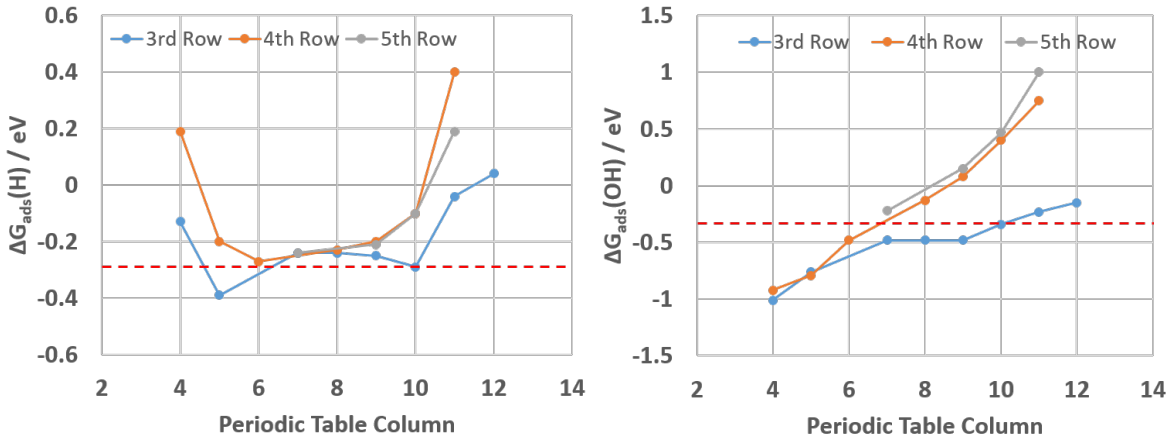

Figure 7.3: Gibbs energies of adsorption of H (left) and OH (right) on the NiM surfaces, with a 25% of content of the second metal. The red dashed lines indicates the values corresponding to the adsorption on a clean Ni(111) surface.

In the case of the adsorption of H, many systems present a similar energy than pure Ni. Surfaces that contain metals with an almost fully or depleted occupied d-band have higher energies than others. Extreme and not suitable cases are Zr and the coinage metals Ag and Au. The energies have values near to zero for Zn, Cu, Pd, and Ti.

The values of the adsorption energies of OH increases monotonically with the position in the Periodic Table, that correlates with the filling and the center of the d-band. Opposite to the adsorption of H, the TiNi surface adsorbs OH to strongly to make it a viable candidate. The values for the surfaces with Cu, Zn, and Pd show that these are still the best candidates. The ReNi, RuNi, and RhNi systems are also interesting systems to consider because they have adsorption energies are higher than for pure Ni and near to zero.

In Figure 7.4 I have compared the Gibbs adsorption energies on the NiM systems with the values on pure M(111) surfaces (ΔG^*_{ads}). The values were obtained from DFT calculations from different sources [109], [110], [111], [112], [113], [114]. The adsorption energies of H and OH on these NiM surfaces follow linear relationships, with some exceptions like Ti, and Nb or Fe for the cases of H or OH, respectively.

Opposite to the cases of surfaces with low content of the second metal M we have systems

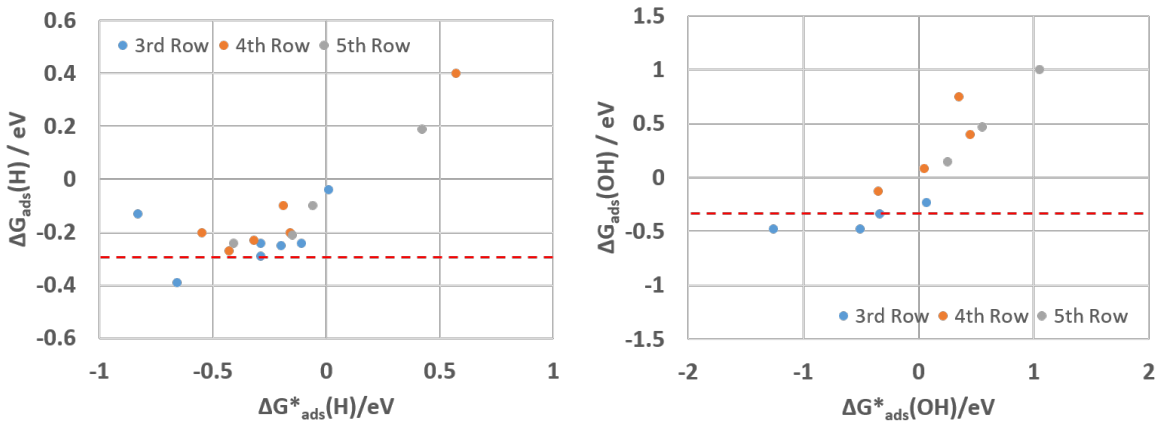

Figure 7.4: Gibbs energies of adsorption of H (left) and OH (right) on the NiM surfaces as a function of the same energies on pure (111) surfaces (ΔG^*_{ads}). The content of the second metal is 25%. The red dashed lines indicates the values corresponding to the adsorption on a clean Ni(111) surface. The values of ΔG^*_{ads} were taken from [109], [110], [111], [112], [113], [114].

with a complete monolayer of M. According to their surfaces energies, systems with lower values will be on top of the Ni substrates. On the other hand, the metals with higher energies will be more stable under one layer of Ni, and in the second position from top to bottom.

The adsorption energies on most surfaces with Ni on top (and M on the second layer) are very similar to the values on pure Ni, showing than the influence of the M layer underneath is minor. Exceptions are Re and Ru for the case of H, where the adsorption is too unfavorable. On the other surfaces the adsorption is too strong to make them suitable candidates. The same trend is observed for the adsorption of OH.

When a complete monolayer of M is on top of the Ni substrate the relationship between ΔG_{ads} and ΔG^*_{ads} seems to be linear. However the values are more positive than on pure M metals probably due to the increasing mismatch between both metals. Unfortunately these NiM systems are also not suitable. Some of the surfaces have adsorption energies of H or OH near to zero values but these systems are not the same.

Figure 7.6 shows the Gibbs energies of adsorption of H and OH only on the surfaces presented in this section. As it can be observed, the systems with energy values near to zero are the ones with low percentage of the second metal. With exceptions of Au and Ag, that

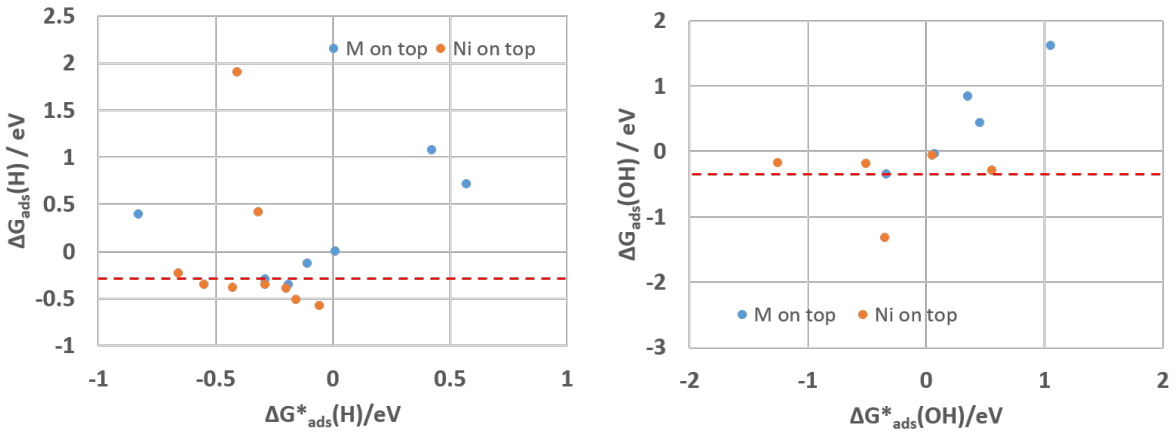

Figure 7.5: Gibbs energies of adsorption of H (left) and OH (right) on the NiM surfaces as a function of the same energies on pure (111) surfaces (ΔG^*_{ads}). Blue and orange circles corresponds to a complete monolayer of M on first or second position of the slab, respectively . The red dashed lines indicates the values corresponding to the adsorption on a clean Ni(111) surface. The values of ΔG^*_{ads} were taken from [109], [110], [111], [112], [113], [114]

have too high adsorption energies, and Ti, Zr, and Nb, that adsorb OH too strongly. Most of the system with a complete monolayer of M under one layer of Ni have too negative H adsorption energies. And in almost all the cases, the surfaces with a monolayer of M adsorb one or both species too strongly or too weakly.

Figure 7.6 makes also easier to choose the best candidates between the systems presented in figs. 7.4 and 7.5. The best systems are the ones with both Gibbs energies of adsorption near to zero, like is the case of the surfaces with low content of Cu, Zn, Rh, or Ir. Co, Mo, Re, and Ru are also interesting candidates but their adsorption energies are very similar to the ones of pure Ni.

These findings correlate well with experimental results. In the case of Zn, Badawy *et al.* have found that ZnNi alloys enhanced the electro-catalytic activity of Ni electrodes towards the HER due to the reduction of cathodic hydrogen overpotential in 254 mV. [115] Zn also reduces the corrosion process in comparison with pure Ni.

According to Vazquez *et al.* the catalytic activity of NiIr is high for HER and it approaches to that of Pt. [116] They observed that Ir spontaneously deposites on Ni, partly covers the surface and increases the electrode area eight times. Similar findings have obtained Lyakhov

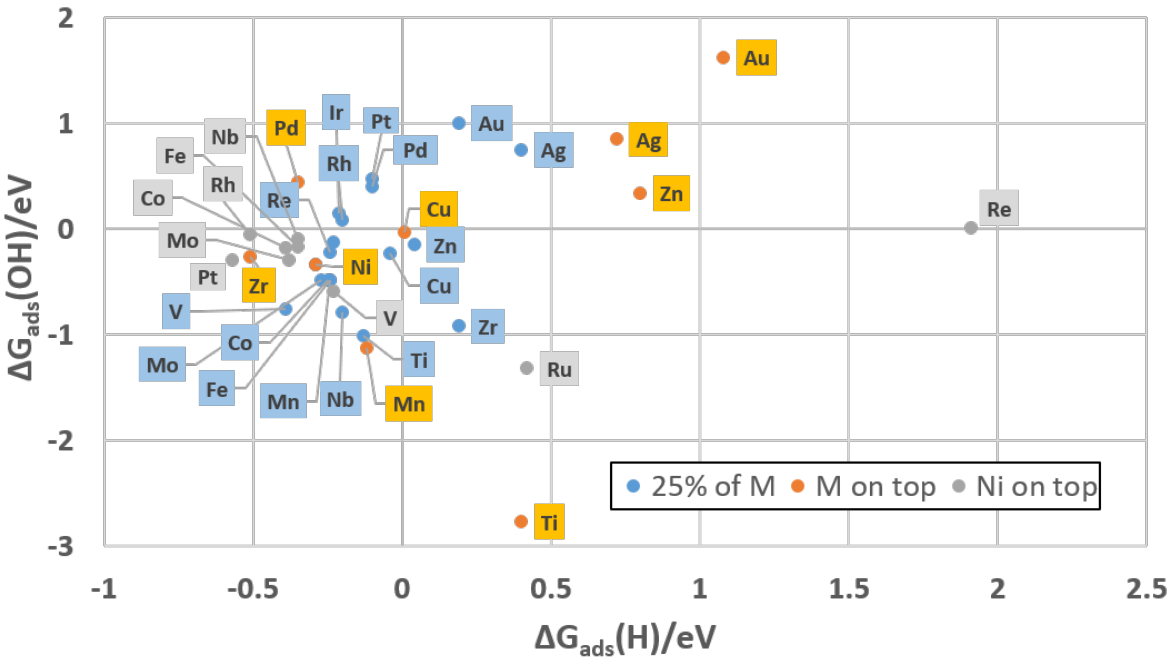

Figure 7.6: Gibbs energies of adsorption of H and OH on the NiM surfaces. Blue circles correspond to a 25% content of the second metal. Orange and grey circles corresponds to a complete monolayer of M on first or second position of the slab, respectively .

using NiRe alloys. [117] According to both of them, the enhancement of the catalytic activity is only a geometric effect but my calculations show that part of it could be due to the synergy between both metals. However and even though Re and Ir present a good catalytic activity when combined with Ni, both alloys are as expensive as platinum, making them not interesting for commercial uses.

Another candidate is Ru and many studies have shown that HER the presence of RuO_2 increases the catalytic activity of Ni. [118], [119], [120] However the low mechanical stability of the catalyst and the high costs of the manufacturing process prevent its practical application.

Sun *et al.* have studied NiCo ordered mesoporous materials with the amount of cobalt varying between 28% and 100%. [121] They have found a maximum in the catalytic activity at 42% of cobalt, that they related to the decreased number of Ni active sites on the surface area, and consequently progressive loss of synergism. My results also support that conclusion.

7.5 Conclusion

In this chapter, the adsorption energies of H and OH were studied in order to find good candidates for combinations with Ni that may have good catalytic activity for hydrogen evolution. At the beginning, a study of preferable sites was performed. On most metals, the fcc site is favored both for the adsorption of H and OH. Exceptions are Ti and Pt for H, and Zr for OH. Based on these data, all calculations for bimetallic systems were performed for fcc sites.

The results form an extensive database; on the basis of my work certain combinations and coverages of transition metals with nickel can be excluded, while others look promising. From the first row of transition metals, the most interesting materials are: Zn and Co. Mn can also be included, even though the OH adsorption energy is lower than the value of pure nickel. From the second row, the selected systems are: Rh and Ru, and from the last one: Re and Ir.

Chapter 8

General Remarks and Conclusions

Hydrogen evolution/oxidation is arguably the most important and best investigated electrochemical reaction. Several concepts of electrochemistry, in particular the Tafel equation and the notion of a transfer coefficient, were developed on the basis of this reaction, and the standard hydrogen electrode still defines the scale of electrochemical potentials.

The hydrogen reaction is also of huge practical importance. One of the visions for meeting the energy demands in the future is the *hydrogen economy*, in which hydrogen is supposed to replace coal, oil and gas as the main energy vectors. This requires efficient hydrogen generation in electrolyzers, and consumption in fuel cells. But even if a pure hydrogen economy will not materialize, there is a general consensus that hydrogen and fuel cells will play an important role in the future.

A principle difficulty with the electrochemical hydrogen reaction is the lack of a cheap and efficient catalyst. In acid solutions platinum is an excellent but expensive catalyst; in addition, oxygen reduction, which occurs at a fuel cell cathode, is slow on all known substrates. In alkaline solution, oxygen reduction is faster and requires less expensive catalysts, but hydrogen oxidation and evolution are slow. It was therefore considered a breakthrough, when the Markovic group announced that it had found a nickel-based catalyst on which it is

fast. They suggested that water formation according to:

$$H_{ad} + OH_{ad} \rightarrow H_2O \tag{8.1}$$

was an important intermediate step, which could operate efficiently at bifunctional surfaces in alkaline solutions.

Up till then this step had never been considered in the context of hydrogen evolution/oxidation. For this reaction step, bifunctional, in particular bimetallic electrodes like those I investigated in this thesis, offer good possibilities. O and OH can adsorb at different, but adjacent sites and then recombine to water. So far this mechanism is unproven, but it is an exciting possibility, and the first really new idea for hydrogen electrocatalysis in decades. This the reason why I chose this for the theoretical investigations I conducted for my thesis. In addition, such bifunctional mechanisms may occur in other reactions as well, but water formation according to eq. (8.1) is of the simplest possible examples. Thus, by studying its mechanism and catalysis, we can lay the foundations for understanding more complicated examples.

In the choice of a suitable bimetallic electrode I was guided by Sabatier's principle, which states that on a good catalyst adsorption should neither be too strong nor too weak; Gibbs energies of adsorption near zero should be optimal. Nickel is known to adsorb both H and OH too strongly, copper adsorbs them too weakly. Although adsorption properties in bimetallic systems are not additive, there was a reasonable expectation that they might offer suitable adsorption sites. In addition, Ni/Cu bimetallics have proved to be good catalysts experimentally.

As method for the theoretical studies I chose DFT, which nowadays is the standard, since it combines reasonable accuracy with reasonable speed. The study of water formation is comparatively simple, since it does not involve charged species – DFT with ions still offers great difficulties. Nevertheless, we had to simplify the system in order to make the calculations tractable. The reaction takes place at an electrochemical interface, so the reactants are in

contact with an aqueous solution, whose presence we completely neglected. Even with this simplification the calculations were lengthy, because nickel exhibits spin polarization, which had to be taken into account. Fortunately the interaction of water both with copper and with nickel is relatively weak, so that the neglect of its presence should not invalidate my results. In any case this is an unavoidable simplification at this stage.

To be on firm ground, I first studied the adsorption of OH and H and water formation on pure Ni(111) and Cu(111), where I could compare my results with literature values. Within the usual DFT error of about ± 0.1 eV I obtained the same results.

As model bimetallic surfaces I chose fcc(111) surfaces with varying Ni/Cu content – $25\%, 50\%$ and 75% Cu. The aim of my study was to explore the kinetics of water formation and find suitable sites where the reaction proceeds rapidly. Before turning to the kinetics I investigated the thermodynamics of the adsorption of H and OH on various sites on these surfaces. Using Sabatier's principle as a guide, this already indicated which sites might be suitable for the recombination reaction. Indeed, I could identify various sites where the Gibbs energies of adsorption either for OH or for H looked promising, i.e. the Gibbs energies of adsorption near 0 V SHE were close to zero.

The most important part of my thesis was the determination of activation energies for water formation on the investigated surfaces from a variety of sites. Usually, within DFT this is done by a technique called nudged elastic band, but this proved to converge slowly. Therefore, I mapped out potential anergy surfaces for the reaction by single point calculations. For this purpose, I placed an adsorbed OH at a suitable site near the center of my unit cell, and mapped out several paths for the reaction.

On each surface I found reaction paths with activation energies of the order of 0.2 - 0.3 eV, which makes for a very fast reaction. All of these favorable paths involved mixed adsorption sites where in the initial states the reactants have both Ni and Cu as neighbors. This proved my initial consideration that the two metals complement each other well. A particularly interesting situation occurred on the surface with 25% Cu: The hydrogen surrounded by

3 Ni atoms is more strongly adsorbed than the hydrogen having 1 Cu atom as neighbor. However, the latter is the more favorable reactant, and the other species is just a bystander. The situation is thus similar to that in hydrogen evolution on Pt(111), where the strongly adsorbed hydrogen does not participate in the reaction.

So, unless the neglect of the presence of the solution is too drastic a simplification, we may conclude that the bifunctional water formation is a very favorable reaction step on bimetallic Ni/Cu surfaces. Indeed, with activation energies of 0.3 eV or less it may be too fast to be observable. This may be the reason why a recent experimental study of Cu/Ni clusters was inconclusive (citation).

Besides this exhaustive study on Cu/Ni, I surveyed bimetallic surfaces of Ni with 18 other metals. The calculation of potential energy surfaces for such a large number of cases was out of the question, so I calculated adsorption energies for H and OH on these surfaces in order to identify suitable surface compositions. Indeed, I could identify several combinations which look promising, viz. bimetallics of Ni with Zn, Co, Rh, Ru, Re and Pt. The latter four metals are too expensive to be of practical use, and the price of Co, which is used in Li-ion batteries, has risen in recent years. So only the combination with Zn could be of practical value. It may be worth while to perform an exhaustive study of this surface and calculate activation energies, preferably in combination experiments. But perhaps the most important result of this part of my thesis is that certain combinations can be excluded because of unsuitable adsorption energies.

As already mentioned, water formation is not the only reaction where a bifunctional mechanism may operate. A case in point is formic acid oxidation on platinum modified by Bi-adatoms [122] The authors could not establish a definite reaction mechanism, but provide evidence that various surface sites cooperate in the reaction steps. I believe that my results encourage to investigate these and similar cases by the techniques that I have used.

Finally, a few words about the technical aspects of my work. As I have already briefly mentioned, the most drastic approximation is the neglect of the solution, especially of water.

For hydrogen adsorption, there is good evidence that the presence of water does not affect the adsorption energy. Calculations by the Nørskov group with an extra layer of water on top of the adsorbed hydrogen gave the same adsorption energies [123]. However, adsorbed OH has a tendency to form hydrogen bonds with adjacent water [124], as was again shown by adding a water layer on top. However, a single water layer at 0 K is a poor representation of liquid water at room temperature, so it is not at all clear if its presence makes the results more realistic.

Other approaches to modeling the presence of water are based on continuum theories for electrolyte solutions, of which there are various versions. They all have a strong empirical component, and are not able to account for hydrogen bonding of adsorbates, nor for the formation of solvation cages. Therefore I have refrained from adding an implicit solvent, even if its implementation does not cost much in terms of computing time.

In summary, in my thesis I have investigated a newly suggested , as yet unproven reaction step for hydrogen oxidation by state of the art theoretical techniques in Ni/Cu bimetallic surfaces. According to my results, this step is advantageous and very fast on certain surface cites. In addition, I explored a multitude of other nickel bimetallic surfaces for their suitability. The methods which I employed and developed, are suitable for the investigation of other bifunctional mechanisms.

Appendix A

Technical details of DFT simulations

A.1 Computational setup

DFT calculations were performed using the GPAW code [97] [98]. Perdew Burke and Erzenhof (PBE) [94] exchange-correlation functional was combined with PAW [125] to solve KS equations. Brillouin-zone integration was done using a 4 x 4 x 1 k-point Monkhorst-Pack grid [126], which corresponds to a (2 x 2) surface unit cell. For relaxations, the two bottom layers were fixed at the calculated positions corresponding to the bulk, and coverage of $\frac{1}{4}$ when there is one adsorbate. The geometry convergence was achieved when the total forces were less than 0.02 eV/Å. Spin polarization was considered.

A.2 Adsorption sites

As shown in Fig. A.1, three highly symmetric adsorption sites have been studied on Ni(111). The top site is on-top a surface atom and it is labeled as A. The 2-fold bridge site is placed between two neighboring atoms and labeled as B. The fcc 3-fold hollow site is labeled C. This site is directly on top of a metal atom in the second layer.

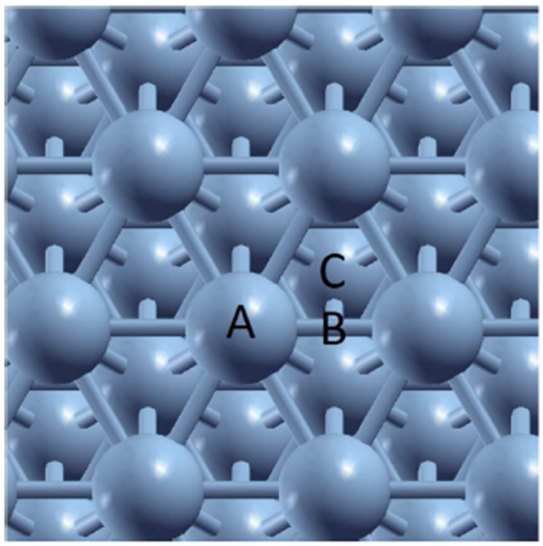

Figure A.1: Different adsorption sites at 111 crystal surfaces: A is a top site, B is a bridge site, C is a fcc hollow site.

Appendix B

French Resume

B.1 Introduction

Depuis la révolution industrielle, la demande d'énergie a augmenté de façon exponentielle: les principales sources d'énergie sont non renouvelables, comme le pétrole, le charbon et le gaz naturel qui correspondent à environ 80% de l'énergie produite et utilisée de nos jours. Ce sont des ressources limitées, donc les sources d'énergie renouvelable (par exemple, géothermie, éolien, solaire, hydroélectrique et biomasse) sont nécessaires pour maintenir le mode de vie de notre société. Mais, elles dépendent de l'influence de la météo, et nécessitent de trouver de nouveaux dispositifs qui convertissent plus efficacement l'énergie chimique d'un combustible en électricité est obligatoire pour répondre à nos besoins en énergie.

L'un des carburants les plus prometteurs est l'hydrogène, obtenu à partir de l'eau de différentes manières : électrolyse, radiolyse, thermolyse, thermolyse, méthode au ferrosilicium, séparation photobiologique ou photocatalytique de l'eau, entre autres. L'étude de son évolution (Hydrogen Evolution Reaction, HER) ou des réactions d'électro-oxydation (Hydrogen Oxidation Reaction, HOR) est devenue très intéressante en raison de leurs rôles dans différents types d'électrolyse et de piles à combustible respectivement.

Récemment, les piles à combustible alcalines à électrolyte solide (SAFC) utilisant de

nouvelles membranes électrolytiques à base de polymères échangeurs d'anions ont été proposées. En comparaison avec les piles à combustible alcalines à électrolyte liquide (AFC), les membranes échangeuses d'anions sont moins sensibles à la contamination par le dioxyde de carbone. De plus, elles ne nécessitent pas l'utilisation des métaux nobles comme les cellules à membrane échangeuse de protons PEM (actuellement considérées comme l'état de l'art pour la propulsion des véhicules électriques à pile à combustible). La réaction de réduction de l'oxygène qui se produit à la cathode des SAFCs est plus efficace en milieu alcalin par rapport aux PEMs, et elle peut être catalysée par des matériaux non précieux tels que l'argent ou les oxydes de métaux de transition. Mais, l'oxydation de l'hydrogène est plus lente en milieu alcalin qu'en milieu acide, ce qui donne lieu à des surtensions importantes sur l'anode des SAFC. Ainsi, le potentiel des SAFC à devenir des cellules commerciales efficaces dépend fortement de la capacité des chercheurs à développer des catalyseurs actifs et stables pour l'évolution de l'hydrogène (pour l'électrolyse) et son oxydation (pour les applications en piles à combustible).

Les électrolyseurs alcalins liquides conventionnels utilisent généralement du Ni comme matériau cathodique. Au-dessus du potentiel d'équilibre de l'électrode d'hydrogène, la surface du nickel s'oxyde facilement, ce qui réduit son activité pour l'oxydation de l'hydrogène, ce qui complique l'utilisation des électrodes monométalliques de Ni à l'anode des SAFCs. La littérature indique quelques exemples de métaux (Pd, Ru, Ir, Mo, Cu et Fe) [116],[127], [68], [128] ayant une influence positive sur l'activité du Ni. Mais origines de l'augmentation de l'activité électrocatalytique ne sont pas encore très claires.

B.2 Résultats et discussion

Il a été postulé [7], qu'en plus des réactions de Heyrovsky, Tafel et Volmer, le mécanisme HOR dans les solutions alcalines comprend également l'étape d'adsorption de OH^- (4) et une réaction chimique entre OH et H adsorbés (5)[26]:

(1) Réaction de Heyrovsky:

$$Surf + H_2 + OH \rightleftharpoons H_{ad} + H_2O + e^-$$

(2) Réaction de Tafel:

$$H_2 + 2Surf \rightleftharpoons 2H_{ads}$$

(3) Réaction de Volmer:

$$H_{ad} + OH^- \rightleftharpoons Surf + H_2O + e^-$$

(4) Adsorption de OH^-:

$$Surf + OH^- \rightleftharpoons OH_{ad} + e^-$$

(5) Recombinaison chimique:

$$H_{ad} + OH_{ad} \rightleftharpoons 2Surf + H_2O$$

Où Surf représente les sites actifs en surface et H ad et OH ad représentent les adsorbats en surface. Comme mentionné précédemment, dans cette thèse, l'accent est mis sur les énergies d'adsorption de H et OH et sur la barrière d'activation de la réaction de recombinaison chimique (étape 5). La réaction de recombinaison chimique n'implique aucun transfert d'électrons et peut donc être étudiée à l'aide de calculs périodiques de DFT. L'avantage principal des calculs DFT est qu'ils permettent d'étudier la cinétique des réactions complexes au niveau atomique. Avec cette théorie, il est possible d'étudier des surfaces bimétalliques pour de nombreux métaux et en faisant varier la teneur, et d'aborder un grand nombre de sites d'adsorption possible. La taille du problème augmente avec la complexité du mécanisme de réaction.

Dans le cas des réactions électrochimiques, certaines conclusions seront obtenues en utilisant le principe de Sabatier. De cette manière, je présente des corrélations semi-empiriques entre la thermodynamique de l'adsorption OH et H et les propriétés cinétiques.

Construction de substrats bimétalliques

Les surfaces ont été modélisées à l'aide de cellules périodiques («périodic slab ») et d'un espace vide de 15 Å entre elles. Les cellules ont quatre couches, et des supercellules (2x2) ont été utilisées. Plusieurs pourcentages de M (métal) dans la couche supérieure ont été simulés en remplaçant différents nombres d'atomes de Ni. Les trois couches inférieures ont été formées uniquement par Ni et la couche supérieure a été comme suit:

- 25% M et 75% Ni,
- 50% M et 50% Ni,
- 75% M et 25% Ni,
- 100% M

Une autre cellule a également été considérée: une couche supérieure de Ni + une 2ème couche de M + deux couches inférieures de Ni. Les surfaces sont représentées sur la Fig. B.1.

Adsorption de H et OH sur des surfaces bimétalliques

L'énergie d'adsorption de H et OH a été calculée sur la position fcc (cubique face centré) pour toutes les surfaces. Les expressions suivantes ont été utilisées pour calculer les valeurs des énergies d'adsorption:

$$E_{ad}(H) = E(Surf - H) - E(Surf) - \frac{1}{2}E(H_2)$$

$$E_{ad}(OH) = E(Surf - OH) - E(Surf) - E(OH)$$

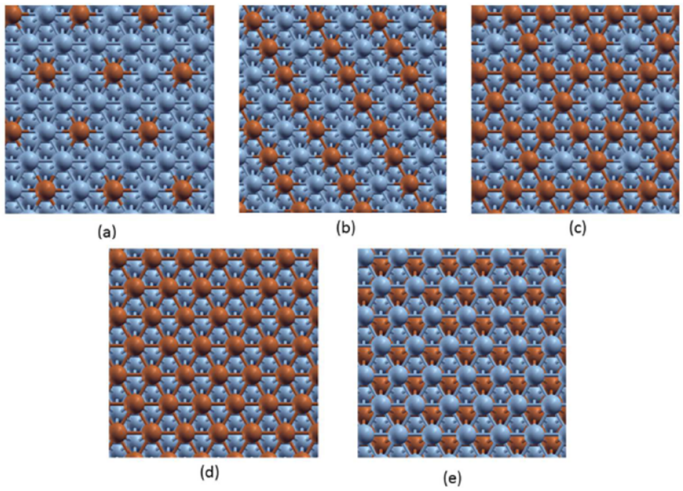

Figure B.1: vues de dessus des cellules utilisées pour représenter les surfaces bimétalliques de NiM. Composition de la couche supérieure: (a) 25% de M et 75% de Ni; (b) 50% de M et 50% de Ni; (c) 75% de M et 25% de Ni; (d) 100% M. Le système (e) a une couche supérieure complète de Ni et une deuxième couche de M. Les sphères grises et oranges représentent respectivement les atomes de Ni et de M.

où E(Surf-X), E(Surf), E(H_2) et E(OH) sont les énergies de l'adsorbat sur la surface, la surface propre et la molécule d'hydrogène ou le radical OH dans le vide respectivement. L'énergie libre d'adsorption de l'hydrogène a été calculée en ajoutant 0,2 eV à E_{ads}, comme l'expliquent Schmickler et al. [129] . Cette valeur tient compte de l'entropie de l'hydrogène gazeux et de l'énergie du point zéro de la molécule H_2 . L'énergie du point zéro de l'atome adsorbé est faible; elle est réduite par la présence du solvant, et aussi partiellement annulée par l'entropie de l'adsorbat. Toutes ces contributions sont pratiquement les mêmes pour tous les métaux, et dans tous les cas plus petites que la précision des calculs DFT.

Le calcul de l'énergie libre d'adsorption de OH n'est pas aussi simple que dans le cas de H. La principale difficulté est qu'après l'adsorption, OH n'est pas complètement déchargé sur la surface. Par conséquent, la sphère de solvatation n'est pas complètement perdue, et les changements sur l'énergie de solvatation sont difficiles à estimer. Néanmoins, on peut supposer que la perte dans la solvatation sera la même pour toutes les surfaces métalliques fcc, de même orientation. Dans cette hypothèse, nous avons estimé les énergies d'adsorption

libre à partir des valeurs de l'adsorption sur la surface Pt(111) comme suit:

$$\begin{aligned} G_{ads}(OH) - E_{ads}(OH) &= G_{ads}^{Pt(111)}(OH) - E_{ads}^{Pt(111)}(OH) \\ G_{ads}(OH) &= (G_{ads}^{Pt(111)}(OH) - E_{ads}^{Pt(111)}(OH)) + E_{ads}(OH) \\ G_{ads}(OH) &= (0.65 - (-2.3)) + E_{ads}(OH) \end{aligned} \tag{B.1}$$

Les énergies 'adsorption G_{ads} obtenues à partir des potentiels électrochimiques expérimentaux (obtenus à partir de la voltampérométrie cyclique) en utilisant l'équation de Nernst, et l'énergie d'adsorption issue des calculs DFT [99].

La relation entre l'activité catalytique d'un métal et l'énergie d'adsorption a fait l'objet d'études approfondies pour l'HER. Les relations entre l'activité catalytique et l'énergie d'adsorption de l'hydrogène (« volcano plot ») ont été rapportées pour une gamme de matériaux, conduisant à la conclusion que la valeur optimale est ΔG_{ads} (H) ≈ 0 [10]. Comme il a été souligné précédemment, de toutes les étapes du mécanisme de l'HOR, nous nous sommes particulièrement intéressés à la recombinaison chimique de OH et H adsorbés (réaction (5)). La réaction ne se produira que pour des catalyseurs qui peuvent adsorber les deux espèces dans la même plage de potentiel (qui est reliée à l'énergie libre par l'équation de Nernst). Par conséquent, nos critères pour trouver les meilleurs catalyseurs sont:

- ΔG_{ads} (H)$\approx$0
- ΔG_{ads} (H)$\approx\Delta G_{ads}$ (OH)

Adsorption de H et OH sur des surfaces bimétalliques Cu / Ni

Dans une publication précédente, Cherstiouk et al. [87] ont découvert qu'une petite quantité de cuivre peut améliorer l'activité catalytique des nanoparticules de nickel vis à vis de l'HOR. Les auteurs supposent que la réaction a eu lieu sur des sites mixtes, où l'énergie d'adsorption

de H_{ads} était plus faible que sur le nickel pur. En revanche, si l'énergie d'adsorption de H_{ads} est trop faible, les premières étapes (réactions (1) et (2)) n'auront jamais lieu. Sur la base de ces résultats expérimentaux, j'ai choisi ce système (surfaces bimétalliques CuNi) pour étudier comment la modification de la composition de la surface affecte la thermodynamique et la cinétique de certaines des étapes de l'HOR. En utilisant les critères que j'ai présentés dans la section précédente, je commencerai à étudier la thermodynamique de l'adsorption, puis je continuerai avec la cinétique de la formation de l'eau.

Le tableau 1 montre les énergies libres d'adsorption de H et OH sur différents sites des surfaces représentées sur la Fig. B.1. Selon le tableau 1, l'adsorption de OH est plus forte sur les surfaces contenant plus de Ni. Ce comportement est attendu. Habituellement, le nickel forme des liaisons fortes avec l'oxygène, ce qui entraîne l'oxydation et le blocage de la surface. Comme prévu, les surfaces avec la même quantité de Cu et Ni ont des énergies d'adsorption intermédiaires, ce qui en fait de bons candidats pour réduire la barrière d'activation de la formation de l'eau (en comparaison avec le Ni pur). D'autre part, le changement de l'énergie d'adsorption de OH affectera également la vitesse de l'étape (4), qui, contrairement à la formation de l'eau, est renforcée par une forte énergie d'adsorption de OH. Par conséquent, nous supposons que les surfaces contenant 25% et 50% de Cu auront un taux de réaction global plus élevé.

Dans le cas de l'énergie d'adsorption H, il n'y a pas de valeurs intermédiaires; les valeurs sont soit plus proches de celles du nickel pur, soit de celles des surfaces de cuivre. Sur la base de ces valeurs, il est difficile de prédire comment la composition des surfaces affectera les barrières d'activation.

Il est très important de souligner que la surface avec 50% de Cu (disposé en lignes) est celle qui suit tous les critères présentés précédemment. L'énergie libre de l'adsorption de H est proche de zéro pour 25% ou 75% de Cu mais l'adsorption de OH se produit à un potentiel différent.

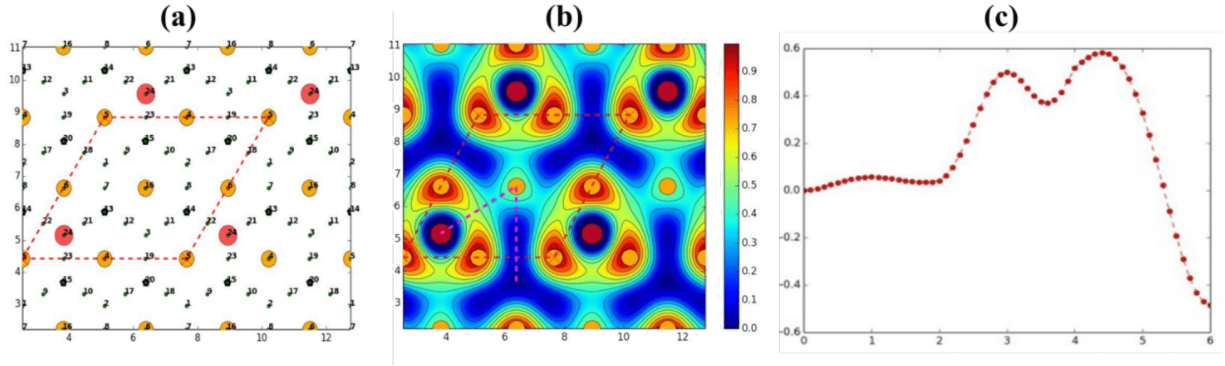

Figure B.2: (a) Les sites d'adsorption possibles H ads , les cercles oranges et rouges correspondent respectivement à Cu et OH. Les lignes rouges pointillées représentent la cellule unité. (b) Carte d'énergie potentielle de H et OH co-adsorbés sur la surface de Cu (111). Dans cette carte, le radical OH est placé sur le site fcc, et les positions de H sont montrées en (a). (c) Coordonnée de réaction pour la recombinaison entre OH et H. La trajectoire en (c) correspond au chemin minimal indiqué en (b) (lignes pointillées en violet). Les valeurs d'énergie sont en eV. L'énergie la plus basse a été prise comme valeur zéro de l'échelle.

Recombinaison chimique OH et H sur des surfaces bimétalliques CuNi

En principe, avec une puissance de calcul suffisante, il est toujours possible de calculer une barrière d'activation à l'aide de la méthode NEB. Il y a un tel nombre de configurations initiales possibles (de H_{ads} et OH_{ads}) sur ces surfaces, que cette méthode est impraticable. Avant de présenter les résultats obtenus, je présenterai la méthode que j'ai utilisée pour trouver les états de transition et les énergies d'activation. J'ai créé des surfaces d'énergie potentielle contrainte (PES) de la manière suivante. H et OH ont été co- adsorbés sur chaque surface, et les énergies ont été obtenues après les considérations suivantes:

- Différentes cartesont été créées pour la même surface CuNi, en maintenant la position de l'atome d'oxygène (du radical OH) à la position d'équilibre;
- Pour la construction de chaque carte, H_{ads} a été placé dans différentes positions : en position top, ponté et fcc, et à différentes distances du radical OH. La distance perpendiculaire à la surface (coordonnée z) a fait l'objet d'une relaxation, mais la

Table B.1: Adsorption de H ou OH sur les systèmes bimétalliques NiCu

Surface	$E_{ads}(H)$	$E_{ads}(OH)$	$\Delta G(H)$	$\Delta G(OH)$
Ni (111)	-0.49	-3.29	-0.29	-0.34
100% Ni on Cu/Ni(111)	-0.63	-3.39	-0.43	-0.44
25% Cu on Ni (111)	-0.57 (3Ni) -0.24 (1Cu)	-3.31 (3Ni) -3.18 (1Cu)	-0.37 -0.04	-0.36 -0.23
50% Cu on Ni (111)	-0.26 (2Cu)	-2.99 (2Cu)	-0.06	-0.04
75% Cu on Ni (111)	-0.21 (1Ni) -0.09 (3Cu)	-2.82 (1Ni) -2.86 (3Cu)	-0.01 0.11	0.13 0.09
100% Cu on Ni (111)	-0.18	-2.98	0.02	-0.03
Cu (111)	-0.19	-2.88	0.01	0.07

position dans le plan (coordonnées x et y) a été maintenue fixe;

- Dans chaque calcul d'énergie, un seul OH et un atome H ont été placés sur la surface;
- La position de l'atome d'hydrogène (du radical OH) a été optimisée lors de la minimisation de l'énergie.

Un exemple de la construction de ces cartes est illustré sur la Fig. B.2(a). Dans le tracé (a), OH est fixé dans une position fcc (cercle rouge) tandis que les différentes positions de H sont numérotées de 1 à 24. Les 24 valeurs énergétiques ont été utilisées pour créer la PES du Cu(111), comme le montre la Fig. B.2 (b). Les valeurs intermédiaires ont été interpolées à l'aide de la fonction de base radiale du code python.

Ces cartes ont été utilisées pour obtenir le chemin réactionnel de formation de l'eau, les énergies de réaction, les barrières d'activation et les états de transition. L'estimation a été améliorée par la suite en relaxant l'état de transition. Cette solution de rechange est beaucoup plus rapide que les calculs NEB correspondants et nécessite des coûts de calcul moins élevés. Néanmoins, les calculs traditionnels de NEB ont été utilisés pour certains systèmes afin de vérifier l'exactitude de notre méthode. Les résultats ont montré une bonne concordance entre les deux méthodes et avec les valeurs publiées précédemment. (*add ref neb)Le chemin réactionnel pour la formation de l'eau sur Cu(111) est illustré à la Fig. B.2 (c).

La barrière d'activation sur les surfaces en Cu, Ni et Cu/Ni(111) bimétallique est présentée

Table B.2: L'énergie d'activation, et l'énergie totale de la formation de l'eau dans différentes surfaces.

Surface	États initiaux	E_{act}	ΔG_{ini}	ΔE
Ni(111)	fcc	0.81	-0.40	0.17
100% Ni on Cu/Ni(111)	fcc	0.70	-0.30	0.51
25% Cu on Ni(111)	H: 3Ni, OH: 3Ni	0.78	-0.61	0.54
	H: 3Ni, OH: 1Cu	0.75	-0.49	0.16
	H: 1Cu, OH: 1Cu	0.26	-0.07	-0.26
50% Cu on Ni(111)	H: 2Cu, OH: 2Cu	0.34	-0.17	0.05
	H: 1Cu, OH: 2Cu	0.20	0.10	-0.23
75% Cu on Ni(111)	H: 2Cu, OH: 2Cu	0.50	-0.04	-0.31
	H: 2Cu, OH: 3Cu	0.20	0.42	-0.54
	H: 3Cu, OH: 3Cu	0.82	-0.33	0.01
100% Cu on Ni(111)	fcc	0.45	0.34	-0.28
Cu(111)	fcc	0.58	0.37	-0.48

dans le tableau B.2. Les résultats pour le Cu pur (111) et le Ni (111) sont en accord avec la littérature [100], [101], [104].

Comme on peut l'observer dans le Tableau B.2, il n'y a pas de corrélation directe entre l'énergie de réaction et l'énergie d'activation. Il est important de noter qu'une telle corrélation existe dans de nombreux systèmes et que le principe Brønsted-Evans-Polanyi est applicable. Nos résultats montrent que dans ces surfaces bimétalliques ce principe ne peut pas être appliqué, et l'analyse de la cinétique de la réaction basée uniquement sur l'énergétique conduira à des conclusions erronées.

Les valeurs peuvent être divisées en trois catégories principales. Un groupe avec des barrières d'activation élevées et des valeurs comprises entre 0,75 et 0,85 eV. Ce groupe correspond à la surface de Ni(111) pur et aux substrats bimétalliques à haute teneur en nickel. Le second groupe a une valeur intermédiaire pour l'énergie d'activation entre 0,45 et 0,58 eV. A ce groupe appartient la surface en cuivre pur. Enfin, le dernier groupe a les barrières d'activation les plus basses, avec des valeurs aussi petites que 0,2 eV. A ce groupe appartiennent les surfaces avec un pourcentage intermédiaire de cuivre. La surface avec 50% de cuivre est aussi celle qui satisfait les deux critères pour les énergies d'adsorption, devenant le meilleur choix pour augmenter l'activité des substrats de nickel.

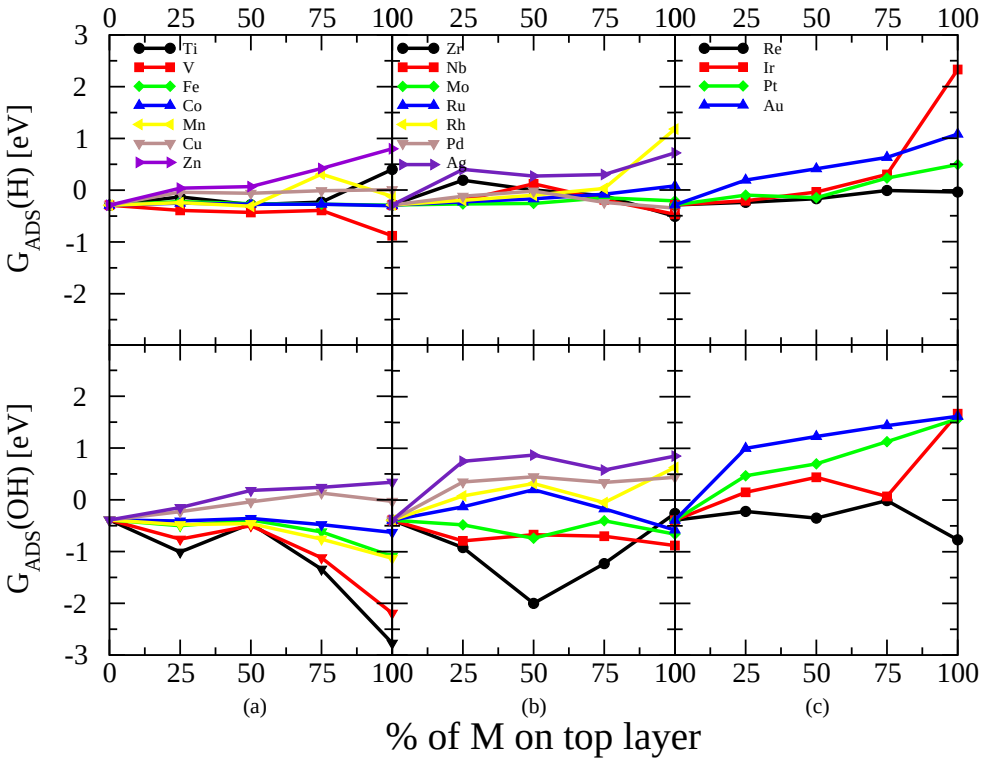

Figure B.3: H (en haut) et OH (en bas) des énergies libres d'adsorption sur les surfaces bimétalliques de NiM. Les résultats sont divisés en fonction de la position de M dans le tableau périodique

La carte de la surface avec la barrière d'activation la plus basse est illustrée sur la Figure xx. On peut constater qu'il y a des sites près des atomes de nickel qui adsorbent H_{ads} plus fortement. Les sites proches des atomes de cuivre sont néanmoins un meilleur choix, en raison de l'adsorption plus faible de H_{ads} et de l'énergie plus faible de l'état de transition.

Adsorption de H et OH sur des surfaces bimétalliques

Dans cette dernière section, j'ai fait des études DFT sur diverses surfaces NiM, afin de prédire des systèmes bimétalliques alternatifs avec une activité HOR plus élevée. En raison du grand nombre de systèmes, je n'ai étudié que l'énergie de l'adsorption H et OH, en me concentrant sur la recombinaison chimique. Les énergies libres d'adsorption, obtenues à l'aide de différents métaux de transition, ont été représentées sur la Fig. B.3. Les résultats ont été triés en fonction de la position du deuxième métal dans le tableau périodique.

Dans tous les graphiques de la Fig. B.3, il y a la région dans laquelle les énergies d'adsorption H et OH répondent aux critères des meilleurs catalyseurs HOR (ΔG_{ads} (H)≈ΔG_{ads} (OH)). Les candidats possibles sont seulement les métaux qui sont inclus dans ces zones pour les deux adsorbats.

La majorité des matériaux étudiés fixent OH ads trop fortement ou trop faiblement lorsque le pourcentage de ce second métal est élevé. Dans la quasi-totalité des cas, seules les surfaces contenant 25% d'un second métal peuvent adsorber les deux espèces dans la plage de potentiel optimale. Les énergies d'adsorption H sont dans la plupart des cas dans la région sélectionnée, la seule exception étant les métaux de la monnaie (Ag et Au).

Du premier groupe, les matériaux les plus intéressants sont: Zn et Co. Le Mn peut également être inclus, même si l'énergie d'adsorption de OH_{ads} est inférieure à la valeur du nickel pur. Dans le deuxième groupe, les systèmes sélectionnés sont: Rh et Ru, et de la dernière: Re et Ir.

Les prédictions théoriques des alliages de NiM prometteurs sont comparées aux données expérimentales. Badawy [115] a montré que les films NiZn sur un substrat en Cu étaient de bons candidats pour l'HER dans 1 M KOH. Selon Aaboubi [67], la performance accrue du NiMn est liée à deux facteurs principaux: l'augmentation de la surface réelle de Ni (porosité et rugosité) et l'adéquation des sites actifs en introduisant du Mn dans l'alliage Ni. Franceschini [63] a observé que l'augmentation de la quantité de Ru conduit à une réduction de l'activité.

B.3 Conclusion générale

L'adsorption de H_{ads} et OH_{ads} et la formation d'eau sur des surfaces bimétalliques en Ni ont été étudiés au moyen de calculs DFT. Selon les “volcano plot” (basés sur le principe de Sabatier), les meilleurs catalyseurs après l'étape de recombinaison chimique devraient avoir:ΔG_{ads} (H)≈ΔG_{ads} (OH).

Le système bimétallique CuNi a été choisi pour étudier en détails la thermodynamique

et la cinétique de la formation de l'eau pendant l'HOR. L'effet de différentes quantités et structures géométriques de Cu sur les surfaces Ni(111) sur H_{ads} et OH_{ads} a été étudié. Dans tous les cas, les énergies d'adsorption se situent entre les valeurs correspondant aux surfaces de Ni ou Cu pur.

Dans cette thèse, une mééthode différente et plus rapide pour obtenir des états de transition a été utilisée et des barrières d'activation de réactions purement chimiques. Habituellement, la méthode de NEB est le choix privilégié pour étudier la cinétique de ce type de réactions sur des surfaces métalliques. Elle est prohibitive dans les systèmes bimétalliques avec de nombreuses configurations initiales et finales possibles, en raison de la complexité et des coûts de calcul. J'ai montré que les PES contraintes sont une alternative fiable pour étudier la formation de l'eau sur ces surfaces. Les résultats obtenus pour les surfaces pures sont en accord avec les valeurs obtenues par la méthode NEB.

Il n'y a pas de corrélation directe entre les barrières d'activation et les énergies de réaction de la formation de l'eau. Ainsi, le principe Evans-Polyani ne tient pas la route. Il est donc obligatoire de calculer les énergies d'activation pour comprendre et prédire la cinétique de la réaction.

La présence de cuivre sur les surfaces de nickel a un effet important sur la formation de l'eau, réduisant la barrière à 0,2 eV. Une petite ou une grande quantité de cuivre n'a presque aucun effet sur la réaction, ce qui signifie qu'un seul atome isolé de cuivre ne changera pas la cinétique. Mais la présence de lignes de Cu améliore l'effet catalytique de la surface bimétallique, quelle que soit la couverture de surface.

Enfin, plusieurs métaux de transition ont été étudiés afin de trouver de nouveaux matériaux qui affaiblissent légèrement l¨interaction entre la surface et les adsorbats, et de créer de nouveaux sites d'activation pour la formation de l'eau. En me basant sur les énergies d'adsorption, j'ai trouvé plusieurs candidats possibles : Zn, Co, Mn, Rh, Ru, Re, Re et Ir. D'autres études expérimentales et théoriques sont nécessaires pour connaître l'exactitude de ces prévisions.

List of Tables

List of Figures

Bibliography

[1] MARCELO LINARDI. *Introdução à ciência e tecnologia de células a combustível*. Artliber, 2010.

[2] Wolf. Vielstich, Arnold. Lamm, Hubert A. (Hubert Andreas) Gasteiger, and Harumi. Yokokawa. *Handbook of fuel cells : fundamentals, technology, and applications*. Wiley, 2003.

[3] Hartmut Wendt, Michael Götz, and Marcelo Linardi. Tecnologia de células a combustível. *Química Nova*, 23(4):538–546, aug 2000.

[4] Hartmut Wendt, Marcelo Linardi, and Eliana M Aricó. CÉLULAS A COMBUSTÍVEL DE BAIXA POTÊNCIA PARA APLICAÇÕES ESTACIONÁRIAS. *Quim. Nova*, 25(3):470–476, 2002.

[5] Géraldine Merle, Matthias Wessling, and Kitty Nijmeijer. Anion exchange membranes for alkaline fuel cells: A review. *Journal of Membrane Science*, 377(1-2):1–35, 2011.

[6] Ming Gong, Di Yan Wang, Chia Chun Chen, Bing Joe Hwang, and Hongjie Dai. A mini review on nickel-based electrocatalysts for alkaline hydrogen evolution reaction. *Nano Research*, 9(1):28–46, 2016.

[7] M W Breiter. Eletrochemical Study of Hydrogen Adsorption on Platinum Metals. *Journal of The Electrochemical Society*, 109(3):C85–C95, 1962.

[8] Perica Paunovic, Orce Popovski, Dragan Slavkov, Aleksandar Dimitrov, and Hadzi Jordanov. Effect of carbon nanotubes support in improving the performance of mixed eclectrocalysts for hydrogen evolution. *Journal of the Serbian Chemical Society*, 26(2):87–93, 2007.

[9] M. Jaccaud, F. Leroux, and J.C. Millet. New chlor-alkali activated cathodes. *Materials Chemistry and Physics*, 22(1-2):105–119, jun 1989.

[10] Paola Quaino, Fernanda Juarez, Elizabeth Santos, and Wolfgang Schmickler. Volcano plots in hydrogen electrocatalysis – uses and abuses. *Beilstein J. Nanotechnol*, 5:846–854, 2014.

[11] Sergio Trasatti. Work function, electronegativity, and electrochemical behaviour of metals: III. Electrolytic hydrogen evolution in acid solutions. *Journal of Electroanalytical Chemistry and Interfacial Electrochemistry*, 39(1):163–184, sep 1972.

[12] Wolfgang Schmickler and Elizabeth Santos. Hydrogen reaction and electrocatalysis. In *Interfacial Electrochemistry*, pages 163–175. Springer Berlin Heidelberg, Berlin, Heidelberg, 2010.

[13] G. (Gerhard) Ertl, Helmut Knözinger, Ferdi Schüth, and Jens Weitkamp, editors. *Handbook of heterogeneous catalysis*. Wiley-VCH Verlag GmbH & Co. KGaA, 2008.

[14] Alexandr G Oshchepkov, Antoine Bonnefont, and Viktoriia A Saveleva. Exploring the Influence of the Nickel Oxide Species on the Kinetics of Hydrogen Electrode Reactions in Alkaline Media. *Topics in Catalysis*, 59(15):1319–1331, 2016.

[15] T. Bligaard, J.K. Nørskov, S. Dahl, J. Matthiesen, C.H. Christensen, and J. Sehested. The Brønsted–Evans–Polanyi relation and the volcano curve in heterogeneous catalysis. *Journal of Catalysis*, 224(1):206–217, may 2004.

[16] S.L. Medway, C.A. Lucas, A. Kowal, R.J. Nichols, and D. Johnson. In situ studies of the oxidation of nickel electrodes in alkaline solution. *Journal of Electroanalytical Chemistry*, 587(1):172–181, feb 2006.

[17] D. S. Hall, C. Bock, and B. R. MacDougall. The Electrochemistry of Metallic Nickel: Oxides, Hydroxides, Hydrides and Alkaline Hydrogen Evolution. *Journal of the Electrochemical Society*, 160(3):F235–F243, jan 2013.

[18] Paul H. Holloway. Chemisorption and oxide formation on metals: Oxygen–nickel reaction. *Journal of Vacuum Science and Technology*, 18(2):653–659, mar 1981.

[19] Tarasevich, M.R, Sadkowski, A., and Yeager, E. *Comprehensive Treatise of Electrochemistry*. Plenum, New York, 1983.

[20] R Adzic. *Electrocatalys*. Wiley-VCH Verlag GmbH & Co. KGaA, New York, 1998.

[21] P. N Ross. *Electrocatalys*. Wiley–VCH, New York, 1998.

[22] DJ Schmidt, TJ: Markovic, NM; Stamenkovic, V; Ross, PN; Attard, GA: Watson. Surface characterization and electrochemical behavior of well-defined Pt-Pd111 single-crystal surfaces: A comparative study using Pt111 and palladium-modified Pt111 electrodes. *Lagmuir*, 18(18):6969–6975, 2002.

[23] D. Floner, C. Lamy, and J.-M. Leger. Electrocatalytic oxidation of hydrogen on polycrystal and single-crystal nickel electrodes. *Surface Science*, 234(1-2):87–97, aug 1990.

[24] Nenad M. Markovića, Stella T. Sarraf, Hubert A. Gasteiger, and Philip N. Ross. Hydrogen electrochemistry on platinum low-index single-crystal surfaces in alkaline solution. *J. Chem. Soc., Faraday Trans.*, 92(20):3719–3725, jan 1996.

[25] Jeff Greeley, Thomas F. Jaramillo, Jacob Bonde, Ib Chorkendorff, and Jens K. Nørskov. Computational high-throughput screening of electrocatalytic materials for hydrogen evolution. *Nature Materials*, 5(11):909–913, nov 2006.

[26] Ram Subbaraman, Dusan Tripkovic, Kee-Chul Chang, Dusan Strmcnik, Arvydas P. Paulikas, Pussana Hirunsit, Maria Chan, Jeff Greeley, Vojislav Stamenkovic, and Nenad M. Markovic. Trends in activity for the water electrolyser reactions on 3d M(Ni,Co,Fe,Mn) hydr(oxy)oxide catalysts. *Nature Materials*, 11(6):550–557, jun 2012.

[27] N. N. Greenwood A. Ernshaw. *Chemistry of Elements*. Elsevier, Oxford, UK, 1997.

[28] L. M. Madeira, M. F. Portela, and C. Mazzocchia. Nickel Molybdate Catalysts and Their Use in the Selective Oxidation of Hydrocarbons. *Catalysis Reviews*, 46(1):53–110, dec 2004.

[29] Neill W. J. Use of high nickel alloy in the petroleum refining industry. *Materials performance*, 40(5):50–54, 1974.

[30] Khaliq Ahmed and Karl Föger. Fuel Processing for High-Temperature High-Efficiency Fuel Cells. *Industrial & Engineering Chemistry Research*, 49(16):7239–7256, aug 2010.

[31] J.H; Chorkendorff I. Larsen. From fundamentals studies of reactivity on single crystals to design of catalysts. *Surface Science reports*, 35(5-8):165–222, 1999.

[32] B. Beverskog and I. Puigdomenech. Revised Pourbaix diagrams for nickel at 25–300 °C. *Corrosion Science*, 39(5):969–980, may 1997.

[33] J. Bode, H. ; Dehmelt, K.; Witte. Zur Kinntnis der nickelhydroxide elektrode - I. Uber das nickel (II)- hydroxidhydrat. *Electrochimica Acta*, 11:1079–1087, 1966.

[34] D. M. MacArthur. The Hydrated Nickel Hydroxide Electrode Potential Sweep Experiments. *Journal of The Electrochemical Society*, 117(4):422, 1970.

[35] Deepika Singh. Characteristics and Effects of γ-NiOOH on Cell Performance and a Method to Quantify It in Nickel Electrodes. *Journal of The Electrochemical Society*, 145(1):116, 1998.

[36] N. Sac-Epee. β-Ni(OH)[sub 2] Transitions during Electrochemical Cycling of the Nickel Hydroxide Electrode. *Journal of The Electrochemical Society*, 145(5):1434, 1998.

[37] B. MacDougall and M. Cohen. Anodic Oxidation of Nickel in Neutral Sulfate Solution. *Journal of The Electrochemical Society*, 121(9):1152, 1974.

[38] S.L. Medway, C.A. Lucas, A. Kowal, R.J. Nichols, and D. Johnson. In situ studies of the oxidation of nickel electrodes in alkaline solution. *Journal of Electroanalytical Chemistry*, 587(1):172–181, feb 2006.

[39] F. Hahn, B. Beden, M.J. Croissant, and C. Lamy. In situ uv visible reflectance spectroscopic investigation of the nickel electrode-alkaline solution interface. *Electrochimica Acta*, 31(3):335–342, mar 1986.

[40] Malgorzata Dmochowska and Andrzej Czerwinski. Behavior of a nickel electrode in the presence of carbon monoxide. *Journal of Solid State Electrochemistry*, 2(1):16–23, 1998.

[41] R. S. Schrebler Guzman, J. R. Vilche, and A. J. Arvia. Non-equilibrium effects in the nickel hydroxide electrode. *Journal of Applied Electrochemistry*, 9(2):183–189, mar 1979.

[42] W. Visscher and E. Barendrecht. Anodic oxide films of nickel in alkaline electrolyte. *Surface Science*, 135(1-3):436–452, dec 1983.

[43] R. S. Schrebler Guzman, J. R. Vilche, and A. J. Arvía. Rate Processes Related to the Hydrated Nickel Hydroxide Electrode in Alkaline Solutions. *Journal of The Electrochemical Society*, 125(10):1578, oct 1978.

[44] N. Krstajić, M. Popović, B. Grgur, M. Vojnović, and D. Šepa. On the kinetics of the hydrogen evolution reaction on nickel in alkaline solution - Part II. Effect of temperature. *Journal of Electroanalytical Chemistry*, 512(1-2):27–35, oct 2001.

[45] M. A. V. Devanathan and M. Selvaratnam. Mechanism of the hydrogen-evolution reaction on nickel in alkaline solutions by the determination of the degree of coverage. *Transactions of the Faraday Society*, 56:1820, 1960.

[46] J.J. Kim S.H. Ahh, S.J. Hwang, S.J. Woo, I. Choi, H.-J. Kim, J.H. Jang, S.W. Nam, T.-H. Lim, T. Lim, S.-K. Kim. Electrodeposited Ni dendrites with high activity and durability for hydrogen evolution reaction in alkaline water electrolysis. *Journal of Materials Chemistry A*, 22:15153–15159, 2012.

[47] R. L. LeRoy. Analysis of Time-Variation Effects in Water Electrolyzers. *Journal of The Electrochemical Society*, 126(10):1674, 1979.

[48] D. M. Soares. Hydride Effect on the Kinetics of the Hydrogen Evolution Reaction on Nickel Cathodes in Alkaline Media. *Journal of The Electrochemical Society*, 139(1):98, 1992.

[49] M Bernardini, N Comisso, G Davolio, and G Mengoli. Formation of nickel hydrides by hydrogen evolution in alkaline media. *Journal of Electroanalytical Chemistry*, 442(1-2):125–135, jan 1998.

[50] J. L Weininger and M. W. Breiter. Hydrogen Evolution and Surface Oxidation of Nickel Electrodes in Alkaline Solution. *Journal of The Electrochemical Society*, 111(6):707, 1964.

[51] N. Danilovic, Ram Subbaraman, D. Strmcnik, Kee-Chul Chang, A. P. Paulikas, V. R. Stamenkovic, and Nenad M. Markovic. Enhancing the Alkaline Hydrogen Evolution Reaction Activity through the Bifunctionality of Ni(OH) ₂ /Metal Catalysts. *Angewandte Chemie International Edition*, 51(50):12495–12498, dec 2012.

[52] Ming Gong, Wu Zhou, Mon-Che Tsai, Jigang Zhou, Mingyun Guan, Meng-Chang Lin, Bo Zhang, Yongfeng Hu, Di-Yan Wang, Jiang Yang, Stephen J. Pennycook, Bing-Joe

Hwang, and Hongjie Dai. Nanoscale nickel oxide/nickel heterostructures for active hydrogen evolution electrocatalysis. *Nature Communications*, 5(1):4695, dec 2014.

[53] Michael K. Bates, Qingying Jia, Nagappan Ramaswamy, Robert J. Allen, and Sanjeev Mukerjee. Composite Ni/NiO-Cr ₂ O ₃ Catalyst for Alkaline Hydrogen Evolution Reaction. *The Journal of Physical Chemistry C*, 119(10):5467–5477, mar 2015.

[54] Xiaodong Yan, Lihong Tian, and Xiaobo Chen. Crystalline/amorphous Ni/NiO core/shell nanosheets as highly active electrocatalysts for hydrogen evolution reaction. *Journal of Power Sources*, 300:336–343, dec 2015.

[55] Alexandr G. Oshchepkov, Pavel A. Simonov, Olga V. Cherstiouk, Renat R. Nazmutdinov, Dmitrii V. Glukhov, Vladimir I. Zaikovskii, Tatyana Yu. Kardash, Ren I. Kvon, Antoine Bonnefont, Alexandr N. Simonov, Valentin N. Parmon, and Elena R. Savinova. On the Effect of Cu on the Activity of Carbon Supported Ni Nanoparticles for Hydrogen Electrode Reactions in Alkaline Medium. *Topics in Catalysis*, 58(18-20):1181–1192, nov 2015.

[56] Ram Subbaraman, Dusan Tripkovic, Dusan Strmcnik, Kee-Chul Chang, Masanobu Uchimura, Arvydas P Paulikas, Vojislav Stamenkovic, and Nenad M Markovic. Enhancing hydrogen evolution activity in water splitting by tailoring Li^+-$Ni(OH)_2$-Pt interfaces. *Science (New York, N.Y.)*, 334(6060):1256–60, dec 2011.

[57] R. Subbaraman, D. Tripkovic, D. Strmcnik, K.-C. Chang, M. Uchimura, A. P. Paulikas, V. Stamenkovic, and N. M. Markovic. Enhancing Hydrogen Evolution Activity in Water Splitting by Tailoring Li+-Ni(OH)2-Pt Interfaces. *Science*, 334(6060):1256–1260, dec 2011.

[58] Gerhard Kreysa, Bo Hakansson, and Per Ekdunge. Kinetic and thermodynamic analysis

of hydrogen evolution at nickel electrodes. *Electrochimica Acta*, 33(10):1351–1357, oct 1988.

[59] P.N Ross. *Handbook of Fuel Cells*. Wiley, New York, 2003.

[60] José L.C. Fajín, M. Natália D.S. Cordeiro, Francesc Illas, and José R.B. Gomes. Generalized Brønsted–Evans–Polanyi relationships and descriptors for O–H bond cleavage of organic molecules on transition metal surfaces. *Journal of Catalysis*, 313:24–33, may 2014.

[61] Daniel Sebastiani and Luigi Delle Site. Adsorption of Water Molecules on Flat and Stepped Nickel Surfaces from First Principles. *Journal of Chemical Theory and Computation*, 1(1):78–82, jan 2005.

[62] Monica Pozzo, Gianluigi Carlini, Renzo Rosei, and Dario Alfè. Comparative study of water dissociation on Rh(111) and Ni(111) studied with first principles calculations. *The Journal of Chemical Physics*, 126(16):164706, apr 2007.

[63] Esteban A. Franceschini, Gabriela I. Lacconi, and Horacio R. Corti. Kinetics of hydrogen evolution reaction on nickel modified by spontaneous Ru deposition: A rotating disk electrode and impedance spectroscopy approach. *International Journal of Hydrogen Energy*, 41(5):3326–3338, feb 2016.

[64] Sergey N. Pronkin, Antoine Bonnefont, Pavel S. Ruvinskiy, and Elena R. Savinova. Hydrogen oxidation kinetics on model Pd/C electrodes: Electrochemical impedance spectroscopy and rotating disk electrode study. *Electrochimica Acta*, 55(9):3312–3323, mar 2010.

[65] R. M. Abouatallah, D. W. Kirk, S. J. Thorpe, and J. W. Graydon. Characterization of Vanadium Deposit Formation at a Hydrogen Evolving Electrode in Alkaline Media. *Journal of The Electrochemical Society*, 148(9):E357, sep 2001.

[66] R.M Abouatallah, D.W Kirk, S.J Thorpe, and J.W Graydon. Reactivation of nickel cathodes by dissolved vanadium species during hydrogen evolution in alkaline media. *Electrochimica Acta*, 47(4):613–621, nov 2001.

[67] Omar Aaboubi, Ahmed-Yassin Ali-Omar, Eunice Dzoyem, Jimmy Marthe, and Mohamed Boudifa. Ni–Mn based alloys as versatile catalyst for different electrochemical reactions. *Journal of Power Sources*, 269:597–607, dec 2014.

[68] I. Danaee and S. Noori. Kinetics of the hydrogen evolution reaction on NiMn graphite modified electrode. *International Journal of Hydrogen Energy*, 36(19):12102–12111, sep 2011.

[69] Michael G. Walter, Emily L. Warren, James R. McKone, Shannon W. Boettcher, Qixi Mi, Elizabeth A. Santori, and Nathan S. Lewis. Solar Water Splitting Cells. *Chemical Reviews*, 110(11):6446–6473, nov 2010.

[70] I. Flis-Kabulska and J. Flis. Electroactivity of Ni–Fe cathodes in alkaline water electrolysis and effect of corrosion. *Corrosion Science*, 112:255–263, nov 2016.

[71] M Metikoš-Huković and A Jukić. Correlation of electronic structure and catalytic activity of Zr–Ni amorphous alloys for the hydrogen evolution reaction. *Electrochimica Acta*, 45(25-26):4159–4170, aug 2000.

[72] L. Mihailov, T. Spassov, and M. Bojinov. Effect of microstructure on the electrocatalytic activity for hydrogen evolution of amorphous and nanocrystalline Zr–Ni alloys. *International Journal of Hydrogen Energy*, 37(14):10499–10506, jul 2012.

[73] J. Halim, R. Abdel-Karim, S. El-Raghy, M. Nabil, and A. Waheed. Electrodeposition and Characterization of Nanocrystalline Ni-Mo Catalysts for Hydrogen Production. *Journal of Nanomaterials*, pages 1–9, feb 2012.

[74] Sandhya Shetty, M. Mohamed Jaffer Sadiq, D. Krishna Bhat, and A. Chitharanjan Hegde. Electrodeposition and characterization of Ni-Mo alloy as an electrocatalyst for alkaline water electrolysis. *Journal of Electroanalytical Chemistry*, 796:57–65, jul 2017.

[75] Mert Manazoğlu, Gökçe Hapçı, and Gökhan Orhan. Effect of electrolysis parameters of Ni–Mo alloy on the electrocatalytic activity for hydrogen evaluation and their stability in alkali medium. *Journal of Applied Electrochemistry*, 46(2):191–204, feb 2016.

[76] István Bakos, András Paszternák, and David Zitoun. Pd/Ni Synergestic Activity for Hydrogen Oxidation Reaction in Alkaline Conditions. *Electrochimica Acta*, 176:1074–1082, sep 2015.

[77] Maria Alesker, Miles Page, Meital Shviro, Yair Paska, Gregory Gershinsky, Dario R. Dekel, and David Zitoun. Palladium/nickel bifunctional electrocatalyst for hydrogen oxidation reaction in alkaline membrane fuel cell. *Journal of Power Sources*, 304:332–339, feb 2016.

[78] V. Pérez-Herranz, R. Medina, P. Taymans, C. González-Buch, E.M. Ortega, G. Sánchez-Loredo, and G.J. Labrada-Delgado. Modification of porous nickel electrodes with silver nanoparticles for hydrogen production. *Journal of Electroanalytical Chemistry*, 808:420–426, jan 2018.

[79] Esteban A. Franceschini, Gabriela I. Lacconi, and Horacio R. Corti. Hydrogen evolution kinetics on Ni cathodes modified by spontaneous deposition of Ag or Cu. *Journal of Energy Chemistry*, 26(3):466–475, may 2017.

[80] V. V. Kuznetsov, Yu. D. Gamburg, M. V. Zhalnerov, V. V. Zhulikov, and R. S. Batalov. Reaction of hydrogen evolution on Co-Mo (W) and Ni-Re electrolytic alloys in alkaline media. *Russian Journal of Electrochemistry*, 52(9):901–909, sep 2016.

[81] Jianrui Feng, Fan Lv, Weiyu Zhang, Peihao Li, Kai Wang, Chao Yang, Bin Wang, Yong Yang, Jinhui Zhou, Fei Lin, Gui-Chang Wang, and Shaojun Guo. Iridium-Based Mul-

timetallic Porous Hollow Nanocrystals for Efficient Overall-Water-Splitting Catalysis. *Advanced Materials*, 29(47):1703798, dec 2017.

[82] M.A. Domínguez-Crespo, E. Ramírez-Meneses, A.M. Torres-Huerta, V. Garibay-Febles, and K. Philippot. Kinetics of hydrogen evolution reaction on stabilized Ni, Pt and Ni–Pt nanoparticles obtained by an organometallic approach. *International Journal of Hydrogen Energy*, 37(6):4798–4811, mar 2012.

[83] Boguslaw Pierozynski and Tomasz Mikolajczyk. Cathodic Evolution of Hydrogen on Platinum-Modified Nickel Foam Catalyst. *Electrocatalysis*, 7:121–126, 2016.

[84] Cristina González-Buch, Isaac Herraiz-Cardona, Emma M. Ortega, Sergio Mestre, and Valentín Pérez-Herranz. Synthesis and characterization of Au-modified macroporous Ni electrocatalysts for alkaline water electrolysis. *International Journal of Hydrogen Energy*, 41(2):764–772, jan 2016.

[85] C. Lupi, A. Dell'Era, and M. Pasquali. In situ activation with Mo of Ni–Co alloys for hydrogen evolution reaction. *International Journal of Hydrogen Energy*, 39(5):1932–1940, feb 2014.

[86] E. Santos, P. Quaino, P.F. Hindelang, and W. Schmickler. Hydrogen evolution on a pseudomorphic Cu-layer on Ni(1 1 1) – A theoretical study. *Journal of Electroanalytical Chemistry*, 649(1-2):149–152, nov 2010.

[87] Olga V. Cherstiouk, Pavel A. Simonov, Alexandr G. Oshchepkov, Vladimir I. Zaikovskii, Tatyana Yu. Kardash, Antoine Bonnefont, Valentin N. Parmon, and Elena R. Savinova. Electrocatalysis of the hydrogen oxidation reaction on carbon-supported bimetallic NiCu particles prepared by an improved wet chemical synthesis. *Journal of Electroanalytical Chemistry*, 783:146–151, dec 2016.

[88] Sang Hyun Ahn, Hee-Young Park, Insoo Choi, Sung Jong Yoo, Seung Jun Hwang, Hyoung-Juhn Kim, EunAe Cho, Chang Won Yoon, Hansoo Park, Hyungbin Son,

Juan Martin Hernandez, Suk Woo Nam, Tae-Hoon Lim, Soo-Kil Kim, and Jong Hyun Jang. Electrochemically fabricated NiCu alloy catalysts for hydrogen production in alkaline water electrolysis. *International Journal of Hydrogen Energy*, 38(31):13493–13501, oct 2013.

[89] Mosaad Negem and H. Nady. Electroplated Ni-Cu nanocrystalline alloys and their electrocatalytic activity for hydrogen generation using alkaline solutions. *International Journal of Hydrogen Energy*, 42(47):28386–28396, nov 2017.

[90] Axel Gross. *Theoretical Surface Science*. Springer edition, 2009.

[91] P. Hohenberg and W. Kohn. Inhomogeneous Electron Gas. *Physical Review*, 136(3B):B864–B871, nov 1964.

[92] W. Kohn. Nobel Lecture: Electronic structure of matter—wave functions and density functionals. *Reviews of Modern Physics*, 71(5):1253–1266, oct 1999.

[93] W. Kohn and L. J. Sham. Self-Consistent Equations Including Exchange and Correlation Effects. *Physical Review*, 140(4A):A1133–A1138, nov 1965.

[94] John P. Perdew, Kieron Burke, and Matthias Ernzerhof. Generalized Gradient Approximation Made Simple. *Physical Review Letters*, 77(18):3865–3868, oct 1996.

[95] R. M. Martin. *Electronic structure: basic theory and practical methods*. Cambridge Univer. Press, Cambridge, repr. edn. edition, 2010.

[96] José M Soler, Emilio Artacho, Julian D Gale, Alberto García, Javier Junquera, Pablo Ordejón, and Daniel Sánchez-Portal. The SIESTA method for ab initio order-N materials simulation. *Journal of Physics: Condensed Matter*, 14(11):2745–2779, mar 2002.

[97] J. J. Mortensen, L. B. Hansen, and K. W. Jacobsen. Real-space grid implementation of the projector augmented wave method. *Physical Review B*, 71(3):035109, jan 2005.

[98] J Enkovaara, C Rostgaard, J J Mortensen, J Chen, M Dułak, L Ferrighi, J Gavnholt, C Glinsvad, V Haikola, H A Hansen, H H Kristoffersen, M Kuisma, A H Larsen, L Lehtovaara, M Ljungberg, O Lopez-Acevedo, P G Moses, J Ojanen, T Olsen, V Petzold, N A Romero, J Stausholm-Møller, M Strange, G A Tritsaris, M Vanin, M Walter, B Hammer, H Häkkinen, G K H Madsen, R M Nieminen, J K Nørskov, M Puska, T T Rantala, J Schiøtz, K S Thygesen, and K W Jacobsen. Electronic structure calculations with GPAW: a real-space implementation of the projector augmented-wave method. *Journal of Physics: Condensed Matter*, 22(25):253202, jun 2010.

[99] Leandro M. C. Pinto, Paola Quaino, Mauricio D. Arce, Elizabeth Santos, and Wolfgang Schmickler. Electrochemical Adsorption of OH on Pt(111) in Alkaline Solutions: Combining DFT and Molecular Dynamics. *ChemPhysChem*, 15(10):2003–2009, jul 2014.

[100] Abas Mohsenzadeh, Kim Bolton, and Tobias Richards. DFT study of the adsorption and dissociation of water on Ni(111), Ni(110) and Ni(100) surfaces. *Surface Science*, 627:1–10, sep 2014.

[101] Peter Ferrin, Shampa Kandoi, Anand Udaykumar Nilekar, and Manos Mavrikakis. Hydrogen adsorption, absorption and diffusion on and in transition metal surfaces: A DFT study. *Surface Science*, 606(7-8):679–689, apr 2012.

[102] Elizabeth Santos, Peter Hindelang, Paola Quaino, Eduardo N. Schulz, Germán Soldano, and Wolfgang Schmickler. Hydrogen electrocatalysis on single crystals and on nanostructured electrodes. *ChemPhysChem*, 12(12):2274–2279, 2011.

[103] Abas Mohsenzadeh, Tobias Richards, and Kim Bolton. DFT study of the water gas shift reaction on Ni(111), Ni(100) and Ni(110) surfaces. *Surface Science*, 644:53–63, feb 2016.

[104] Fanglin Che, Jake T Gray, Su Ha, and Jean-Sabin Mcewen. Catalytic Water Dehy-

drogenation and Formation on Nickel: Dual Path Mechanism in High Electric Fields. *Journal of Catalysis*, 332:187–200, 2015.

[105] Guichang Wang, Ling Jiang, Cai, Pan, Zhao, Wei Huang, Xie, Li, Sun, and Bing Zhong. Surface Structure Sensitivity of the Water-Gas Shift Reaction on Cu(h kl) Surfaces: A Theoretical Study. *The Journal of Physical Chemistry B*, 107(2):557–562, 2003.

[106] José L.C. Fajín, M. Natália D.S. Cordeiro, Francesc Illas, and José R.B. Gomes. Descriptors controlling the catalytic activity of metallic surfaces toward water splitting. *Journal of Catalysis*, 276(1):92–100, 2010.

[107] M.Y. Gao, C. Yang, Q.B. Zhang, Y.W. Yu, Y.X. Hua, Y. Li, and P. Dong. Electrochemical fabrication of porous Ni-Cu alloy nanosheets with high catalytic activity for hydrogen evolution. *Electrochimica Acta*, 215:609–616, oct 2016.

[108] H. L. Skriver and N. M. Rosengaard. Surface energy and work function of elemental metals. *Physical Review B*, 46(11):7157–7168, sep 1992.

[109] G. S. Karlberg. Adsorption trends for water, hydroxyl, oxygen, and hydrogen on transition-metal and platinum-skin surfaces. *Physical Review B - Condensed Matter and Materials Physics*, 74(15):3–6, 2006.

[110] S.; Li. Y; Liu. X.; Zhang. D.; Gao. J. Shen. Hydrogen diffusion into the subsurfaces of metal catalysts from first principles. *Physical Chemistry Chemical Physics*, page 3557, 2017.

[111] E. Kristinsdottir, L.; Skulason. A systematic DFT study of Hydrogen diffusion on transition metal surfaces. *Surface Science*, 606:1400–1404, 2012.

[112] M. Ferrin, Peter; Kandoi, S.; Nilekar. A.; Mavrikakis. Hydrogen Adsorption, Absorption and Diffusion on and in transition metals surfaces: A DFT study. *Surface Science*, 606:679–689, 2012.

[113] M. Greeley, Jeff; Markvrikakis. Surface and Subsurface Hydrogen: Adsorption Properties on Transition Metals and Near Surface Alloys. *Journal of Physical Chemistry Physical Chemistry Physical Chemistry B*, 109:3460–3471, 2005.

[114] J. ko, J.; kwon. H.; kang, H.; kim, B.; Han. Universality in surface mixing rule of adsorption for small adsorbates on binary transition metal alloys. *Physical Chemistry Chemical Physics*, 17:3123, 2015.

[115] W.A. Badawy, H. Nady, and G.M. Abd El-Hafez. Electrodeposited Zn-Ni alloys as promising catalysts for hydrogen production-Preparation, characterization and electrocatalytic activity. *Journal of Alloys and Compounds*, 699:1146–1156, mar 2017.

[116] Lourdes Vázquez-Gómez, Sandro Cattarin, Paolo Guerriero, and Marco Musiani. Hydrogen evolution on porous Ni cathodes modified by spontaneous deposition of Ru or Ir. *Electrochimica Acta*, 53(28):8310–8318, nov 2008.

[117] Yu. D. Gamburg, V. V. Zhulikov, and B. F. Lyakhov. Electrodeposition, properties, and composition of rhenium–nickel alloys. *Russian Journal of Electrochemistry*, 52(1):78–82, jan 2016.

[118] A.C Tavares and S Trasatti. Ni+RuO2 co-deposited electrodes for hydrogen evolution. *Electrochimica Acta*, 45(25-26):4195–4202, aug 2000.

[119] U.Č. Lačnjevac, B.M. Jović, V.D. Jović, V.R. Radmilović, and N.V. Krstajić. Kinetics of the hydrogen evolution reaction on Ni-(Ebonex-supported Ru) composite coatings in alkaline solution. *International Journal of Hydrogen Energy*, 38(25):10178–10190, aug 2013.

[120] M. Jaccaud, F. Leroux, and J.C. Millet. New chlor-alkali activated cathodes. *Materials Chemistry and Physics*, 22(1-2):105–119, jun 1989.

[121] Tingting Sun, Jia Cao, Jing Dong, Hanying Du, Haijiang Zhang, Jianfeng Chen, and Lianbin Xu. Ordered mesoporous NiCo alloys for highly efficient electrocatalytic hydrogen evolution reaction. *International Journal of Hydrogen Energy*, 42(10):6637–6645, mar 2017.

[122] Juan Victor Perales-Rondón, Adolfo Ferre-Vilaplana, Juan M. Feliu, and Enrique Herrero. Oxidation Mechanism of Formic Acid on the Bismuth Adatom-Modified Pt(111) Surface. *Journal of the American Chemical Society*, 136(38):13110–13113, sep 2014.

[123] G. S. Karlberg, T. F. Jaramillo, E. Skúlason, J. Rossmeisl, T. Bligaard, and J. K. Nørskov. Cyclic Voltammograms for H on Pt(111) and Pt(100) from First Principles. *Physical Review Letters*, 99(12):126101, sep 2007.

[124] * J. K. Nørskov, J. Rossmeisl, A. Logadottir, , L. Lindqvist, J. R. Kitchin, T. Bligaard, and H. Jónsson. Origin of the Overpotential for Oxygen Reduction at a Fuel-Cell Cathode. *The Journal of Physical Chemistry B*, 108(46):17886–17892, 2004.

[125] Yi Pan, Haigang Zhang, Dongxia Shi, Jiatao Sun, Shixuan Du, Feng Liu, and Hongjun Gao. Highly Ordered, Millimeter-Scale, Continuous, Single-Crystalline Graphene Monolayer Formed on Ru (0001). *Advanced Materials*, 21(27):2777–2780, jul 2009.

[126] Hendrik J. Monkhorst and James D. Pack. Special points for Brillouin-zone integrations. *Physical Review B*, 13(12):5188, jun 1976.

[127] Stefania Fiameni, Isaac Herraiz-Cardona, Marco Musiani, Valentín Pérez-Herranz, Lourdes Vázquez-Gómez, and Enrico Verlato. The HER in alkaline media on Pt-modified three-dimensional Ni cathodes. *International Journal of Hydrogen Energy*, 37(14):10507–10516, jul 2012.

[128] R Šimpraga, G Tremiliosi-Filho, S Y Qian, and B E Conway. In situ determination of the 'real are factor' in H2 evolution electrocatalysis at porous Ni-Fe composite electrodes. *Journal of Electroanalytical Chemistry*, 424(1-2):141–151, 1997.

[129] E. Santos, A. Lundin, K. Pötting, P. Quaino, and W. Schmickler. Model for the electrocatalysis of hydrogen evolution. *Physical Review B*, 79(23):235436, jun 2009.